Doctoral dissertation

Non-Fermi Liquid Behavior in $Ce(Ru_{1-x}Rh_x)_2Si_2$

Yoshikazu Tabata
Graduate School of Science, Osaka University

January, 2001

Doctoral dissertation

Non-Fermi Liquid Behavior in $Ce(Ru_{1-x}Rh_x)_2Si_2$

Yoshikazu Tabata
Graduate School of Science, Osaka University

January, 2001

Contents

Abstract

In this thesis I show the results of study of the non-Fermi liquid (NFL) behavior in $Ce(Ru_{1-x}Rh_x)_2Si_2$ system from the viewpoint of the quantum phase transition (QPT), which occurs at the quantum critical point (QCP) at $T = 0$ due to the instability of the quantum critical fluctuation. $Ce(Ru_{1-x}Rh_x)_2Si_2$ system has three magnetic QCP $x_c \sim 0.04$, 0.4 and 0.5. First I investigate the FL behavior for $x = 0.03$, where the concentration is close to the QCP and the chemical disorder is expected to be small. In the low Rh-concentration region $x \leq 0.03$, the self consistent renomalization (SCR) theory for the antiferromagnetic case works well. On the other hand, in a wide region of the intermediate Rh-concentration $0.35 \leq x \leq 0.5$, the NFL behavior was observed. In this region, it has been revealed that the zero field properties originate from the quantum Griffiths singularity at $T = H = 0$ from the detailed study of the resistivity and the susceptibility as a function of a temperature and magnetic field. This singularity is caused by the interplay between the quantum critical phenomena and the disorder effect due to the alloying. In the high field region the resistivity at each magnetic field can be scaled onto one universal curve. It means that the quantum critical description is applicable in the high field region. On the other hand, in the low field region we discovered the scaling form of the susceptibility, which is considered to be in a different regime from that in the high field region. It should be driven by the interplay between the 'chemical' disorder and the quantum critical fluctuation.

Chapter 1

Introduction

1.1 Heavy Fermion System

Since K. Andres *et al.* discovered the anomalous large electronic coefficient γ ($\sim$ 1620 mJ/molK^2) in $CeAl_3$ in 1975 [1], such "heavy fermion" properties observed in many Ce and U-based intermetallic compounds have been studied by many theoreticians and experimentalists as a central issue in strongly correlated electron systems. The γ-value of metal is proportional to the effective mass of conduction electrons m^*, therefore these materials are called "heavy fermion (HF) system". These heavy mass also given an enhanced Pauli paramagnetic susceptibility and a huge coefficient A of T^2-term of the resistivity. The ratio between the square of γ and A has a universal value, $A/\gamma^2 \sim 1 \times 10^{-5}$ (Kadowaki-Woods relation) [2]. These thermodynamic and transport properties of HF system can be understood in term of Landau's Fermi Liquid (FL) theory. In the FL theory the correlation between conduction electrons is renormalized to the effective mass of quasi-particles which can be handled in the free electron approximation. In the HF systems the enhancedment of m^* reaches around 100 or 1000. This anomalous mass-enhancedment is due to the Kondo effect which is the hybridization between conduction electrons and localized f-electrons.

Kondo effect was originally discovered in the nonmagneic metal with magnetic impurity, which is described with the *sd* hamiltonian,

$$\mathcal{H} = -Js\boldsymbol{S} \tag{1.1}$$

where $\boldsymbol{s}$ and $\boldsymbol{S}$ is the spin of the conduction electron and the magnetic impurity respectively and J is a exchange coupling constant between the both spins. According to this single impurity Kondo model, the electorn of the magnetic impurity (d or f-electron) localized on the magnetic atom at high temperature, and the conduction electrons are scattered by the localized moment of this d or f-electron through the *sd* interaction. J. Kondo calculated the resistivity with this *sd* model within the second order Born approximation and obtained the $-\log T$ dependence [3]. At low temperature such a localized moment strongly couples with the spin of conduction electrons antiferromagnetically, then, forms the singlet state (Kondo singlet). At present exact solution for the Kondo effect is obtained, which tells us that at low temperature the resistivity and the susceptibility continuously approaching to the finite value at $T = 0$ (unitarity limit) with the temperature dependence, $1 - AT^2$ and $(1 + BT^2)^{-1}$ respectively. The physical properties of single impurity Kondo system can be scaled by Kondo temperature T_K which is the coupling

energy of the Kondo singlet state given by,

$$k_{\rm B}T_{\rm K} = W\exp(-\frac{N}{\mid J \mid \rho(\epsilon_F)}) \tag{1.2}$$

where N is the number of the conduction electron, W is the half width of the conduction electron band and $\rho(\epsilon_F)$ is the density of state (DOS) at Fermi energy. The coupling constant J in the *sd* hamiltonian can be derived from the impurity Anderson hamiltonian

$$\mathcal{H} = \sum_{\boldsymbol{k},\sigma} \epsilon_{\boldsymbol{k}} c^{\dagger}_{\boldsymbol{k},\sigma} c_{\boldsymbol{k},\sigma} + \sum_{\sigma} E_f f^{*}_{\sigma} f_{\sigma} + U n_{f\sigma} n_{f-\sigma} + \sum_{\boldsymbol{k}\sigma} (V_{\boldsymbol{k},f} c^{\dagger}_{\boldsymbol{k},\sigma} f_{\sigma} + V^{*}_{\boldsymbol{k},f} f^{\dagger}_{\sigma} c_{\boldsymbol{k},\sigma}) \tag{1.3}$$

where $\epsilon_{\boldsymbol{k}}$ is the energy of the conduction electron with the wave vector $\boldsymbol{k}$, E_f is the energy level of the impurity f-electron, U is the intra-atomic Coulomb repulsion between the f-electron and $V_{\boldsymbol{k},f}$ is the matrix element for the hybridization between the impurity f- and conduction electron. $c_{\boldsymbol{k},\sigma}$, $c^{\dagger}_{\boldsymbol{k},\sigma}$, f_{σ} and $f^{\dagger}_{\sigma}$ denote the annihilation and creation operators for the conduction and f-electron respectively. When the fourth term is treated perturbatively and only the freedom of the spin is considered, J is given by,

$$J = N_0 \mid V \mid^2 (\frac{1}{U+E_f} + \frac{1}{E_f}) < 0 \tag{1.4}$$

The negative J can be derived from the Anderson hamiltonian naturally.

However such a single impurity Kondo model cannot explain the physical properties of HF systems perfectly because Ce or U-atom construct the regular lattice (Kondo lattice), which should be described by the periodic Anderson hamiltonian,

$$\begin{aligned}\mathcal{H} \;=\; & \sum_{\boldsymbol{k},\sigma} \epsilon_{\boldsymbol{k}} c^{\dagger}_{\boldsymbol{k},\sigma} c_{\boldsymbol{k},\sigma} + \sum_{\boldsymbol{k},\sigma} E_{\boldsymbol{k},f} f^{\dagger}_{\boldsymbol{k},\sigma} f_{\boldsymbol{k},\sigma} + \frac{U}{N} \sum_{\boldsymbol{q}} \sum_{\boldsymbol{k},\boldsymbol{k}'} f^{\dagger}_{\boldsymbol{k}} - q_{\sigma} f^{\dagger}_{\boldsymbol{k}'} + q_{,-\sigma} f_{\boldsymbol{k}',-\sigma} f_{\boldsymbol{k},\sigma} \\ & + \sum_{\boldsymbol{k}\sigma} (V_{\boldsymbol{k},f} c^{\dagger}_{\boldsymbol{k},\sigma} f_{\boldsymbol{k},\sigma} + V^{\dagger}_{\boldsymbol{k},f} f^{\dagger}_{\boldsymbol{k},\sigma} c_{\boldsymbol{k},\sigma})\end{aligned} \tag{1.5}$$

As reflect to the periodicity of the magnetic ion, quite different behavior is observed at low temperature, especially in the resistivity. At high temperature Kondo effect is realized at each Ce or U-site and the resistivity shows $-\log T$ dependence, then shows a broad maximum around $T_{\rm K}$ and decreases as decreasing a temperature. It can be considered as the appearance of the coherent state; far below $T_{\rm K}$ f-electrons form not the Kondo-singlet on each Ce or U-site, but the quasi-particle band which has a large DOS at Fermi energy $\epsilon_{\rm F}$. In Fig. 1.1 the schematics of the DOS of the HF system is shown. These quasi-particles behave as heavy fermions, and show FL properties. $T_{\rm K}$ is the width of the heavy quasi-particles bands. In Fig. 1.2 [4] the magnetic resistivity of $Ce_xLa_{1-x}Cu_6$ is shown. In this figure we can see the drastic change from single impurity Kondo system to Kondo lattice system as increasing the Ce-concentration. Kondo effect is the key to understand the physical properties of the HF system.

On the other hand the magnetic interaction, RKKY interaction, between the localized moments of f-electrons also due to the hybridization between conduction electrons and f-electrons tends to develop the long range magnetic order in Kondo lattice systems. It causes the competition between magnetic interaction and Kondo effect. Because of this competition HF systems show rich variety in their ground state. They can be roughly divided into three groups :

1. non-magnetic state : $CeRu_2Si_2$, $CeCu_6$, $CeNi_2Ge_2$ *etc.*

2. magnetic state : $CeRh_2Si_2$, $CeRu_2Ge_2$, $CePd_2Si_2$ *etc.*

3. superconducting state : $CeCu_2Si_2$ (S-phase), URu_2Si_2 , UPt_3 *etc.*

The energy of the RKKY interaction can be given by using J as,

$$T_{\rm RKKY} \sim J^2/W \tag{1.6}$$

and $T_{\rm K}$ is given by Eq. 1.2. Both $T_{\rm K}$ and $T_{\rm RKKY}$ are the functions of the dimensionless parameter J/W with different dependences. S. Doniach obtained the schematic phase diagram of the Kondo lattice shown in Fig. 1.3 [65]. In the low J/W region where $T_{\rm RKKY} \gg T_{\rm K}$, magnetic ground state, usually antiferromagnetic ground state, is realized. As increasing J/W $T_{\rm K}$ increases more rapidly and $T_{\rm N}$ decreases because the development of magnetic order is suppressed by Kondo effect more and more strongly. Then at certain value $(J/W)_{\rm c}$, magnetic instability point, magnetic ground state is collapsed and above $(J/W)_{\rm c}$ where $T_{\rm RKKY} \ll T_{\rm K}$ non-magnetic ground state is realized. In the magnetic region near the magnetic instability point magnetic order has a itinerant character with a partly reduced magnetic moment ($\sim 10^{-1}$ $\mu_{\rm B}$), for example UPd_2Al_3($\sim$ 0.85 $\mu_{\rm B}$) [5], $CePd_2Si_2$ ($\sim$ 0.66 $\mu_{\rm B}$) [6], or ultra small moment ($10^{-2} \sim 10^{-3}$ $\mu_{\rm B}$), for example UPt_3 ($\sim$ 0.02 $\mu_{\rm B}$) [7], URu_2Si_2 ($\sim$ 0.02 $\mu_{\rm B}$) [8]. The problem of the ultra small moment has been studied from the point of view of the time-dependent order parameter which should fluctuate slowly. Even in the nonmagnetic region where FL with heavy quasi-particle is realized, strong antiferromagnetic fluctuation exist and can dominate their low temperature properties. In this region, the ground state can be changed by tuning an external parameter such as a pressure or composition very easily. Many interesting properties of heavy fermion systems, like exisotic superconductivity or non-Fermi liquid (NFL) behavior *etc.* , come from this magnetic instability.

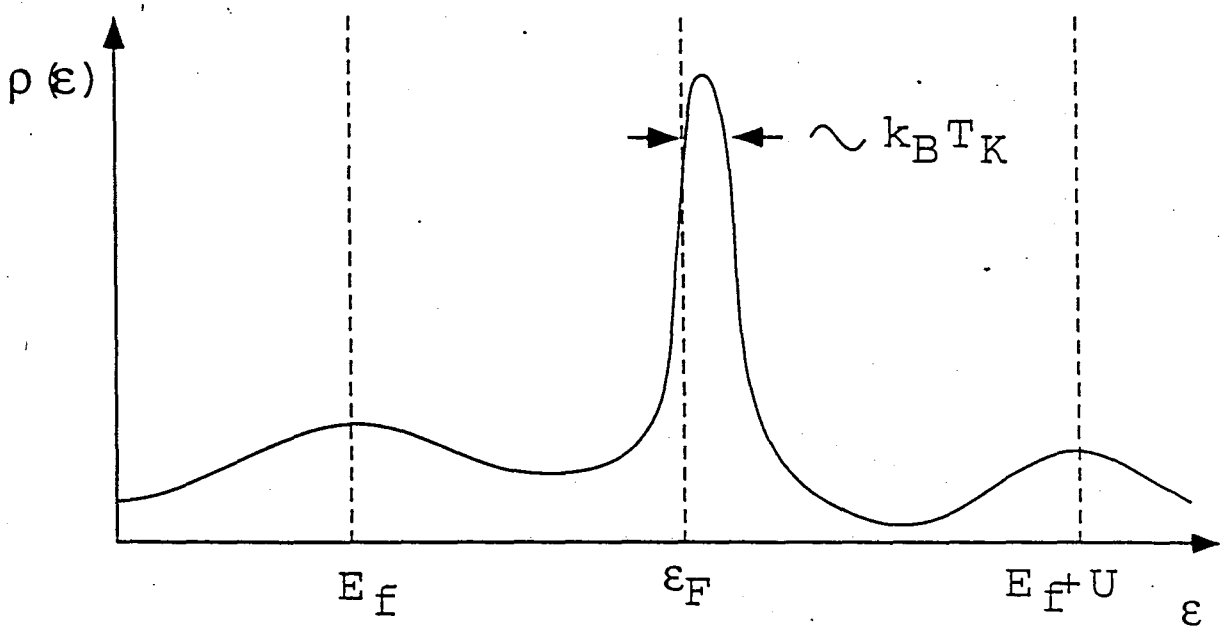

Figure 1.1: The schematic of the DOS of HF system is shown. By the hybridization the energy level of f-electron is broadened and the quasi-particle band with a half width $\sim k_B T_K$ is formed near the Fermi level.

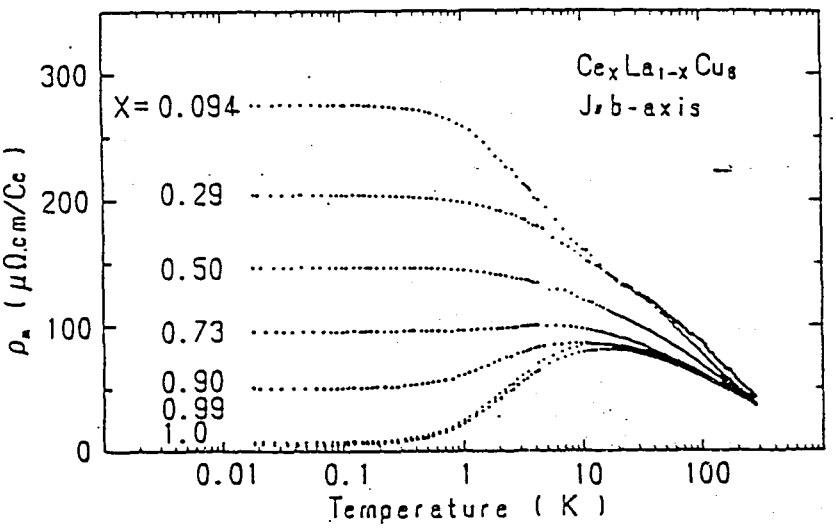

Figure 1.2: The resistivity of $Ce_xLa_{1-x}Cu_6$ is shown [4].

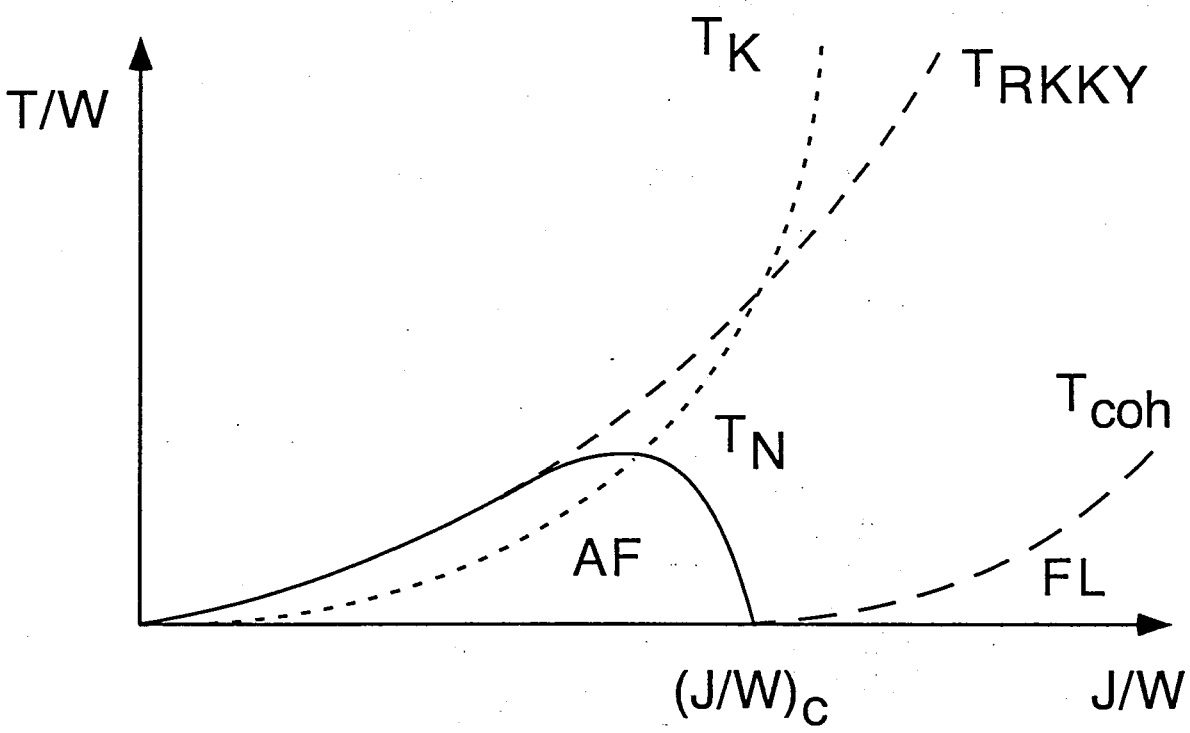

Figure 1.3: The schematic phase diagram of HF system (Doniach phase diagram) [65].

1.2 Non-Fermi Liquid Behavior

FL is a keyword to describe the low temperature properties of the HF systems which show no magnetic or superconducting phase transition down to 0 K, which is characterized by,

- specific heat is proportional to the temperature ($C(T) = \gamma T$)
- magnetic susceptibility shows no temperature dependence ($\chi(T) \sim$ const.)
- electrical resistivity shows a T^2-dependence ($\rho(T) = AT^2$)

These FL behavior are led from the one particle excitation at low energy region.

Recently so called non-Fermi liquid (NFL) behavior has been observed in some HF compounds which locate very close to the magnetic instability point, for example $CeCu_{6-x}Au_x$, $U_xY_{1-x}Pd_3$ [9, 10]. Characteristic feature of NFL is a weak divergent or much stronger temperature dependence of the physical quantities than that expected from conventional FL theory;

- $C/T \sim -\log T$
- $\chi \sim 1 - T^a$ $(a \sim 1/2)$
- $\rho \sim T^n$ $(n < 2)$

The temperature dependences of some physical quantities in typical compounds which show NFL behavior are shown in Tab. 1.1.

As I mentioned in the last section, the ground state of the HF system can be changed from magnetic to nonmagnetic on the $T = 0$ line caused by the enhancedment of the Kondo effect. The Kondo effect quenches the degree of freedom of the localized spin dynamically, which plays a role of quantum fluctuation to suppress and collapse the long range magnetic order at $T = 0$. It means that the magnetic-nonmagnetic transition in HF system by changing the parameter J/W is a quantum phase transition (QPT), and we can call $(J/W)_c$ magnetic quantum critical point (QCP). Some theoreticians expect the anomalous temperature dependences of the physical quantities considered as NFL behavior in HF system near the QCP caused by the anomalous low energy excitation due to the quantum critical fluctuation [11, 12, 13, 14]. For example, T. Moriya *et al.* predicts the temperature dependence of the specific heat and the resistivity near the antiferromagnetic QCP, which is $C(T)/T \sim 1 - \sqrt{T}$ and $\rho(T) \sim T^{1.5}$ respectively [13]. These predictions are quite same to that based on the renormalization group theory developed by A. J. Millis [11]. In Fig. 1.4 the schematics of the NFL near the QCP is shown. The Neel line in Fig. 1.4 is the static phase transition temperature caused by the RKKY interaction, while the coherent line is the crossover line to FL state caused by the quantum fluctuation (Kondo fluctuation). These theory tell me that the NFL behavior in HF system can be the evidence for the QPT in itinerant magnetic system. It is the reason why the study on NFL behavior is one of the central issues in HF physics.

Experimentally it is not obvious whether the NFL behavior is caused by the QPT, yet. One of the reasons the NFL is considered to be associated with the QPT is it has been observed in the system near the QCP, however there is two doubts. One of them is a disorder effect for the system. There are several ways for tuning the parameter $(J/W)_c$, for example alloying or applying a pressure. In alloying system we must consider some kind of disorder effect, crystallographic or magnetic disorder, which is caused by the random substitution of the constituent atoms for the different atoms. A crystallographic

disorder produces the distribution of the local unit cell volume randomly, and it distributes the Kondo temperature T_K. The distribution of the Kondo temperature is also possible senario for the NFL in alloying system as well as the QPT. In this senario the NFL behaviors, anomalous strong temperature dependences of physical quantities, are caused by the remaining local spins which has the low Kondo temperature. When the distribution is sufficiently wide as whose tail extends down to $T_K = 0$, FL is unstable and the singularity which causes the NFL behavior is given rise to at 0 K. E. Miranda *et al.* predict the weak divergent behavior of thermodynamic quantities, and anomalous low energy excitation based on this 'Kondo Disorder' model [15]. $UCu_{5-x}Pd_x$ system is considered to be a typical example for the Kondo Disorder model, whose thermodynamic and transport properties can be explained very well by assuming the distribution of the Kondo temperature [16]. In alloying system the frustration or randomness of the magnetic interaction can be also occurred, which produces random magnetic order, especially spin glass order. S. Sachdev predict the NFL behavior near the QCP in the metallic spin glass case, which is very similar to that in the antiferromagnetic case [14]. The origins of the randomness of the magnetic order and the distribution of the Kondo temperature are same, which is the random distribution of the coupling constant J between conduction electrons and f-electron, because the magnetic interaction in Kondo lattice system is RKKY interaction. Therefore there can be the combination the distribution of the Kondo temperature with the random magnetic interaction. In a recent paper, A. H. Castro-Neto *et al.* has proposed the possibility of the 'Quantum Griffiths Phase' near the QCP in a disordered system, where the NFL behavior is expected [17]. In 3.3.2 I will discuss on this model again and in detail.

Another doubt is the existence of the case the NFL behavior is not observed in spite of the system can be considered to be near the QCP. $CeRh_2Si_2$ is an antiferromagnetic compound with $T_N = 35$ K, whose T_N decreases as applying a pressure and vanishes around 11 kbar, however very near the critical pressure, even at 11.5 kbar, the NFL behavior has not been observed in a resistivity measurement [18]. There are at least three possible interpretation for the FL near or at the QCP, like $CeRh_2Si_2$, as,

1. The region where the NFL behavior is observed is very narrow, only just on or extremely close to the QCP.

2. The magnetic-nonmagnetic transition is not second order but first order phase transition, in which case T_N jumps from finite value to 0 discontinuously therefore there can be no quantum critical region.

3. For the NFL the disorder effect is necessary in substance. Most of compounds which show NFL behavior are the alloying system. However the difficulty of this interpretation is the experimental fact of the appearance of the NFL behavior in pure system, for example $CePd_2Si_2$ at p_c ($\sim$ 28 kbar) [18].

It is very important step to clarify the difference between the case which the NFL behavior is shown and is not to know the physical origin of the NFL.

Above mentioned, there is no consensus for the origin of the NFL behavior in HF system although many experimental works have been concentrated to clarify it. Both QPT and disorder are possible origins for the NFL. In this thesis I will introduce our experimental result for the NFL and FL behavior in $Ce(Ru_{1-x}Rh_x)_2Si_2$ system which has three QCP (will be introduced in more detail in next section) , and discuss the important role of the disorder and the combination it with quantum critical phenomena for the NFL.

Table 1.1: Typical compounds which show NFL behavior

	$C(T)/T$	$\chi(T)$	$\Delta\rho(T)$	Ref.
$CeCu_{5.9}Au_{0.1}$	$-\log T$	$1-T^{1/2}$	T	[9]
$U_xY_{1-x}Pd_3$	$-\log T$	$T^{-0.3}$	$1-T$	[10]
$CeNi_2Ge_2$	$1-T^{1/2}$	$1-T^{1/2}$	$T^{3/2}$	[19]
$UCu_{5-x}Pd_x$	$-\log T$	$-\log T$	$1-T^{3/2}$	[16]

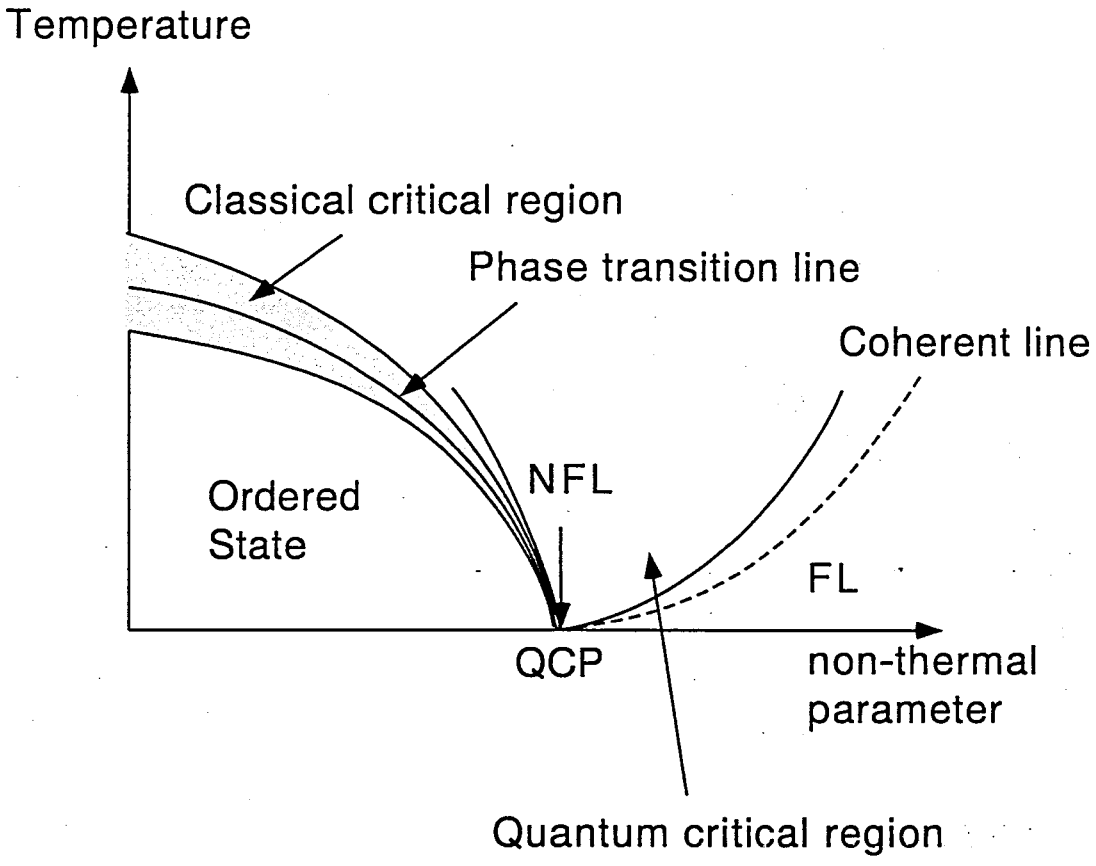

Figure 1.4: The schematics for the QPT. On the $T = 0$ line QPT is occurred at QCP with varying non-thermal parameter. In the quantum critical region NFL beahvior is expected.

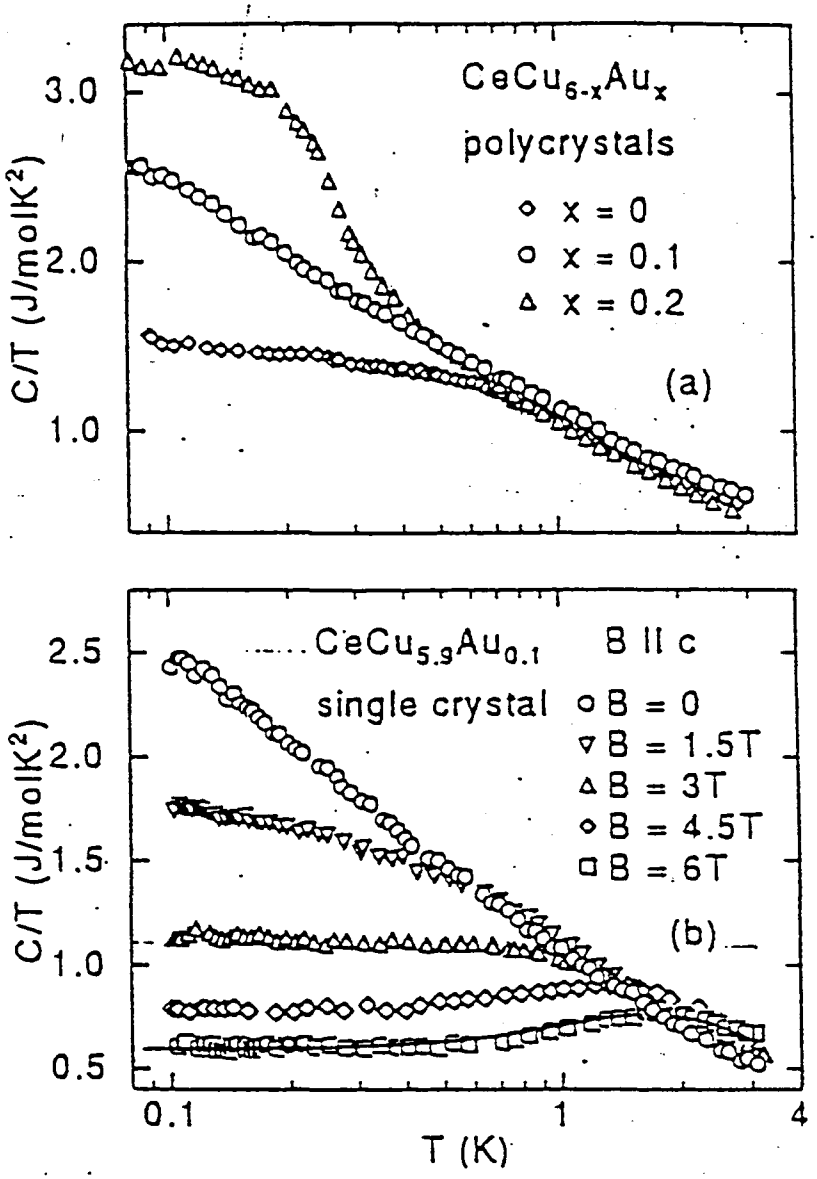

Figure 1.5: NFL behavior in $CeCu_{5.9}Au_{0.1}$ in the specific heat. The logarithmic temperature dependence of $C(T)/T$ is found.

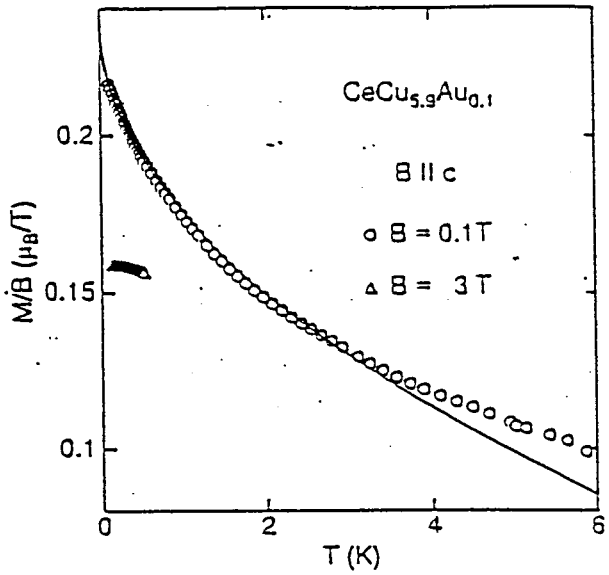

Figure 1.6: NFL behavior in $CeCu_{5.9}Au_{0.1}$ in the susceptibility. The solid line represents the temperature dependence $\chi(T) \sim 1 - T^{1/2}$.

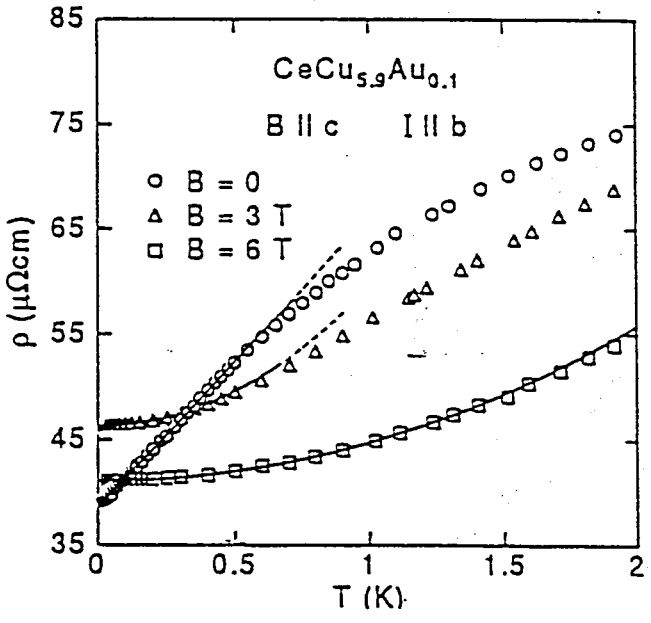

Figure 1.7: NFL behavior in $CeCu_{5.9}Au_{0.1}$ in the resistivity. At zero field the resistivity shows a T-linear dependence. Under a finite magnetic field FL behavior ($\rho(T) \sim T^2$) is recovered.

1.3 The mixed compound system $Ce(Ru_{1-x}Rh_x)_2Si_2$

1.3.1 Physical properties of $CeRu_2Si_2$

$CeRu_2Si_2$ is known to be a moderate heavy fermion compound with a body-centered tetragonal $ThCr_2Si_2$ -type crystal structure, which is shown in Fig. 1.8. This compound shows no long-range magnetic order or superconductivity at least down to 20 mK [20], whose physical properties behave as a typical nonmagnetic heavy fermion system, which shows the FL properties at low temperature and behaves as a localized spin system at high temperature. In Fig. 1.9, 1.10 and 1.11 the specific heat, the susceptibility and the resistivity of $CeRu_2Si_2$ are shown respectively [20, 21, 22].

The electronic specific heat coefficient γ is almost independent of temperature below 5 K, whose value is about 360 mJ/molK^2. Around 10 K the specific heat shows a broad peak which is considered to be related with the Kondo effect. They obtained $T_K \sim 24$ K based on a phenomenological theory for the Kondo effect 'resonant-level model' [24]. Another peak around 110K is ascribed to be as the Schottkey peak by the crystal electric field (CEF) excitation, from which the energy splitting between the ground state and the first excited state has been estimated $\sim$ 220 K. The susceptibility shows the Curie-Weiss behavior at high temperature, and shows a broad maximum around 10 K. Below this maximum susceptibility goes to the constant down to 0 K, as the Pauli paramagnetic. The constant γ and the Pauli paramagnetic susceptibility is a characteristic feature of FL, which indicate that the heavy quasi-particle band is formed in $CeRu_2Si_2$. The resistivity shows also FL behavior, a T^2 dependence, below 0.4 K. Around 25 K the resistivity along the c-axis shows a shoulder, which can correspond to the crossover from a localized spin regime to HF regime. Any thermodynamic or transport properties indicate that the ground state of $CeRu_2Si_2$ is a nonmagnetic FL.

On the other hand from the neutron scattering experiment the development of the antiferromagnetic correlation has been found. In the left figure in Fig. 1.12 the constant E-scans with energy transfer $\hbar\omega = 1.6$ meV around (1 1 0) (= $\boldsymbol{G}$) in r.l.u. at 4.2 K is shown [26]. The magnetic scattering peaks at $\boldsymbol{G} \pm \boldsymbol{q}_1$ or $\boldsymbol{G} \pm \boldsymbol{q}_2$, with $\boldsymbol{q}_1 = (0.3\ 0\ 0)$ and $\boldsymbol{q}_2 = (0.3\ 0.3\ 0)$ respectively, indicate that the correlation with the magnetic wave vector $\boldsymbol{q}_1$ and $\boldsymbol{q}_2$ is developed. The right one in Fig. 1.12 shows the temperature dependence of the half width Γ of the energy spectrum of the magnetic excitation at $\boldsymbol{q}_2$, which has a finite value at 0 K. According to this result the magnetic correlation does not developed to the long-range order down to 0 K. It is consistent with the result of the thermodynamic or transport measurements. Recently Sato *et al.* has discovered the new magnetic correlation with $\boldsymbol{q}_3 = (0\ 0\ 0.35)$ [27], which is also fluctuating in the time and space. These inelastic neutron scattering experiments strongly indicate that $CeRu_2Si_2$ locate near the magnetic instability point. In fact the long-range magnetic order is easily appeared by substitution of small amount of other element for the constituent one. By substitution of La for Ce the correlation with $\boldsymbol{q}_1$ [28] and by substitution of Rh for Ru the one with $\boldsymbol{q}_3$ [29] are stabilized respectively. In the next section I will investigate on the latter system, $Ce(Ru_{1-x}Rh_x)_2Si_2$ system in more detail.

One of the most peculiar properties of $CeRu_2Si_2$ is a magnetization process at low temperature. In spite of the ground state of $CeRu_2Si_2$ is a nonmagnetic FL, as mentioned above, the magnetization process shows a metamagnetic behavior around 7.8 T. In Fig. 1.14 the magnetizations at 4.2 and 1.35 K are shown. Only along the c-axis, which is a magnetic easy axis, the metamagnetic behavior is found, which become sharper as temperature decreasing. This metamagnetic behavior can be considered to be correspond to

the crossover from HF state to localized spin state by applying a magnetic field from the experimental result of dHvA effect [30]. The origin of this metamagnetism is on discuss now by several experimentalists and theoreticians [31, 32].

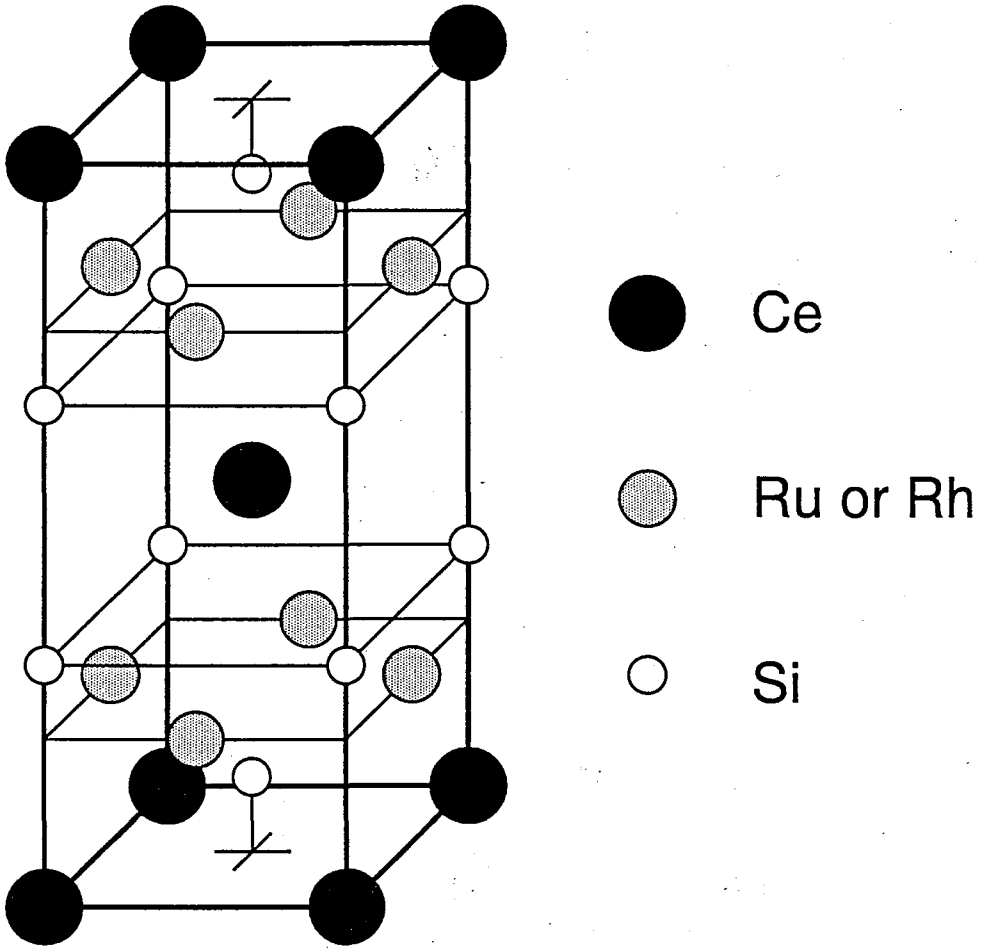

Figure 1.8: The cryatal structure of $CeRu_2Si_2$.

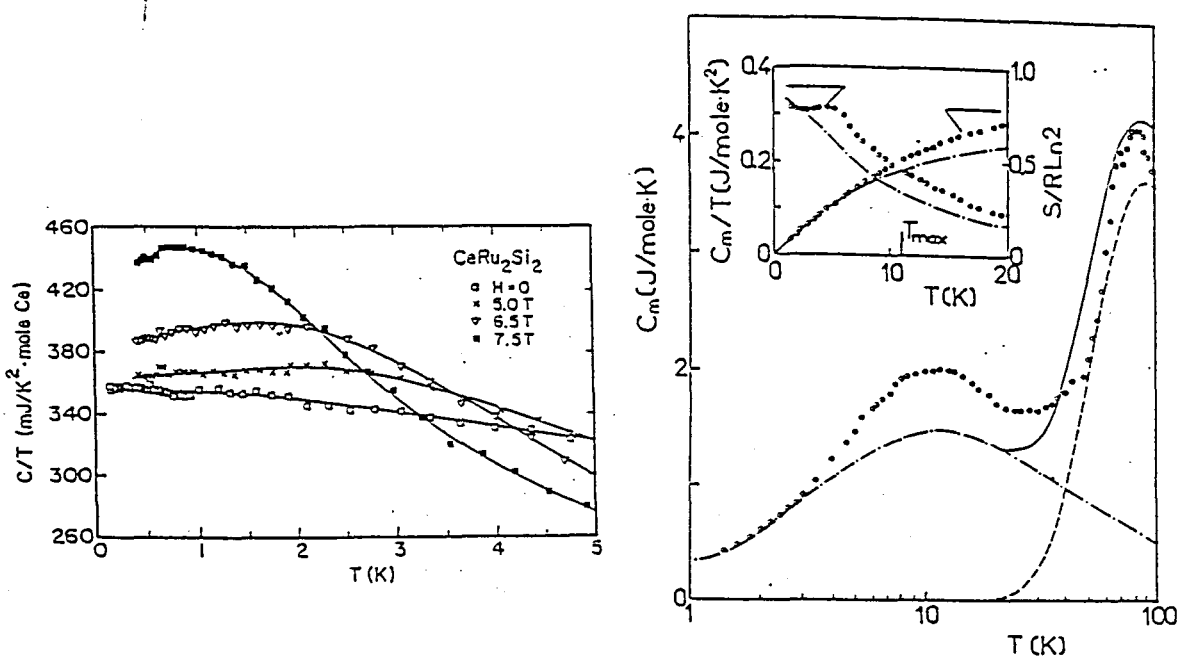

Figure 1.9: The specific heat of $CeRu_2Si_2$ [21, 22]. The left figure is C/T in the low temperature region, which shows a FL behavior, $C/T \sim$ const.. The right one shows a high temperature specific heat, in which we can find the two broad peak explained in the text.

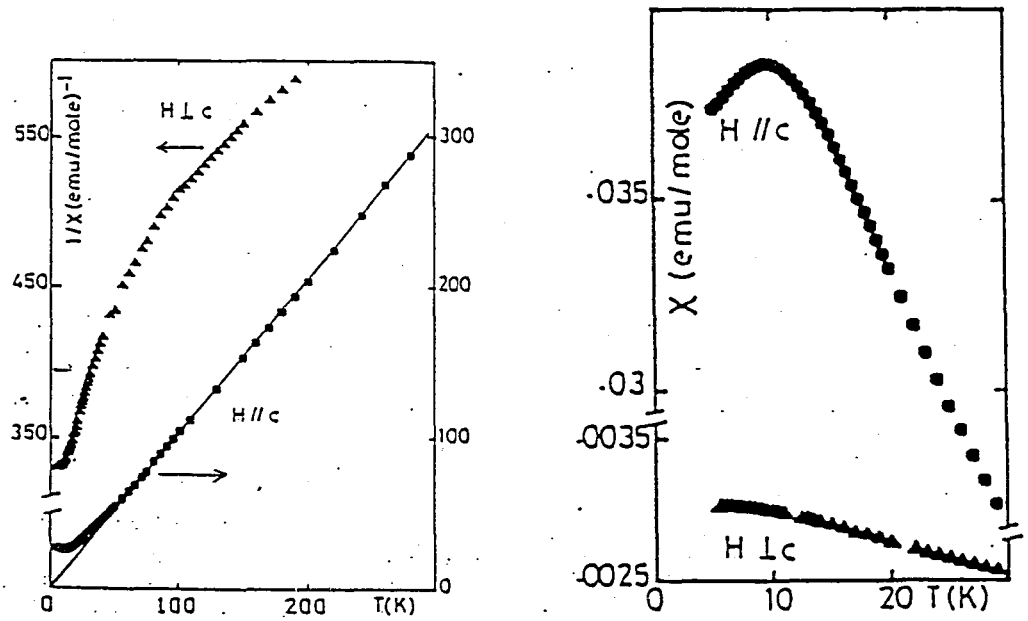

Figure 1.10: The susceptibility of $CeRu_2Si_2$ [20]. The susceptibility shows a very strong anisotropy, the ratio of $\chi_c/\chi_a \sim 15$ at 10 K. Below the broad maximum around 10 K the susceptibility shows a temperature dependence as $\chi(T) \sim \chi_0 + AT^2$. χ_0 is also enhanced as much as γ.

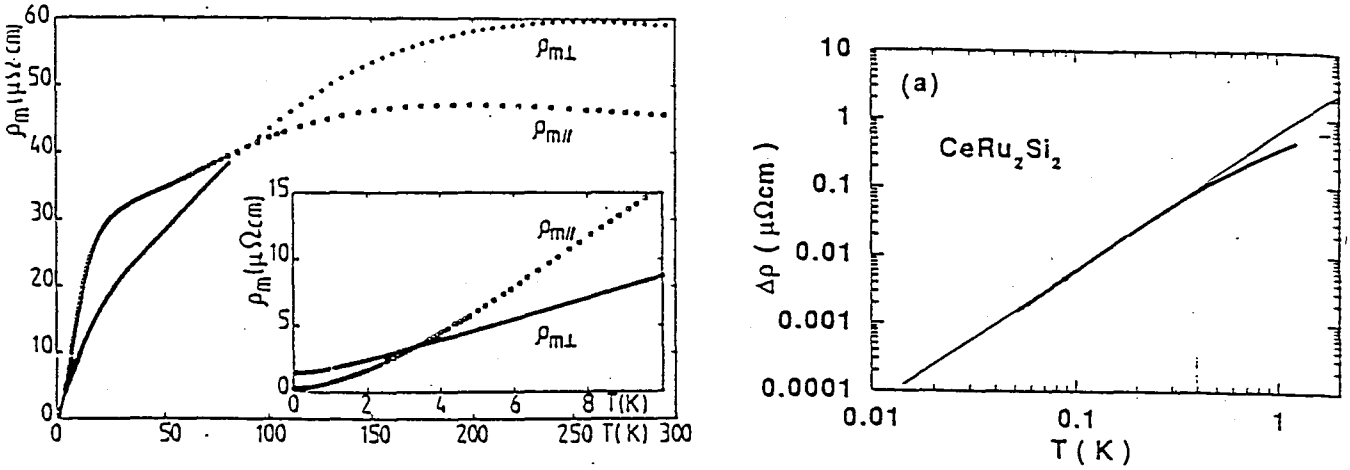

Figure 1.11: The resistivity of $CeRu_2Si_2$ [23, 25]. In the left figure the log-log plot of the low temperature resistivity is shown, which indicate a T^2 dependence is found below 0.4 K. In the right one we can see the shoulder around 25 K is observed in the curve along the c-axis, which indicate the crossover from localized spin regime to HF regime.

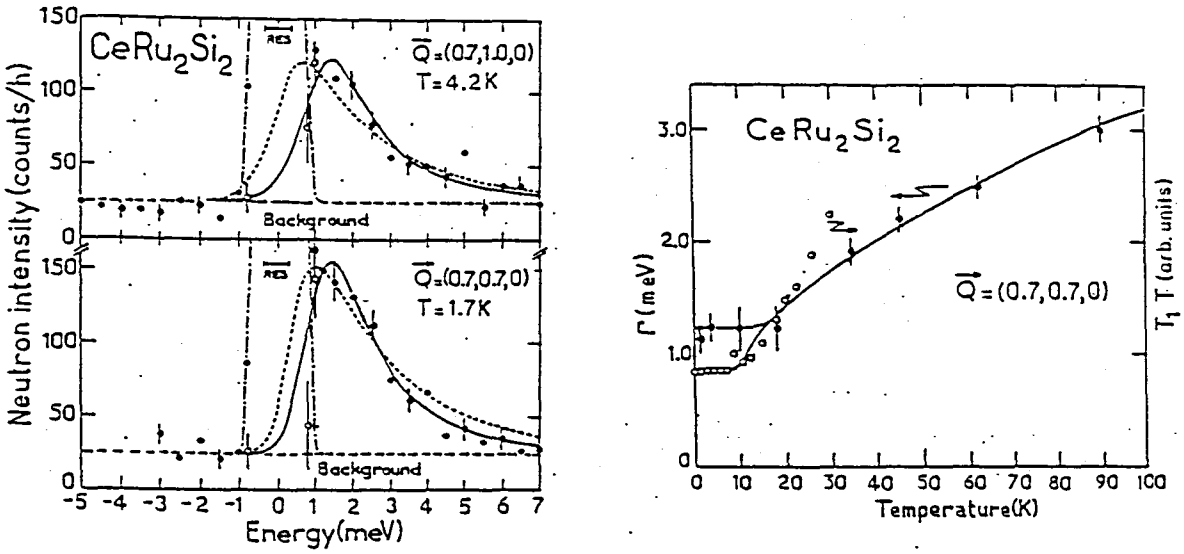

Figure 1.12: The inelastic neutron scattering experiment by Regnault *et al.* [26]. The left figure shows the constant E-scan around (1 1 0) in r.l.u., and the right one shows the temperature dependence of the half width Γ of the energy spectrum of the magnetic excitation at (0.3 0.3 0).

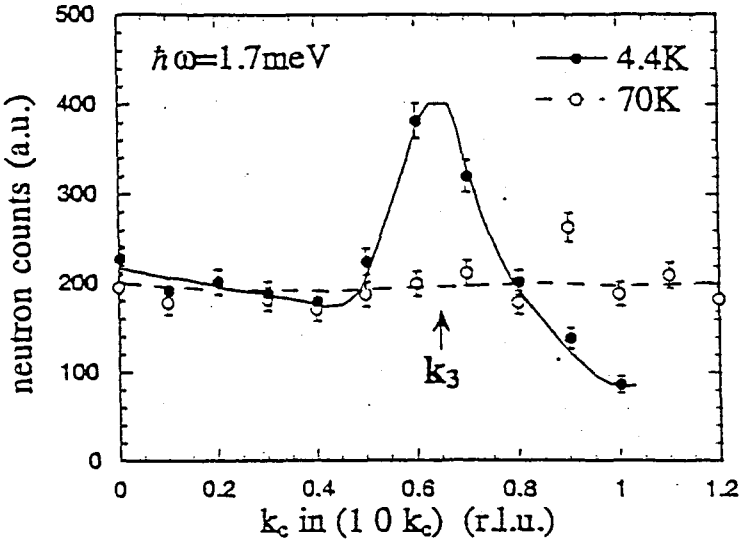

Figure 1.13: The magnetic scattering in (1 0 k_c) line, which indicate the correlation with the magnetic wave vector q_3 is developed below 70 K [27].

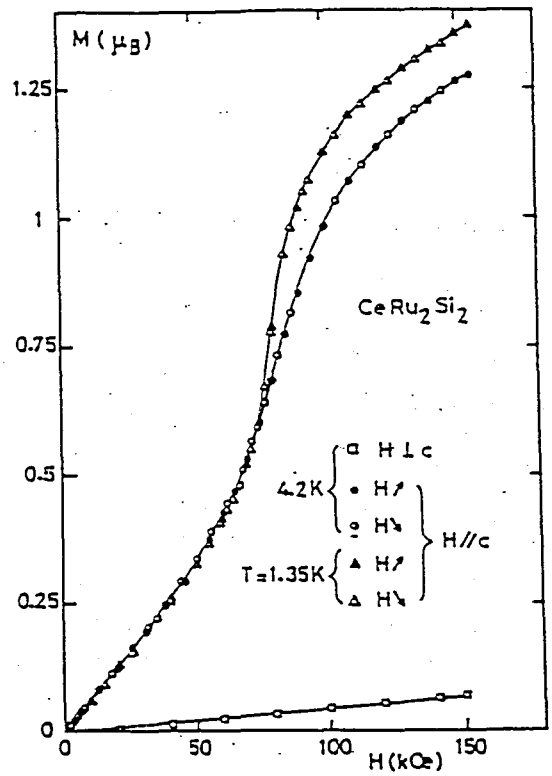

Figure 1.14: The magnetiaztion of $CeRu_2Si_2$ [20]. The metamagnetic behavior is found around 7.8 T along c-axis.

1.3.2 Physical properties of $Ce(Ru_{1-x}Rh_x)_2Si_2$

The mixed compound $Ce(Ru_{1-x}Rh_x)_2Si_2$ is a very interesting system because we can tune the hybridization between the $4f$-electrons of Ce atom and the conduction electrons without destroying the periodicity of the Ce-site. By several authors the magnetic phase diagram of this system was obtained, which is shown in Fig. 1.15 [33, 34, 35]. As mentioned in the last subsection, the pure compound $CeRu_2Si_2$ is a typical HF system, and this nonmagnetic ground state can easily change to the magnetic ordered one by substitution of Rh for Ru. For $x > 0.03$, the antiferromagnetic ordered state is developed. This ordered phase vanishes around $x \sim 0.4$. On the other hand the other pure compound in this mixed system $CeRh_2Si_2$ is an antiferromagnetic compound with $T_N = 35$ K. This magnetic ordered phase vanishes around $x \sim 0.5$. According to this phase diagram, we can divide this system into four regions.

I. $x < 0.03$ nonmagnetic FL state

II. $0.03 < x < 0.4$ spin density wave (SDW) state

III. $0.4 < x < 0.5$ nonmagnetic state

IV. $0.5 < x$ antiferromagnetic state

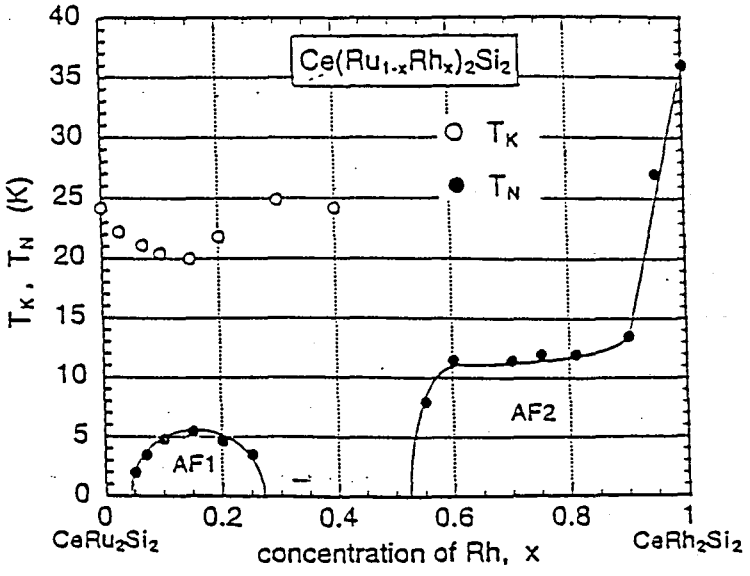

Figure 1.15: Phase diagram of $Ce(Ru_{1-x}Rh_x)_2Si_2$ system obtained from some previous works. This figure is refered from Ref.[33]

In this system we can see two different magnetic ordered phase in region II and IV. In the region II, the antiferromagnetic order developed from the antiferromagnetic correlation with the magnetic wave vector q_3 in $CeRu_2Si_2$, and has a itinerant character. S. Kawarazaki *et al.* performed the neutron scattering experiment in this region, for x = 0.15, and observed an incommensurate sinusoidal modulation of c-oriented magnetic moments with magnetic wave vector (0 0 0.42) [36]. The magnetic wave vector (0 0 k) changes as a function of the Rh-concentration. The pure sinusoidal modulation indicates that the magnetic order belongs to the same category of SDW in Cr. In the macroscopic properties the SDW character has been observed. The resistivity along the c-axis shows a hump at T_N , while that along a-axis shows no anomaly [37, 38], which indicates the anisotropic gap opening at Fermi surface is occurred. It can be explained by the nesting of the hole band which causes the SDW transition. The temperature dependence of specific heat below T_N also indicates such a gap opening [39].

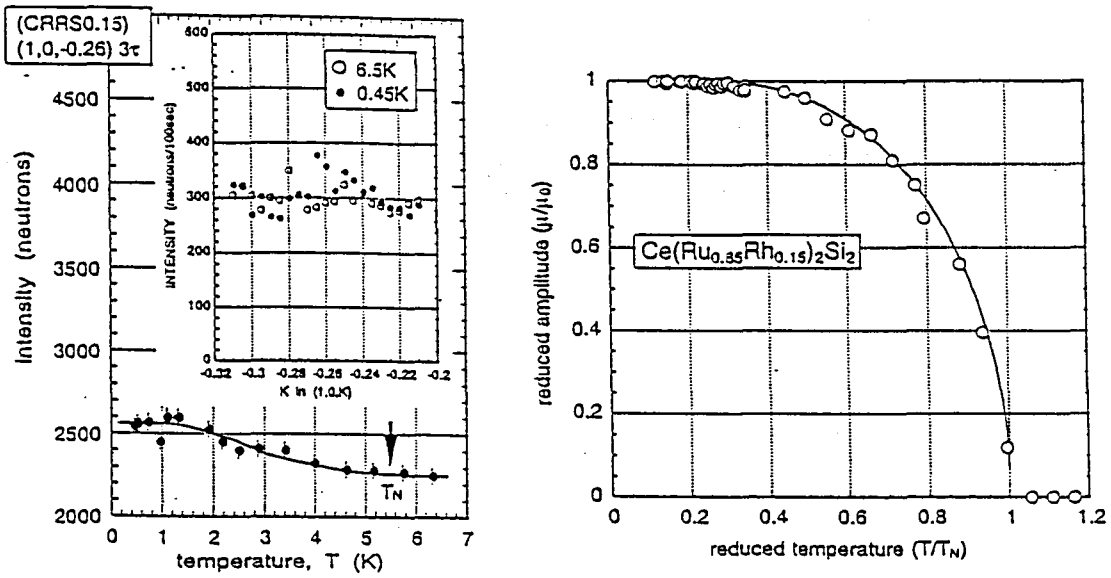

Figure 1.16: The temperature dependence of the intensity of the third-higher harmonic diffraction of the ordered state in x = 0.15 is shown in the left figure. The right one shows the intensity of the primary one. The development of the intensity of third-higher harmonic one is much weaker than that of primary one. [36]

The ordered phase in region IV has a quite different character from that in region II. $CeRh_2Si_2$ shows two magnetic phase transition; one occurs at 36 K (T_{N1}) and the other does at 26 K (T_{N2}) [40]. In the high temperature ordered phase the moments align along the c-axis with the commensurate magnetic wave vector q_H = (1/2 1/2 0), in which the two equivalent magnetic domain with q_H^+ = (1/2 1/2 0) and q_H^- = (-1/2 1/2 0) respectively coexist. On the other hand in the low temperature one the homogeneous multiple-q structure with q_H^+, q_H^-, q_L = (1/2 1/2 1/2) and q_L with $\pi/2$ phase-shifted is realized [41]. As Ru-concentration increasing T_{N2} rapidly decreases and disappears around 30 %, which is equivalent for x = 0.7. At x = 0.7 T_{N1} remains around 6 K, and for x < 0.6 any magnetic order was not observed.

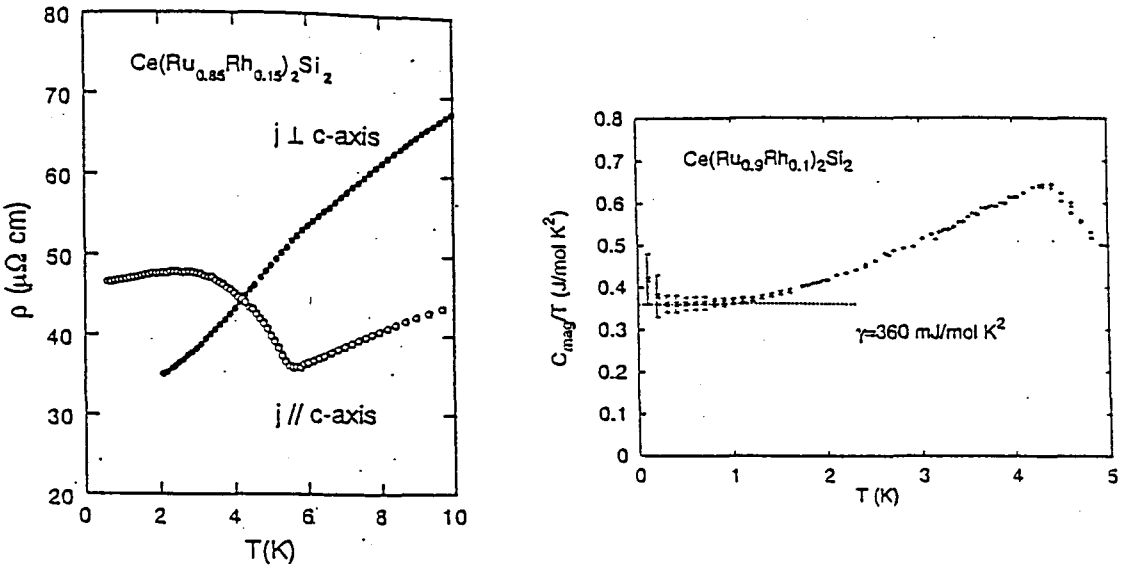

Figure 1.17: The resistivity of $x = 0.15$ is shown in left figure, in which the resistivity along the c-axis jumps at T_N although that along a-xis does not show any anomaly [38]. The right one shows the specific heat of $x = 0.1$ in the form C/T vs T [39]. The large γ-value below T_N can be contributed from the remaining Fermi surface.

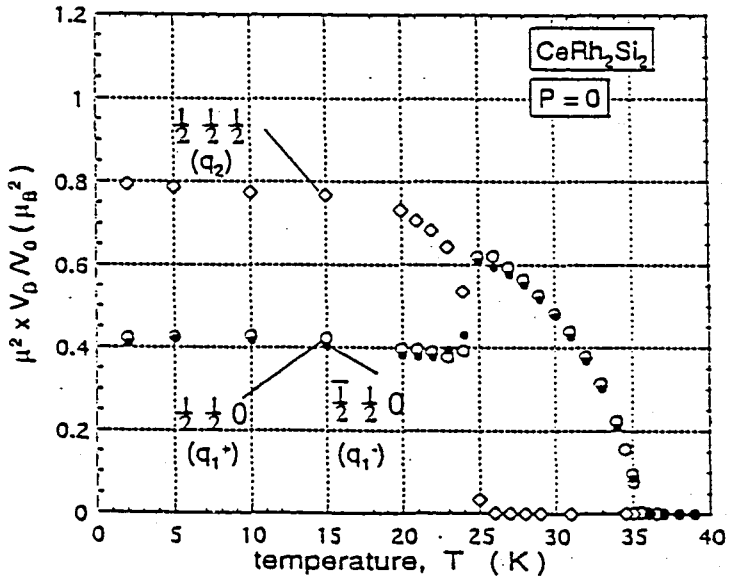

Figure 1.18: The temperature dependences of the intensities of the three magnetic Bragg peaks of single crystalline $CeRh_2Si_2$, with magnetic wave vector q_H^+, q_H^- and q_L respectively [41]. The details is mentioned in the text.

1.3.3 The purpose of this study

The main purpose of this study is to clarify the physical origin of the NFL behavior in some HF system near the magnetic QCP, and to discuss on the role of the disorder effect for the quantum critical phenomena. As mentioned in Sec. 1.2 there are many experimental results to show the NFL behavior near the QCP, however most of case is found in the alloying system. Therefore we cannot neglect the effect of the disorder by alloying for the physical properties. There are some ways to study and understand the NFL behavior and its physical background from the experiments; one of them is to study the NFL behavior in the stoichiometric magnetic compound as applying a pressure, for example, to exclude the effect of the disorder. At a critical pressure P_c the NFL behavior is expected to be observed. The study in the non-disordered system is very important to prove the NFL behavior is the appearance of the quantum critical phenomena. On the other hand it is also important to understand what kind of roles the disorder plays near the QCP, for which we must compare the strong disordered system and non- or weak disordered system.

In Fig 1.15 we can see three QCP, at concentration $x \sim 0.03$, 0.4 and 0.5 in $Ce(Ru_{1-x}Rh_x)_2Si_2$ system. It means that this system is appropriate to study the NFL behavior by comparing with the character at or near each QCPs. At $x = 0.03$ the amount of disorder can be expected to be much less than that at $x = 0.4$ or 0.5. Therefore we can discuss on the effect of the disorder to the quantum critical phenomena by comparing the low temperature thermodynamic or transport properties at three concentrations. And in the region III the frustration of magnetic interactions can exist, probably in random, because this nonmagnetic region locates between two different antiferromagnetic region II, IV. Such a frustration of magnetic interactions reduces the Neel temperature and can lead a spin glass like random ordered state, however in this region the ground state is nonmagnetic. In the previous there are few works about this region, and nearly nothing is known on the physical properties. Therefore we are interested in the physical feature of the nonmagnetic state in this region furthermore.

In this thesis I write the experimental results of the thermodynamic and the transport properties, specific heat, DC and AC susceptibility, Magnetization and resistivity, at the concentrations near the three QCPs in $Ce(Ru_{1-x}Rh_x)_2Si_2$ system, at $x = 0.03$, 0.4, 0.5 and some other concentrations. And in order to answer the questions above mentioned, I have compared the experimental results with several theories to explain the NFL or the QPT in HF system. In the following the main contents of this study is grouped.

1. **The study on the physical properties at $x = 0.03$.**
   Near the critical concentration in the Rh-poor side of the SDW phase the NFL behavior has not been observed. In order to see how the system develops the antiferromagnetic fluctuation as approaching to the QCP, I have compared the experimental results with the self consistent renomalization (SCR) theory, and discussed on the reason of the lack of the NFL behavior.

2. **The study on the physical properties at $x = 0.4$ and 0.5.**
   Near the two critical concentrations in the intermediate Rh-concentration region the characteristic feature of the NFL behavior has been observed. For comparing with the result at $x = 0.03$, I try to analyze the experimental data based on the SCR theory and the Kondo-disorder model.

3. **Field effect on the NFL behavior of $Ce(Ru_{1-x}Rh_x)_2Si_2$ in the intermediate Rh-concentration region.**

I have studied the recovery of the FL by applying an external magnetic field, in the intermediate Rh-concentration region, especially at $x = 0.5$ and 0.6. From experimental results the NFL like tendency is strongly enhanced as approaching to zero field and the QCP of the antiferromagnetic phase in region IV. This is not the case when approaching to the QCP of the SDW phase in region II on the Rh-rich side. I present that two mechanisms usually considered to explain the NFL behavior coexist for this concentration region; one is due to the quantum critical fluctuation and the others due to the Kondo disorder. The quantum critical description is valid for the high field region, above 1 T, and can explain the recovery of the FL very well. On the other hand the zero or low field properties can be described by the unified description of the quantum critical phenomena and the disorder, quantum Griffiths description.

Chapter 2

Experimental Procedures

2.1 Sample preparation

All samples used for measurements are single crystalline samples, which are grown from the botton of the polycrytalline ones. At the starting point, the polycrystalline sample were prepared by arc-melting with nominal stoichiometric amounts of the constituent elements which are listed in Table 2.1 in argon atmosphere. In the melting process no significant loss of elements was found. (The over all weight loss was at most about 0.3 % .) Then the single crystalline samples were grown by the Czochralski method using a tri-arc furnance in an argon atmosphere.

The crystallographic axes were determined by X-ray back Laue method. Some as grown samples were annealed with wrapped by Ta foil loosely in a evacuated silica tube at 1000 °C for 1 week. In a macroscopic measurement of single crystalline samples we did not found any significant differences between as grown and annealed samples. We checked the chemical homogeneity of samples by the microprobe technique like Electron Probe Micro Analyzer (EPMA). The details of the characterization of samples was written in Ref.[42].

2.2 Specific heat measurement

The general and simplest method for measuring the specific heat is an adiabatic method. In this method the sample is isolated thermally from the surroundings, and its temperature is controlled at a certain temperature T_0. Then it is heated during the heating period Δt, and the temperature of the sample raises up to $T_0 + \Delta T$. Finally the heat capacity of the

Table 2.1: The list of the starting materials for making samples.

Element	Electronic configuration	Purity	Shape
Ce	$(Xe)4f^15d^16s^2$	3N, 4N	ingot
Ru	$(Kr)4d^75s^1$	3N5	powder
Rh	$(Kr)4d^85s^1$	3N5	powder
Si	$(Ne)3s^23p^2$	5N	ingot

Table 2.2: The list of samples used for measurement

Rh-concentration x	DC-χ	DC-M	AC-χ	ρ	C
0	○	○	–	–	○
0.03	○	○	–	○	○
0.05	○	○	–	○	○
0.10	○	○	–	○	○
0.15	○	○	–	–	○
0.30	○	○	–	○	○
0.35	○	○	–	–	–
0.40	○	○	–	–	○
0.50	○	○	○	○	○
0.60	○	○	○	–	–
0.70	○	○	–	–	○

sample is obtained as following,

$$C(T_0 + \frac{\Delta T}{2}) = \frac{\Delta Q}{\Delta T} \tag{2.1}$$

where ΔQ is a heat value supplied to the sample. This technique is a fundamental method to obtain the absolute value of the heat capacity thermodynamically, whose accuracy is very high in general. However it is difficult to keep the thermal isolation of the sample in practice because the heat leaks through the electrical line of the thermometer or the heater must exist, which cause the systematic error in the measured value of the heat capacity. In such a case the heat capacity can be obtained with the correction of the heat leaks. For a low temperature measurement it is more difficult, because some degree of heat leaks should be necessary for cooling the sample.

A thermal relaxation method is a technique to measure the low temperature specific heat rather easily. This method has the advantage of that it is not necessary to isolate the sample thermally from the surroundings. In this method, sample is connected to the heat bath which is controlled at a certain temperature T_0 with a weak thermal link which has a thermal conductance k. In Fig. 2.1 the schematics of this method is shown. Because of this weak thermal link the sample reaches to an another thermal equivalent state with the temperature $T = T + \Delta T$ when the heater supplies a power P to the sample. ΔT satisfies the relation, $k\Delta T = P$. After the heater is off at $t = 0$, the temperature of the sample T_s(t) is decayed to the initial value T_0 exponentially with a relaxation time τ as following equation.

$$T_s(t) = T_0 + \Delta T \exp(-t/\tau) \tag{2.2}$$

τ is given as, $\tau = C/k$, where C is the heat capacity of the sample at $T = T_0 + \Delta T/2$. We can obtain the value of ΔT and τ at each T_0 as fitting parameters from the relaxation curve. And C is obtained from these parameters. In Fig. 2.2 I shows the schematic heating or relaxation curves in an adiabatic and a thermal relaxation technique.

Another advantage of a thermal relaxation method is to be possible to measure a very small sample, about a few mg, while a few g of sample is needed for an adiabatic method. Sometimes we cannot obtain a large amount of sample because of the difficulty for growing

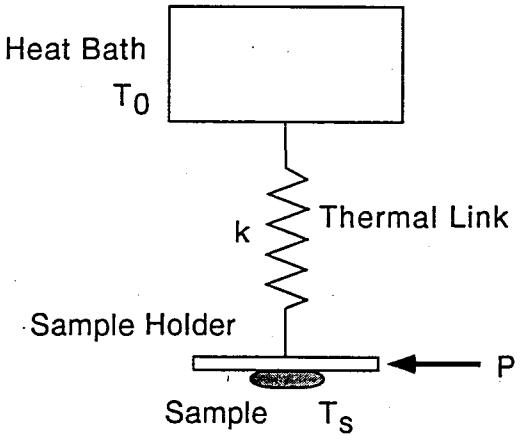

Figure 2.1: Schematics of the thermal relaxation method.

it, when we try to grow a new compound. A thermal relaxation method is very efficient for measuring a very small piece of sample in such a case. On the other hand this method also has some disadvantages, one of which is the less accuracy of measurement than that in an adiabatic method. It comes from the complexity of getting the heat capacity in a thermal relaxation method. In a real measurement, we must take special care that the thermal connection between the sample and the sample holder is so good as we can consider the both temperature is always same. Otherwise we must consider the thermal impedance between both, which makes the relaxation curve deviates from the exponential one.

In Fig. 2.4 the schematic view of the measurement system of (a) ^{4}He-cryostat and (b) ^{3}He/^{4}He dilution refrigerater, which were used for the measurement in the temperature range 1.6 K $\sim$ 20 K and 0.1 K $\sim$ 2.0 K, are shown respectively . In both system we used the copper block as a heat sink whose temperature was controlled by a PID technique and the gold wire(0.05ϕ mm) as a weak thermal link. In general a copper plate is used for a sample holder in the specific heat measurement, however we used a sapphire plate (10 $\times$ 10 $\times$ 4t mm). Sapphire has so high thermal conductivity as that of copper between 1 and 10 K and the less heat capacity because sapphire does not have a electronic heat capacity. In order to measure the small heat capacity of sample precisely the heat capacity of the sample holder is necessary to be very small. For the reason above mentioned the sapphire plate is very appropriate to the sample holder. In Fig. 2.3 the view of sample holder is shown. We used the Cernox-thermometer (Lakeshore Inc.) in the temperature range 1.6 K $\sim$ 20 K and the RuO-thermometer in 0.1 K $\sim$ 2.0 K. A strain gauge (350 Ω) was used as a heater. Both the thermometer and the heater were mounted on the sapphire plate by GE varnish. A sample was mounted by thermal compound (Oxford Inc.). For the good thermal connection between the sample and the sapphire plate we utilized the cleavage c-plane of the $Ce(Ru_{1-x}Rh_x)_2Si_2$ samples. The weights of all the sample we measured were about 10 mg.

For the precise measurement we considered the small drift of the base temperature and used the following function for fitting the relaxation curve,

$$T(t) = T_0 + at + \Delta T \left\{ 1 - \left[1 - \exp\left(-\frac{t - t_0}{\tau} \right) \right] \theta(t - t_0) \right\} \tag{2.3}$$

where the second term represent the drift of the base temperature and t_0 is time when

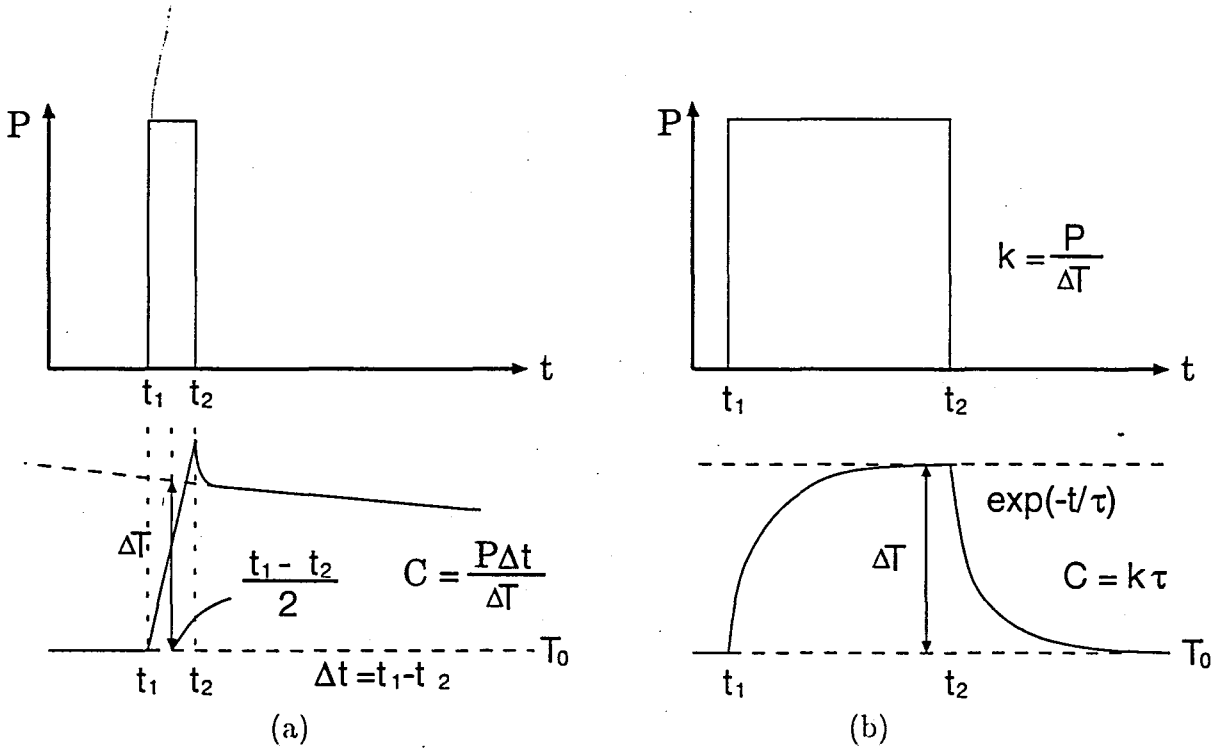

Figure 2.2: Schematic heating and relaxation curves in both method; (a) an adiabatic method (b) a thermal relaxation method

the heater is off. T_0, a, ΔT, t_0 and τ are the fitting parameters. We obtained the heat capacity of the sample after subtracting that of the sample holder measured previously. Finally we succeeded to develop the measuring system which can measure such a small heat capacity as 1 μJ/K with a noise less than 10 %.

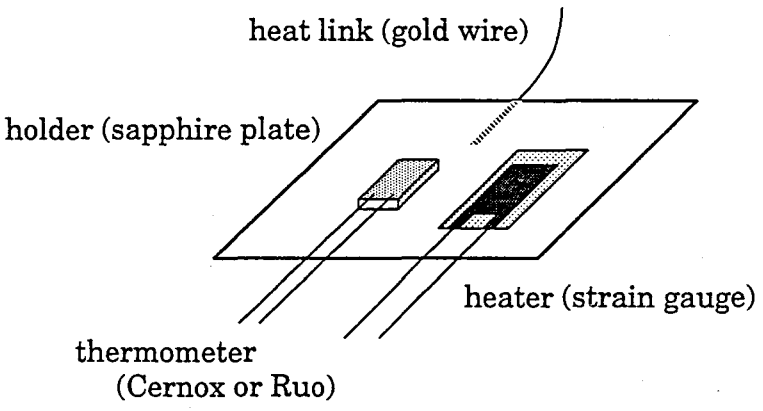

Figure 2.3: The view of sample holder.

(a)

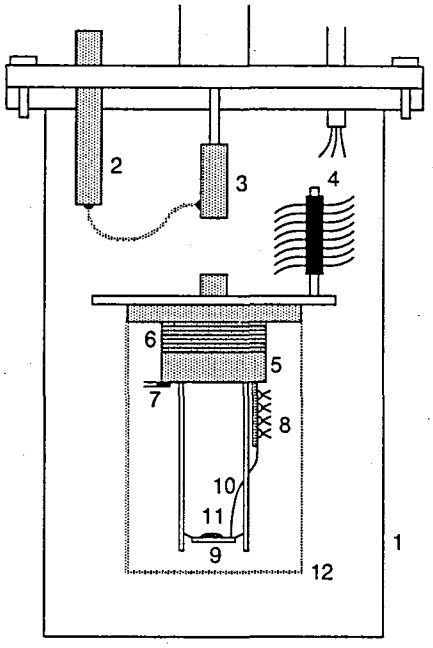

1 brass vacum can
2 Cu heat sink
3 heat switch
4 heat anchor
5 Cu heat reserver
6 heater(Constantan)
7 Ge-themometer
8 heat anchor
9 sample holder(sapphire)
10 heat link(Au-wire)
11 sample
12 Cu radiation shield

(b)

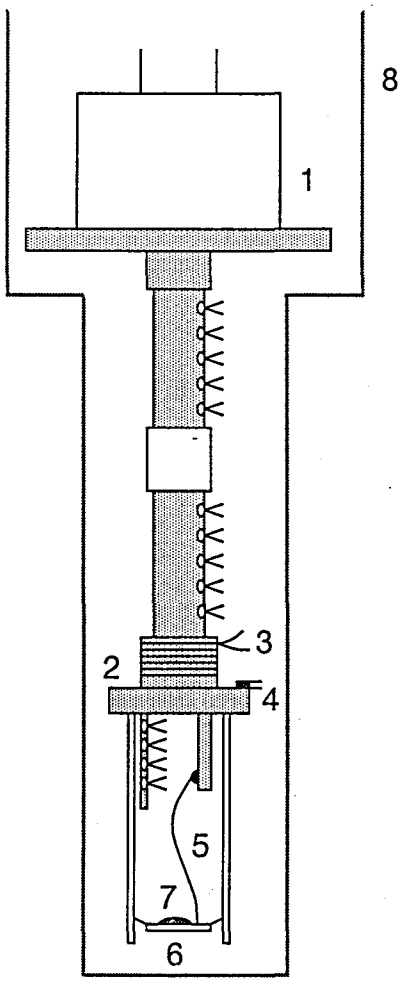

1 mixing chamber
2 heat reserver
3 heater(manganin)
4 RuO thermometer
5 heat link(Au-wire)
6 sample holder(sapphire)
7 sample
8 Cu radiation shield

Figure 2.4: The schemaic view of the measuring system of (a) ^{4}He-cryostat and (b) ^{3}He/^{4}He dilution refrigerator.

2.3 DC magnetization and DC susceptibility measurement

DC magnetization and susceptibility measurements were performed by using a superconducting quantum interference device (SQUID)-magnetometer (MPMS-7, Quantum Design), in the temperature range from 1.8 K to 300 K and the magnetic field range up to 7 T. The principle of the measurement by the SQUID system is schematically shown in Fig. 2.5. The sample is magnetized in the uniform magnetic field H generated by a superconducting magnet. When the sample is moving in the pick-up coil (the second-order differential gradiometer) from the top to bottom, the variation of the flux, which is caused by the movement of the sample, generates the screening current in the pick-up coil. The screening current is detected finally as the output voltage of the rf-SQUID system through the signal coil. The magnetic moment is calibrated by measuring the paradium standard over the magnetic field range and adjusting the system calibration factors to obtain the correct moment value for the standard. The magnetization of the sample is calculated from the signal automatically.

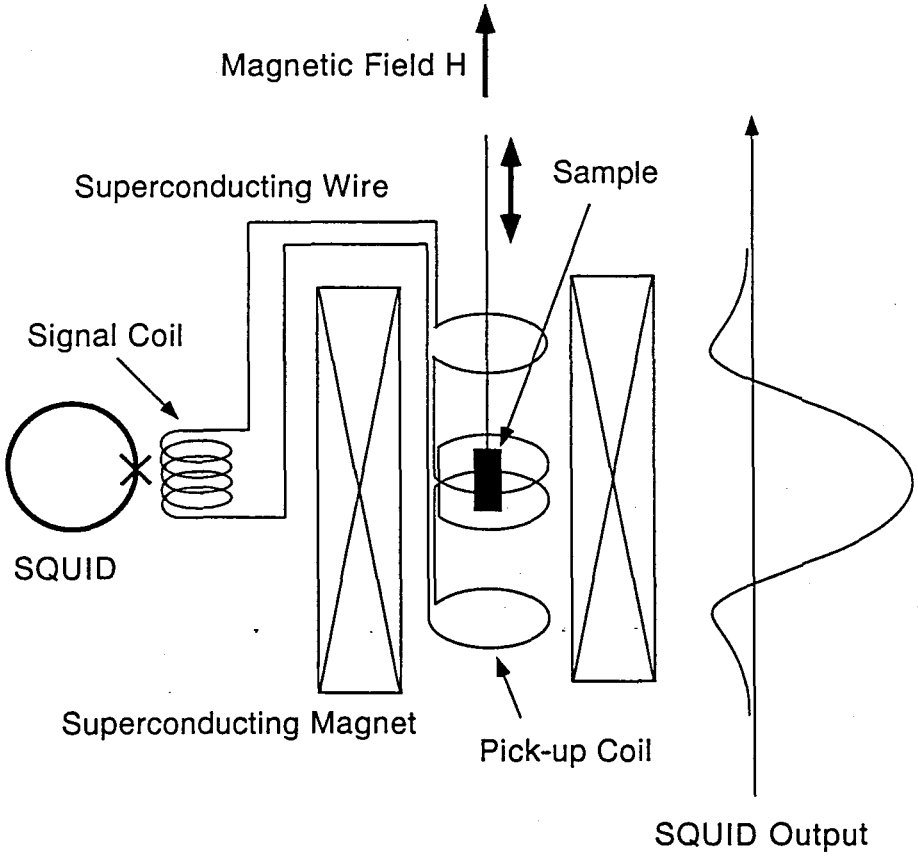

Figure 2.5: The schematic view of the SQUID system.

2.4 AC susceptibility measurement

In the low temperature range (40 mK $\sim$ 3.0 K) the AC susceptibility was measured with the Corson's type mutual inductance bridge by using a dilution refrigerator. The principle

of the AC susceptibility measurement is simple. Figure 2.6 shows the schematics of the AC susceptibility measurement. The mutual inductance between the primary and secondary coil is compensated without the sample. With the sample inside the secondary coil, the mutual inductance is proportional to the susceptibility of the sample. When we supply a AC-current into the primary coil, we can obtain the susceptibility as a induced voltage in the secondary coil.

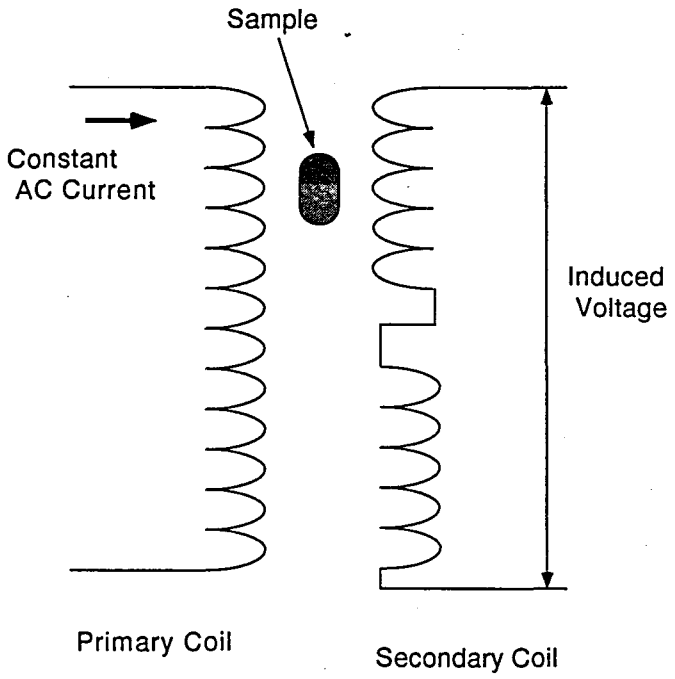

Figure 2.6: The schematics of the AC susceptibility measurement

The magnetization M has an inversion time symmetry, therefore M is written as a function of an external magnetic field H as,

$$M = \chi_0 H + \chi_2 H^3 + \chi_4 H^5 + \cdots \tag{2.4}$$

where χ_0 is a linear susceptibility and χ_2, χ_4, $\cdots$ are non-linear susceptibility. When we apply an AC magnetic field $H_{AC} = h_0 \cos\omega t$, the AC magnetic response $m(t)$, which consists of the in-phase and the out-of-phase components with various frequencies as $m_n = m'_n - im''_n$, is given by,

$$m(t) = \sum_{n=0} \infty [m'_{2n} \cos(2n+1)\omega t - m''_{2n} \sin(2n+1)\omega t] \tag{2.5}$$

where $m'_0 = \chi'_0 h_0 + \frac{3}{4}\chi'_2 h_0^3 + \cdots$, $m''_0 = \chi''_0 h_0 + \frac{3}{4}\chi''_2 h_0^3 + \cdots$, $m'_2 = \frac{1}{4}\chi'_2 h_0^3 + \frac{5}{16}\chi'_4 h_0^5 + \cdots$, $m''_2 = \frac{1}{4}\chi''_2 h_0^3 + \frac{5}{16}\chi''_4 h_0^5 + \cdots$, $\cdot, \cdot, \cdot$. And an induced voltage in a secondary coil by the sample is given by,

$$E \propto -\frac{dm(t)}{dt} \tag{2.6}$$

$$= \omega h_0 \left[\chi_0^{t'} \sin\omega t + \chi_0^{t''} \cos\omega t + \frac{3}{4} h_0^2 (\chi_2^{t'} \sin 3\omega t + \chi_2^{t''} \cos 3\omega t) + \cdots\right] \tag{2.7}$$

where $\chi_0^t = m_0/h_0$, $\chi_2^t = m_2/h_0$, $\cdots$. If h_0 is very small, we can consider as $\chi_0^t \approx \chi_0$, $\chi_2^t \approx \chi_2$, $\cdots$. Therefore we can measure the linear (χ_0', χ_0'') and the non-linear (χ_2', χ_2'', $\cdots$) susceptibilities simultaneously by detecting ω, 3ω, $\cdots$ components of the induced volatge using a two phase lock-in amplifier. When we apply the DC magnetic field H_0, the above equations are modified. And we obtain following, $\chi_0^t \approx \chi_0 + 3\chi_2 H_0^2$ if h_0 is much smaller than H_0, which is the differential susceptibility.

Figure 2.8 shows the circuit diagram of the mutual inductance bridge. An AC voltage is supplied by the inner oscillator of the lock-in amplifier (EG&G, Model 7260), which is put into the primary coil as an AC current driven by the current buffer. The induced voltage in the secondary coil is detected by the lock-in amplifier with the reference voltage, which has the same frequency and the same phase of the input AC current. Through the pre-amplifier the signal enlarges 50 times larger. By using the two phase lock-in amplifier we can detect both the in-phase ($\theta = 0$) and the out-of-phase ($\theta = \pi/2$) components respectively, where θ is the phase delay from the reference voltage.

In Fig. 2.7 the schematic view of the present measurement system is shown. The measuring coils were carefully designed and wound onto the bobbin made of an eppoxi resin (stycast 1266) using a superconducting wire (0.1 ϕ) for the primary coil and a copper wire (0.1 ϕ) for the secondary coil respectively. The sample is wrapped by a copper sleeve strictly, which is connected on the copper cold-stage whose temperature is controlled by a PID technique. The amplitude of the AC field driven by the primary coil was in the range $0 \sim 5$ Oe with the frequency $\omega = 130$ Hz. The measurement process is as following. First we made a balance with the variable resister A and B (see in Fig. 2.8) to compensate the both components of the signal at 2.0 K. Then we measured the variation of the signal voltage as a function of the temperature, which is proportional to χ_0(T)-χ_0(2.0K). The absolute value of the susceptibilities were obtained by comparing the variation of the susceptibility measured by the SQUID magnetometer in the temperature range 1.8 K $\sim$ 3.0 K.

2.5 Resistivity measurement

The resistivity measurements were carried in the low temperature range (20 mK $\sim$ 2.5 K) and the high temperature range (1.5 K $\sim$ 300 K) by using a dilution refrigerator and a standard ^{4}He-cryostat respectively. In the high temperature range a standard DC technique was employed for the measurements, while in the low temperature range we measured by an AC technique to avoid the self-heating of the sample due to the excitation current. For the measurement we put the low excitation current, $\sim$ 0.1 mA, into the sample with the frequency $\omega = 17$ Hz.

The samples for the resistivity measurements were cut to an appropriate size ($\sim$ 0.5 $\times$ 0.5 $\times$ 10 mm^3) using a spark cutter to avoid the crack due to a mechanical tension. The electric contacts were made by the spot-welding aluminium wire (0.025 ϕ mm). The measurements were performed with the excitation current parallel to the both crystallographic a and c-axes. The error of the absolute value of the resistivity is about 20 % becausue of rather poor precision in the absolute value of the sample dimension, however the relative error was less than 0.5 % .

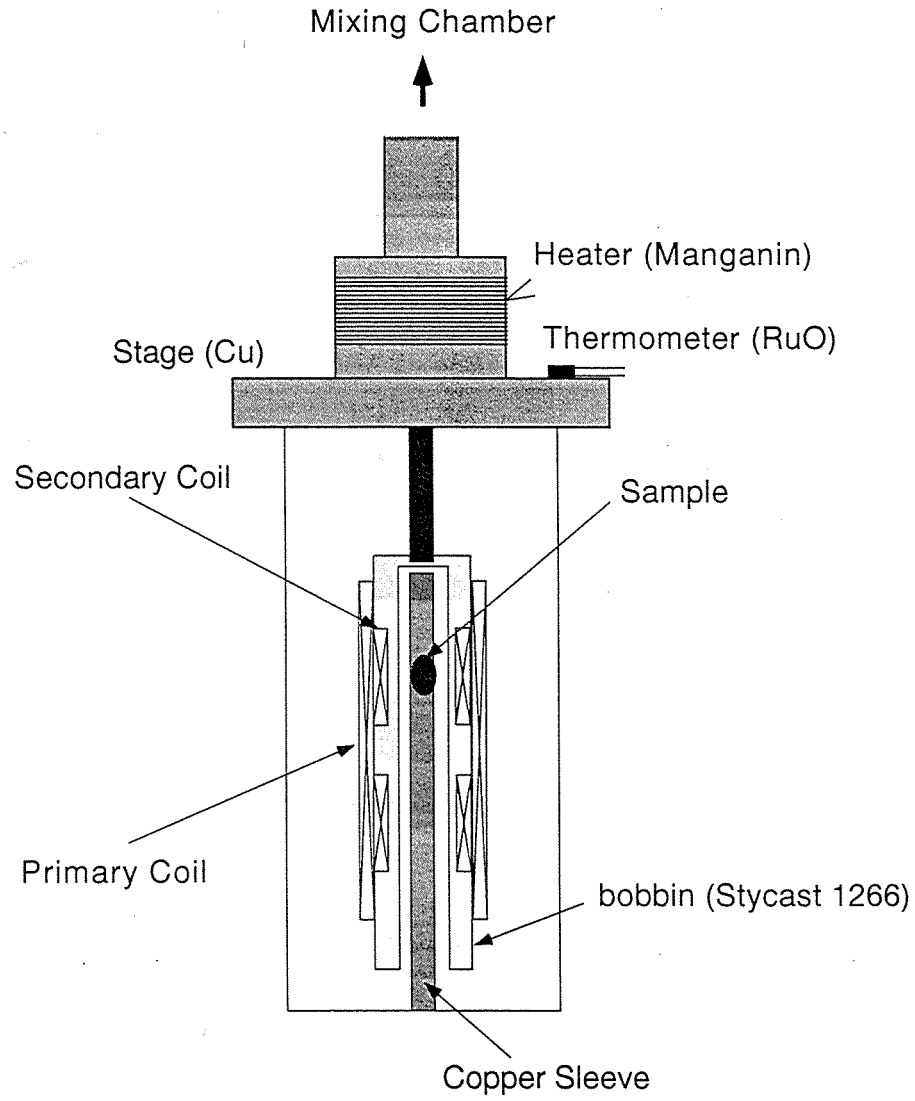

Figure 2.7: The schematic view of the present AC susceptibility measurement system.

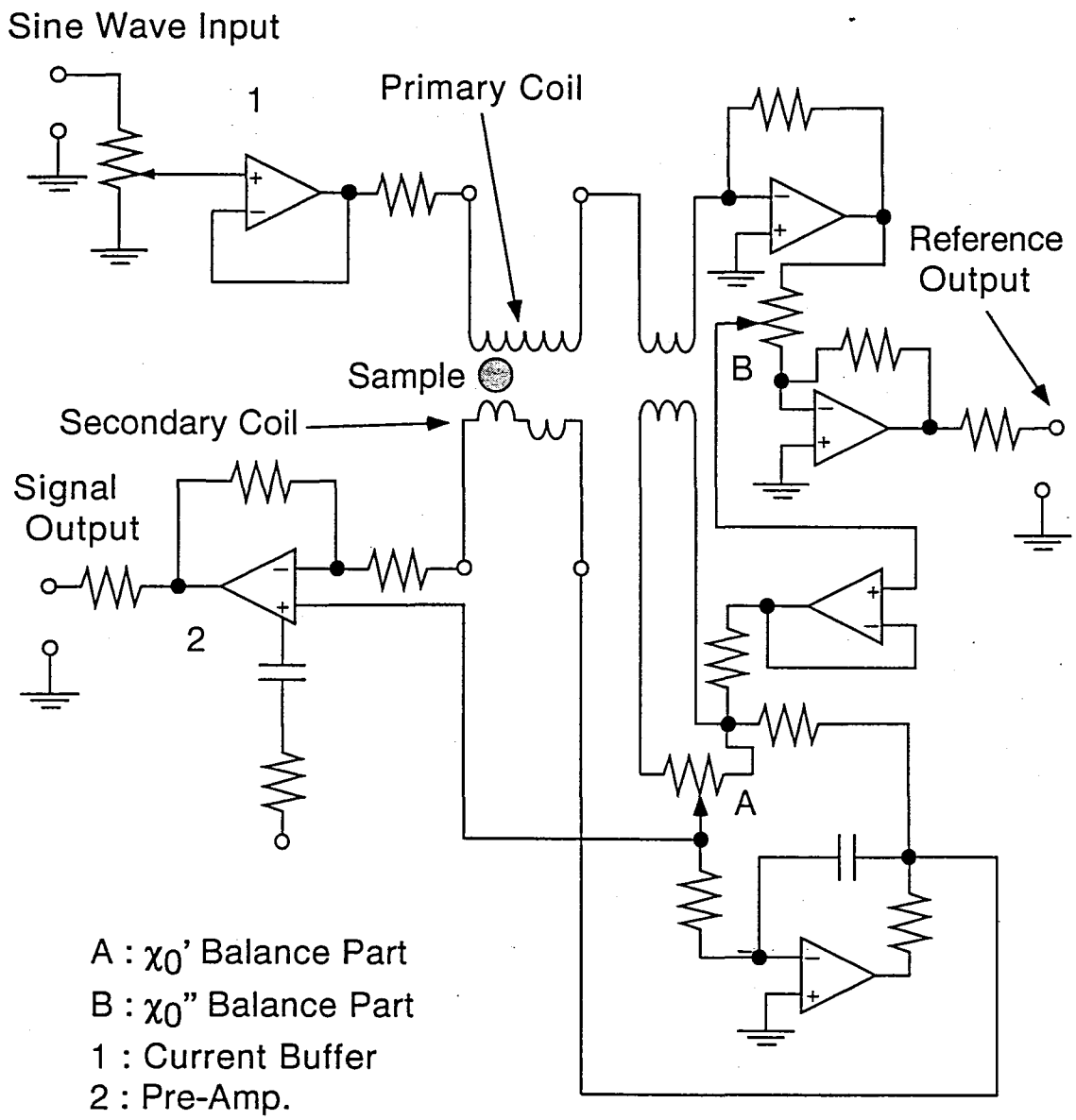

Figure 2.8: The circit diagram of the Corson's type mutual inductance bridge.

Chapter 3

Experimental results and discussions

3.1 Magnetic properties of $Ce(Ru_{1-x}Rh_x)_2Si_2$

In this section I will show the experimental results of the thermodynamic and the transport properties of $Ce(Ru_{1-x}Rh_x)_2Si_2$ in the low Rh-concentration region ($x \leq 0.15$) and in the intermediate Rh-concentration region ($0.3 \leq x \leq 0.5$). As I mentioned in Sec 1.3.2 $Ce(Ru_{1-x}Rh_x)_2Si_2$ system has a rich variety of the ground state and three different QCPs in their magnetic phase diagram. First I will survey the magnetic properties of the $Ce(Ru_{1-x}Rh_x)_2Si_2$ system with taking a special notice of the magnetic instability properties near the critical concentrations, $x = 0.03$, 0.4 and 0.5.

3.1.1 Specific heat

Figure 3.1 shows the magnetic specific heats in the temperature range $0.1 \sim 10$ K in the low Rh-concentration region. I considered that the phonon parts for all Rh-concentrations are same as that of $LaRu_2Si_2$. The specific heat for $x = 0$ does not show any anomaly due to the magnetic phase transition down to the lowest temperature, whose electronic specific heat coefficient γ is almost constant ($\sim$ 380 mJ/molK^2) below 5 K. For $x =$ 0.05, 0.1 and 0.15 the SDW phase transitions were found at $T_N = 2.0$, 4.4 K and 4.8 K, respectively. The anomaly for $x = 0.05$ is very small which may be correspond to the small ordered moment. In a recent neutron diffraction measurement the ordered moment for $x = 0.05$ was observed about 0.2 μ_B [43]. For each concentrations C/T are almost constant far below T_N , whose values are about 460, 342 and 374 mJ/molK^2, respectively. These large γ-values in the SDW state can be considered to come from the remaining Fermi surface after the anisotropic gap opening. Below T_N the specific heats of $x = 0.05$, 0.1 and 0.15 show the exponential-type behavior, $\gamma T + A\exp(-\Delta/T)$. The solid lines in Fig. 3.1 (b) represent the fitting results with this function for these concentrations. The parameters Δ/T_N are 2.2, 1.7 and 1.6 for $x = 0.05$, 0.1 and 0.15 respectively, which are not so different from that of Cr ($\Delta/T_N \sim 2.3$), which is the typical compound shows a SDW transition. The specific heat anomalies after subtracting the electronic part γT have the quite similar shape for each concentrations, even for $x = 0.05$. It means that the character of the phase transition does not change as increasing Rh-concentration.

$x = 0.03$ is the very close concentration to hte QCP of SDW phase on the Rh-poor side, however the specific heat does not show the NFL behavior, logarithmic divergent behavior in C/T, like $CeCu_{5.9}Au_{0.1}$. C/T for $x = 0.03$ is nearly constant below 3 K, whose value is about 500 mJ/molK^2, which is enhanced from that of $x = 0$. This enhancedment of C/T can be thought to be caused by the enhancedment of the antiferromagneic spin

fluctuations or the reducement of the Kondo temperature. I will discuss on the effect of the spin fluctuation for the low temperature properties for this concentration later.

Figure 3.3 shows the specific heats in the intermediate Rh-concentration region. For $x = 0.4$, which is near another critical concentration of the SDW phase, C/T diverges logarithmically down to the lowest temperature in contrast with that for $x = 0.03$. This is the characteristic feature of the NFL behavior in the specific heat. For $x = 0.5$, where the concentration is close to the QCP of the different antiferromagnetic ordered phase in the Rh-rich region, C/T also shows the logarithmic divergent behavior. Because we did not measure the specific heat for other concentration in the intermediate non-magnetic region III (see in Sec. 1.3.2), it's not clear the $-\log T$ dependence of C/T for $x = 0.4$ and 0.5 is attributed to the QCP. For $x = 0.3$ the $-\log T$ dependence is found down to 2 K as well as for $x = 0.4$, however at 2.0 K the SDW phase transition is occured. Below T_N (= 2.0 K), which is determined from the extremely small anomaly in the C/T vs $\log T$ plot, C/T is almost constant. It means $x = 0.3$ is the FL in the SDW state, below 2.0 K, on the other hand in the paramagnetic state, above 2.0 K, is the NFL. It indicates that the NFL behavior may be caused by the spin fluctuation in the paramagnetic state, which is suppressed in the ordered phase and the FL is recovered.

3.1.2 Susceptibility and magnetization

Figure 3.4 shows the susceptibilities in the whole temperature range, between 1.8 K and 300 K. In both the low and the intermediate Rh-concentration region, no x-dependence is observed in the susceptibilities at high temperature, $T > 100$ K. For each concentrations a strong magnetic anisotropy is shown; the ratio of χ_c/χ_a reaches about 20 at 2 K. Above 100 K the susceptibility shows the Curie-Weiss behavior, whose effective Bohr magnetron is about $2.91\mu_B$, along the c-axis. As I will discuss in Sec. 3.2.2, the strong magnetic anisptropy can be explained by a tetragonal crystalline electric field (CEF) model. It indicates that magnetic moments of Ce-atom are localized at each Ce-atom and fluctuate thermally in the high temperature region.

On the other hand, in the low temperature region there is a strong x-dependence. In Fig.3.5 the low temperature susceptibilities ($T \leq 20$ K) are shown. For $x = 0$ and 0.03 the susceptibilities do not show any anomaly down to 1.8 K due to the phase transition. For both concentrations the susceptibilities show the broad maximum around 10.5 K and 7.0 K respectively, and slightly decrease. Below 4 K the susceptibilities are almost constant, which are correspond to form the FL state. In the susceptibility the NFL behavior is not observed for $x = 0.03$ as well as in the specific heat. For $x = 0.05$, 0.10 and 0.15 the sharp drops are found at 2.2 K, 4.7 K and 5.5 K respectively, which are correspond to the SDW phase transition. These temperatures are slightly different, a little high, from T_N determined from the specific heat measurements. It is the general tendency in the case of the antiferromagnetic phase transition. The 'true' phase transition temperature should be determined from the specific heat. The temperature where the broad maximum is found, $T_{\chi max}$, decrease as increasing x, which can be associated with the reduction of the Kondo temperature.

Figure 3.6 shows low temperature susceptibilities in the intermediate Rh-concentration region. From the susceptibility measurements above 1.8 K the critical concentration of the SDW phase on the Rh-rich side is rather $x = 0.35$ than 0.4. Similarly, the QCP of antiferromagnetic phase in high Rh-concentration region is rather $x = 0.6$ than 0.5. For $x = 0.3$ the cusp due to the SDW transition is found around 2 K as well as in the specific heat. Above T_N the susceptibility has a $1 - T$ dependence. In the nonmagnetic ground

state region, for $x = 0.35$, 0.4 and 0.5, $1 - T^a$ behaviors are observed down to 1.8 K, which is the characteristic behavior in the susceptibility of NFL as well as the logarithmic divergent behavior in C/T. In contrast with C/T the NFL behavior in the susceptibility is not universal, but varies with compounds. The value of a varies as a function of x, which is 3/4, 1/2, 1/3 and 1/2 for $x = 0.35$, 0.4, 0.5 and 0.6, respectively. As well as in the specific heat, the NFL behavior is observed in the intermediate Rh-concentration region in the susceptibility, and the deviation from the FL becomes stronger as x increasing.

The magnetization processes and the differential magnetizations at 1.8 K along c-axis are shown in Fig. 3.7 (a) and (b) respectively. For $x = 0.03$, 0.05 and 0.15 the metamagnetic transition was found at 6.85, 6.50 and 5.35 T respectively, which are denoted as H_M in Fig. 3.7 (b). This metamagnetic transition is considered to be not the phase transition but the crossover from the HF regime to the localized moment regime. Therefore the field where the metamagnetic transition is shown H_M can be related with the Kondo temperature T_K . And the sharpness of the metamagnetic transition is very sensitive to x, which is broaden as x increasing. It might be the effect of the disorder by alloying. For $x = 0.15$ much sharper metamagnetic transition is found at 3.35 T, which is denoted as H_c in Fig. 3.7 (b). At H_c the phase transition from the SDW state to the HF state is occurred. Near the critical concentration, $x = 0.03$, the magnetization process is quite similar to that far from the critical concentration, $x = 0$. It is consistent with the FL behavior in the specific heat and the susceptibility at $x = 0.03$.

In Fig. 3.8 the magnetization in the intermediate Rh-concentration region are shown. In contrast with that in the low Rh-concentration region, the metamagnetic transition does not appear at least up to 7 T. From the fact the metamagnetic transition is broaden as x increasing from 0 to 0.15, the disappearance of it can be thought to be the result of the broadening, not the drop of H_M down to 0. Instead of the metamagnetic transition, there is a negative non-linearity in the magnetization process, which becomes more evident as x increasing. I will discuss on this non linearity in the magnetization in Sec.3.3.2.

In the low Rh-concentration region there is the crossover temperature $T_{\chi max}$ in the susceptibility and the crossover field H_M in the magnetization. In the region $T < T_{\chi max}$ and $H < H_M$, the system can be considered to be a itinerant electron regime, and out of this region, a localized moment regime. On the other hand in the intermediate Rh-concentration region such a evident crossover temperature or field can not be found in the magnetic response.

3.1.3 Resistivity

Figure 3.9 shows the resistivities in the whole temperature range along a- and c-axis. There is not a big variation of the resistivity with the Rh-concentration. Along c-axis we can find the maximum around 20 K, which is associated with the crossover from the single-site Kondo regime to the coherent regime, as I mentioned in Sec. 1.1. This crossover behavior can be found even in the intermediate Rh-concentration region, $x =$ 0.3 and 0.5, very clearly, in contrast with the susceptibility and the magnetization. This temperature, $T_{\rho max}$, shows a little variation in x. $T_{\rho max}$ is related with the single-site Kondo temperature T_K in the system, whose variation in x is very similar to that of T_K estimated from the specific heat [34].

The low temperature resistivities ($T \leq 2.5$ K) are shown in Fig. 3.10 and 3.11. For x = 0.05, 0.10 and 0.30 there is the humps of the resistivities along the c-axis caused by the anisotropic gap opening on the Fermi surface at T_N , while along the a-axis there are not evident anomaly at T_N , which are not shown in the figure. Below a certain temperature,

T_{coh}, a T^2 behavior can be found for each Rh-concentrations, except for $x = 0.5$. For $x = 0.5$, a $T^{1.6}$ dependence is found along both axes, instead of a T^2 one. It means that the ground state for $x \leq 0.3$ is FL, even for $x = 0.03$. On the other hand for $x = 0.5$ the NFL behavior is kept at least down to the lowest temperature, 20 mK. These results of the resistivity measurements are consistent with that of other experiments.

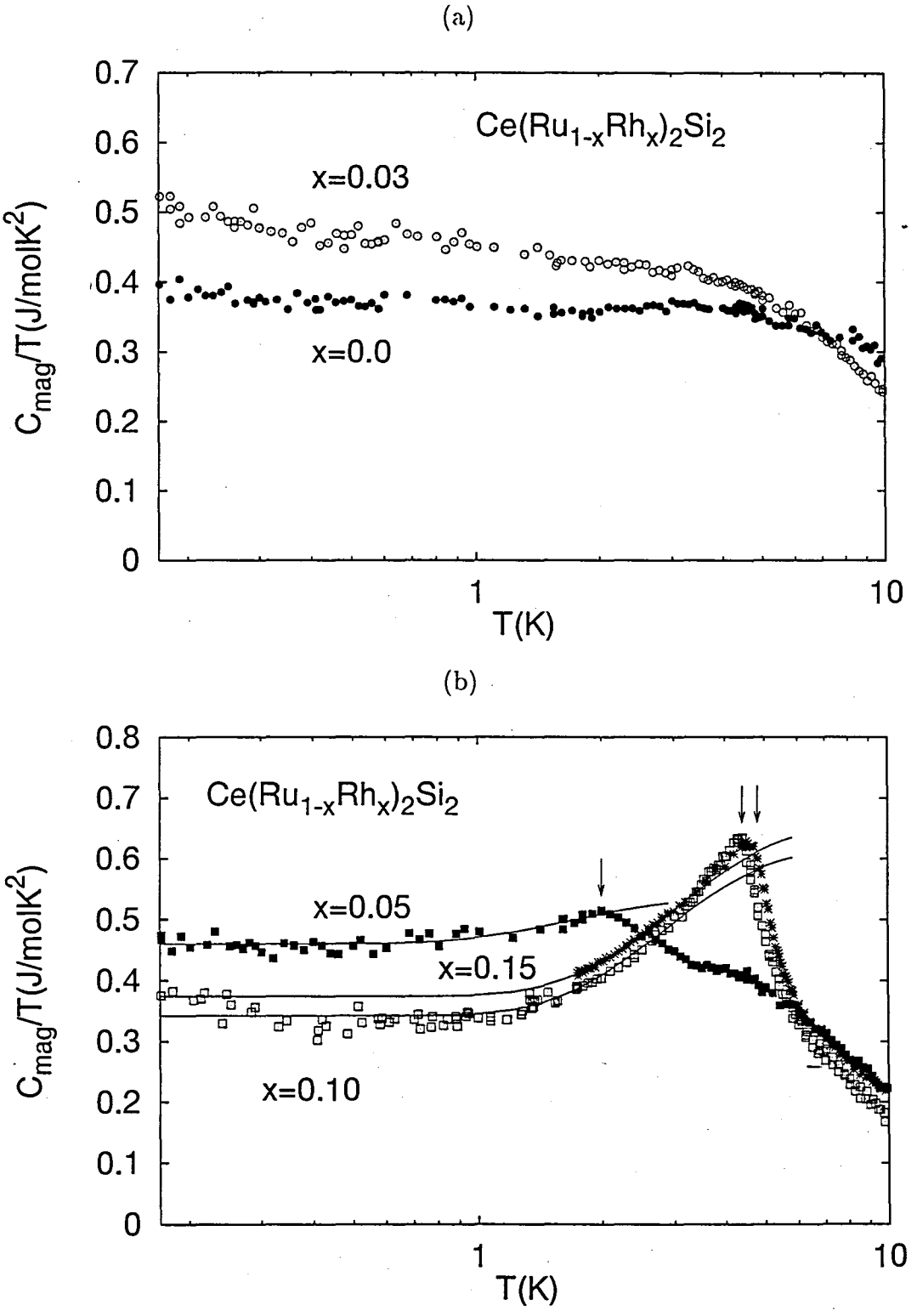

Figure 3.1: The specific heat of $Ce(Ru_{1-x}Rh_x)_2Si_2$ in the low Rh-concentration region, whose ground state is (a) non-magnetic FL (b) SDW. The arrows in (b) indicate T_N for each concentrations. The solid line represent the gap type of behavior, $C(T) = \gamma T + A\exp(-\Delta/T)$.

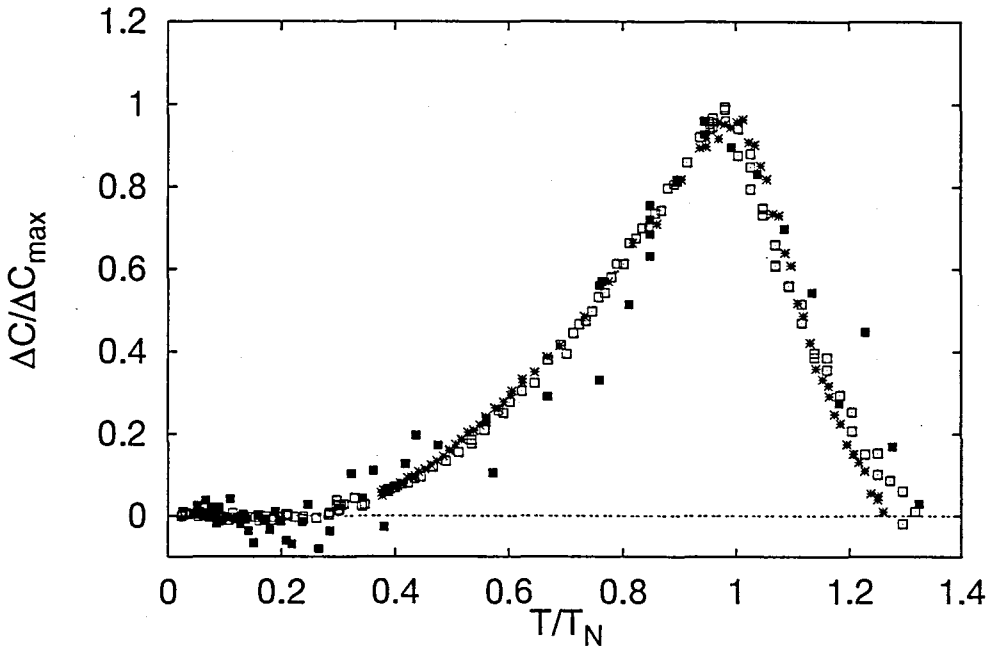

Figure 3.2: The anomaly parts of the specific heats due to the SDW phase transition are shown. The symbols in this figure indicate the same concentration in Fig. 3.1 (b).

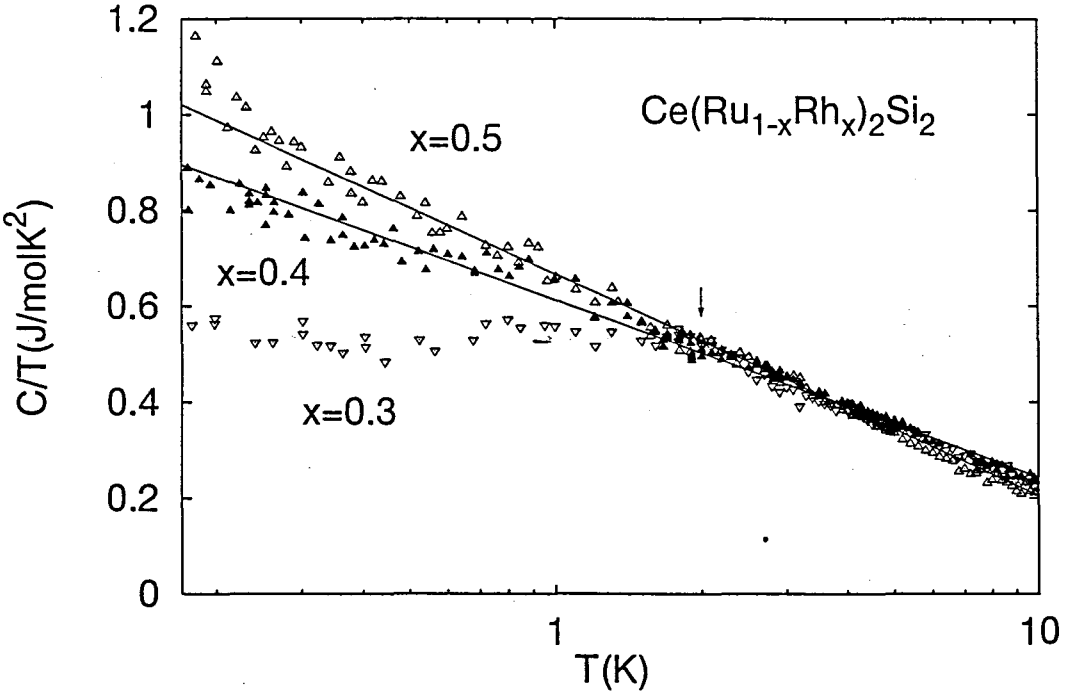

Figure 3.3: The specific heats in the intermediate Rh-concentration region are shown. The arrow in the figure indicates T_N for $x = 0.3$. For $x = 0.4$ and 0.5 the logarithmic divergent behavior is observed down to the lowest temperature.

(a)

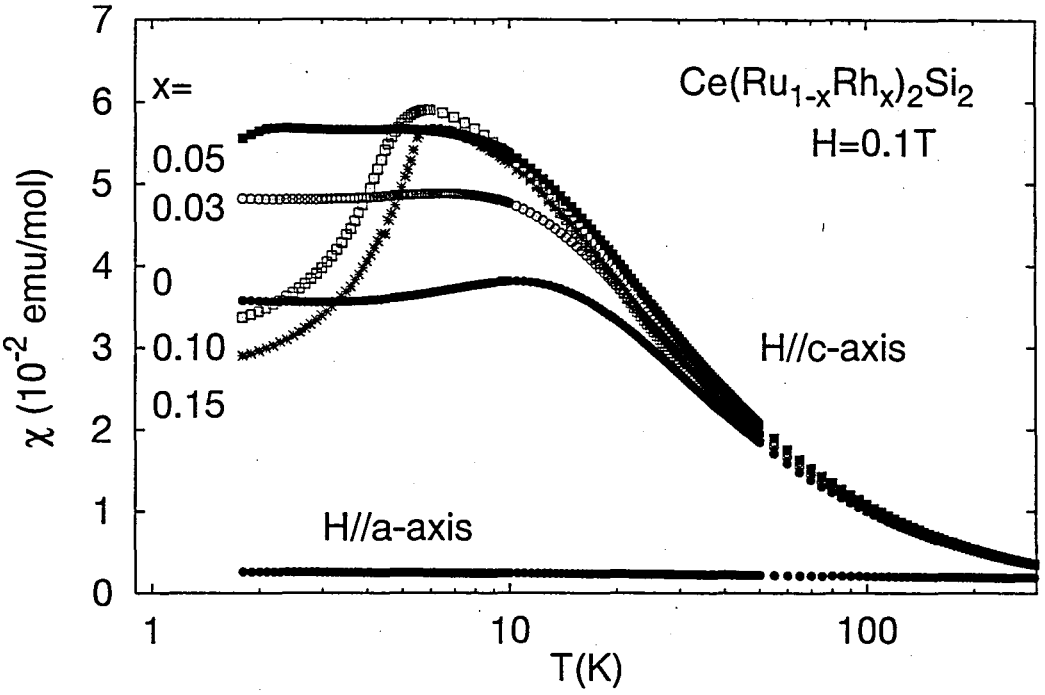

(b)

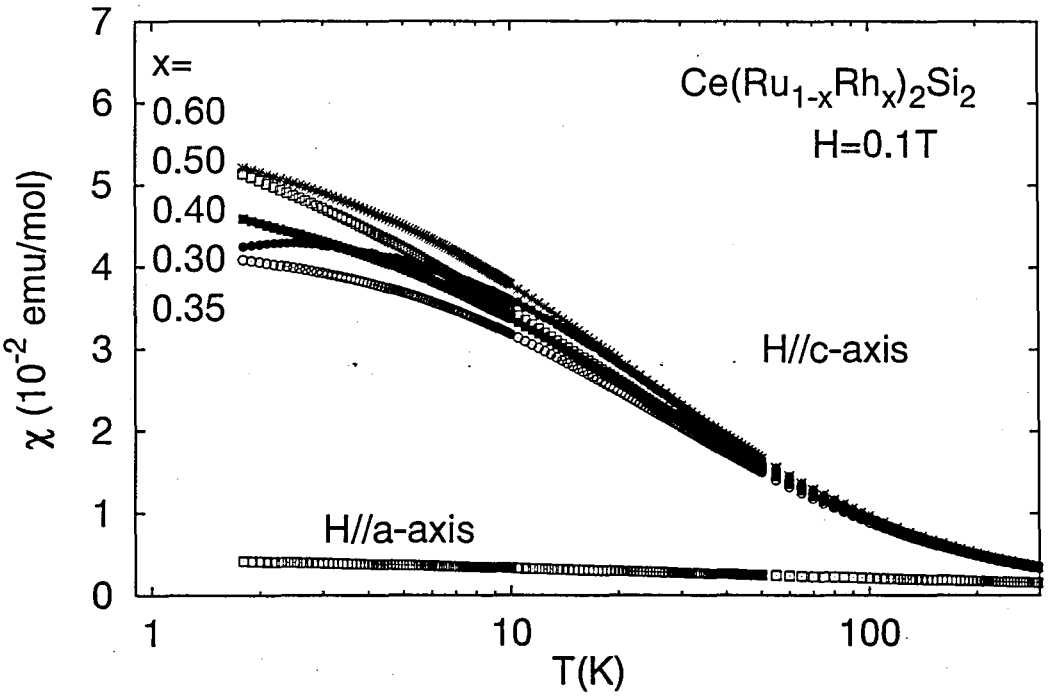

Figure 3.4: The susceptibilities (a) in the low Rh-concentration region and (b) in the intermediate Rh-concentration region.

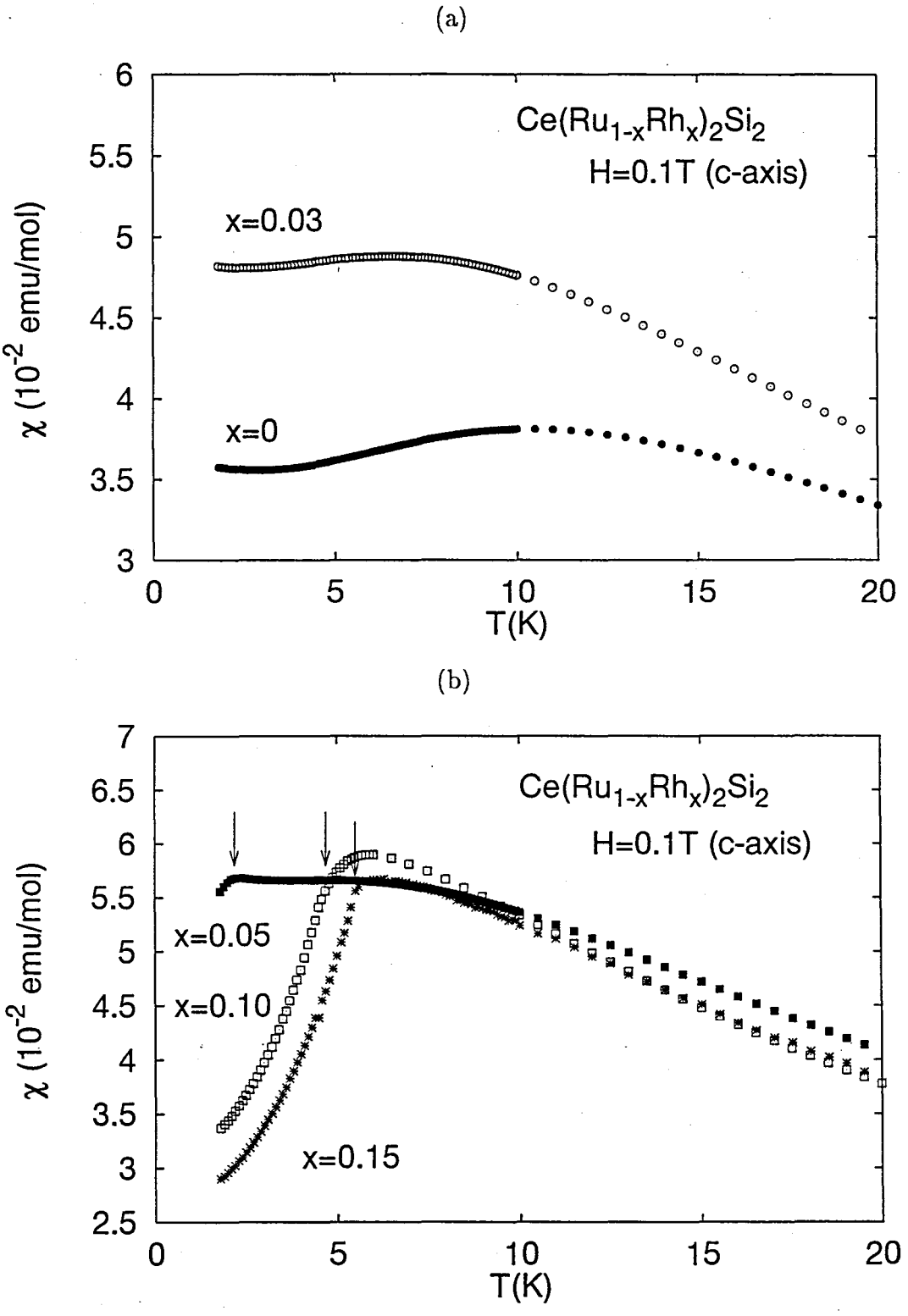

Figure 3.5: The susceptibilities in the low temperature region ($0 \sim 20$ K) for x = (a) 0 and 0.03 (b) 0.05, 0.10 and 0.15 are shown. The arrows in (b) represent the temperature where the susceptibilities show sharp drops.

(a)

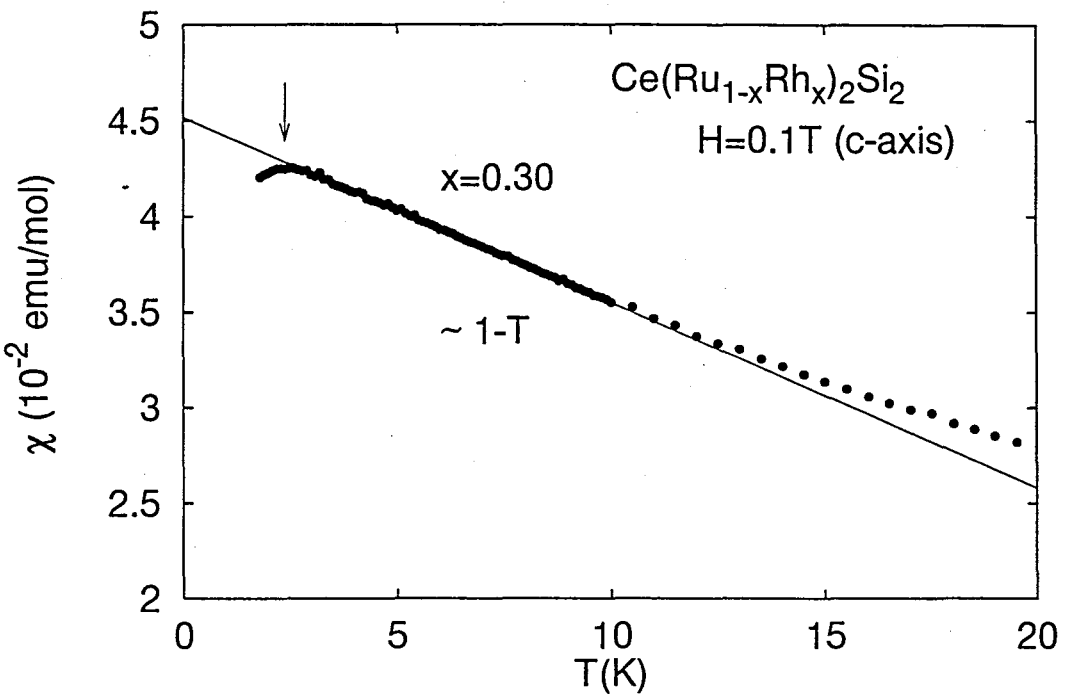

(b)

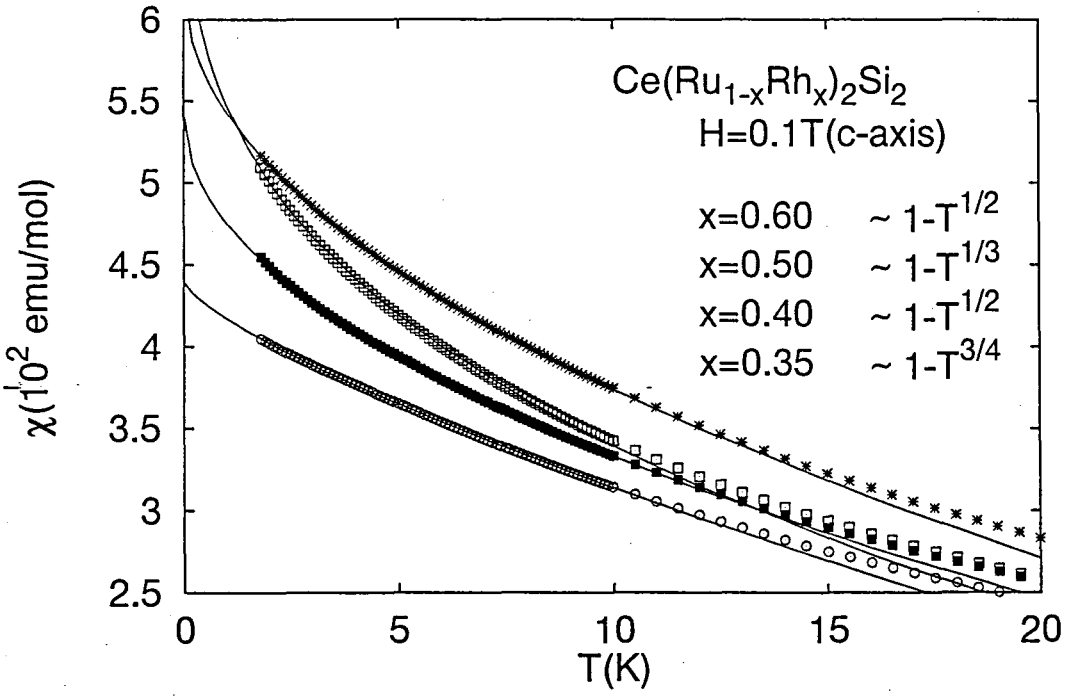

Figure 3.6: The susceptibilities in the low temperature region (0 ~ 20 K) for x = (a) 0.3 (b) 0.35, 0.40, 0.50 and 0.60 are shown. The arrows in (a) represent T_N . The solid line represent the temperature dependence of the susceptibility below 10 K.

(a)

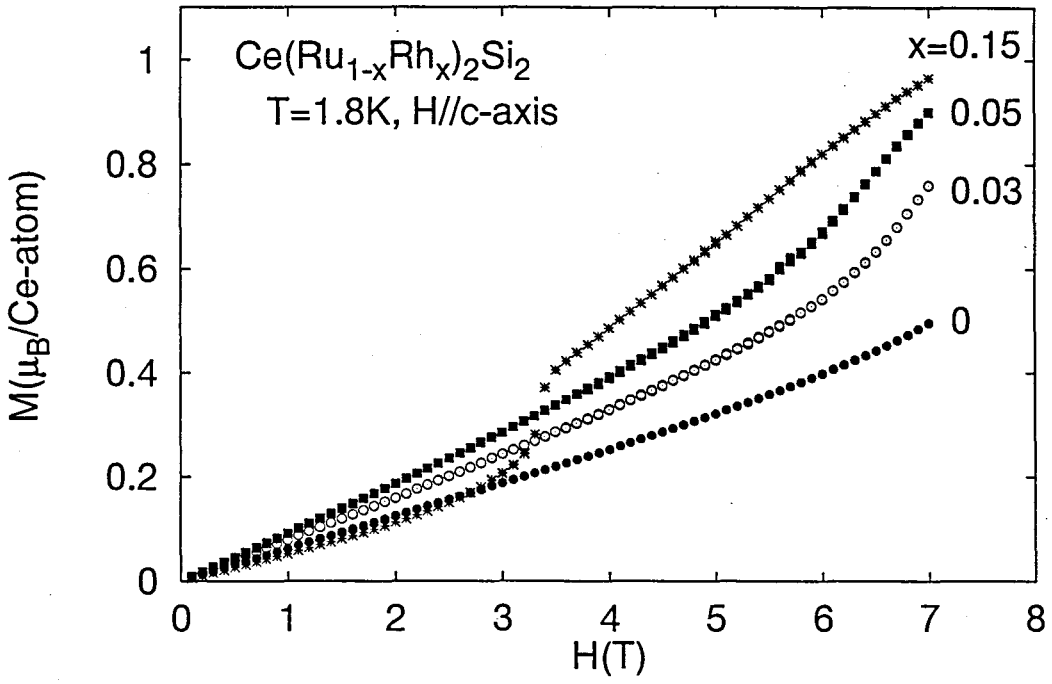

(b)

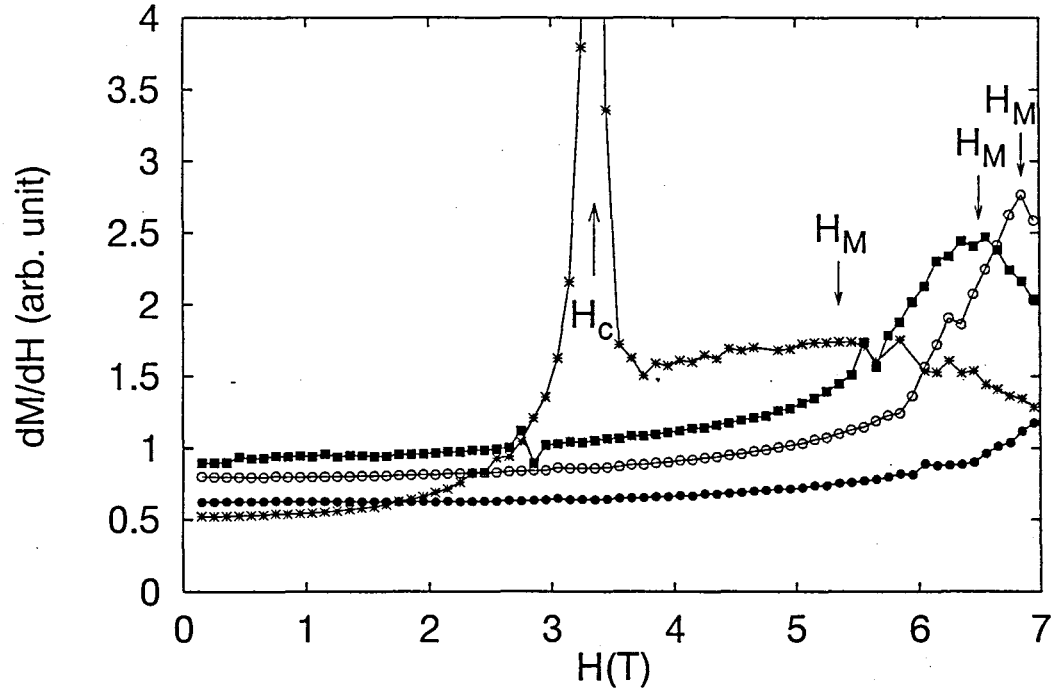

Figure 3.7: The magnetization processes in the low Rh-concentration region are shown (a). (b) is the figure in the form dM/dH-H plot. $H_{\rm M}$ and $H_{\rm c}$ in (b) are described in the text.

(a)

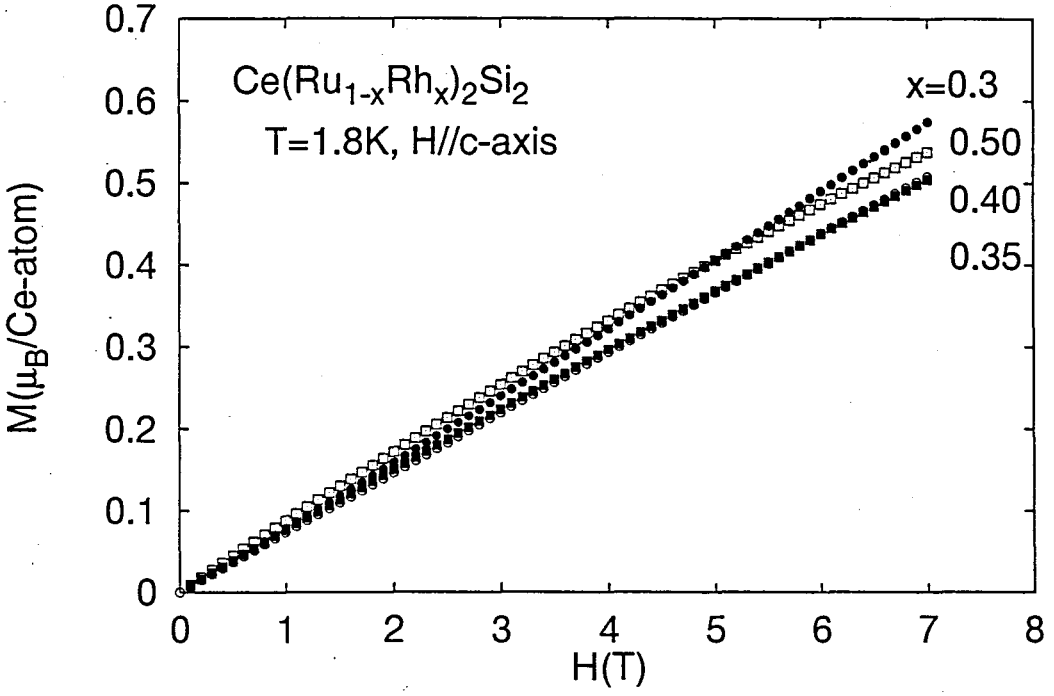

(b)

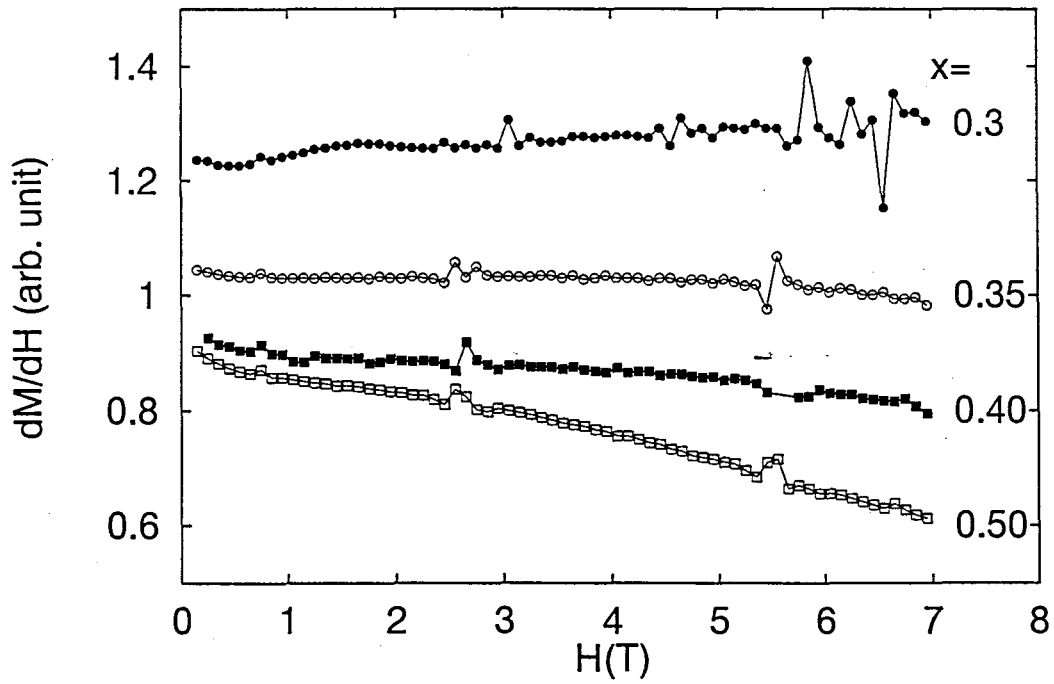

Figure 3.8: The magnetization processes in the intermediate Rh-concentration region are shown (a). (b) is the figure in the form dM/dH-H plot.

(a)

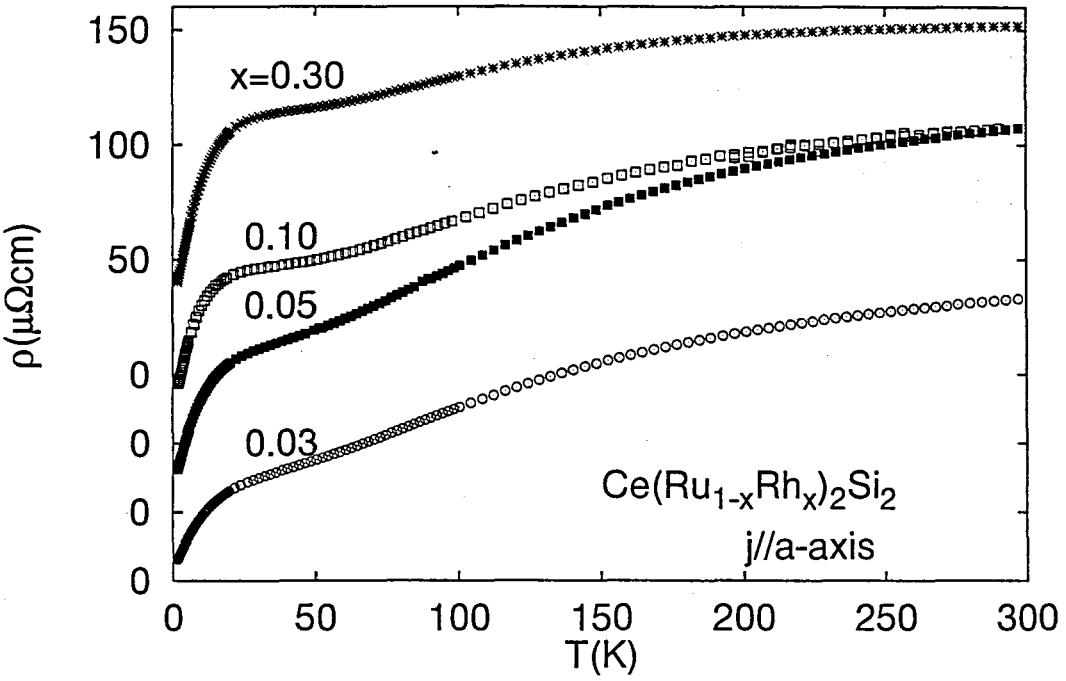

(b)

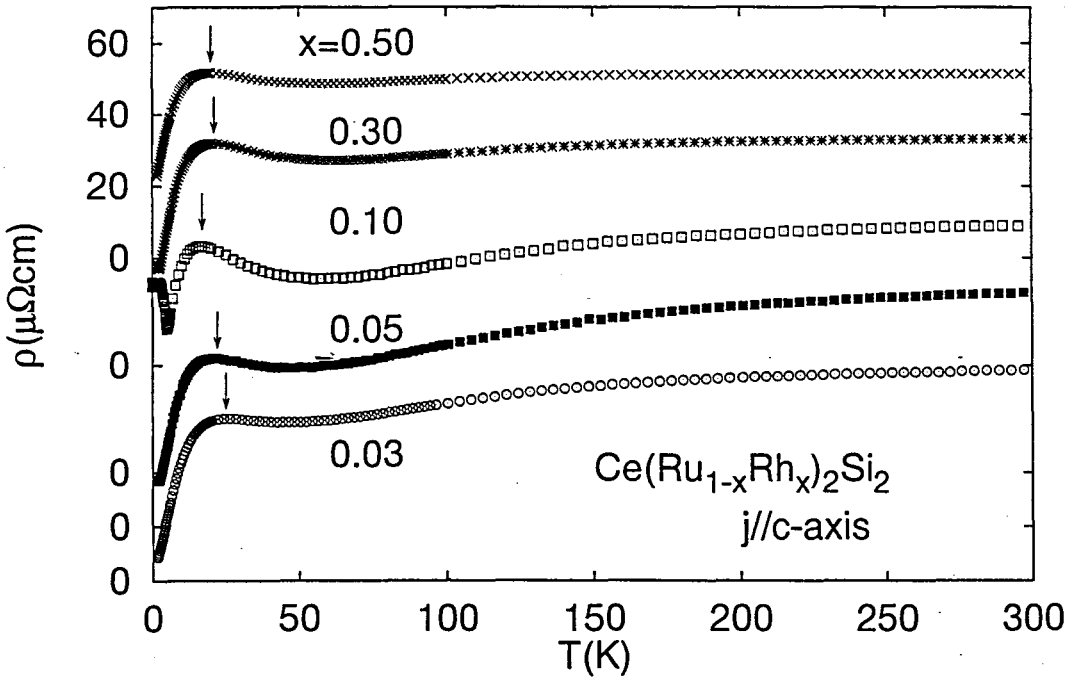

Figure 3.9: The resistivities (a) along a-axis and (b) along c-axis are shown. The arrows indicate the temperatures where a maximum in the resistivity is seen , $T_{\rho max}$ for each x.

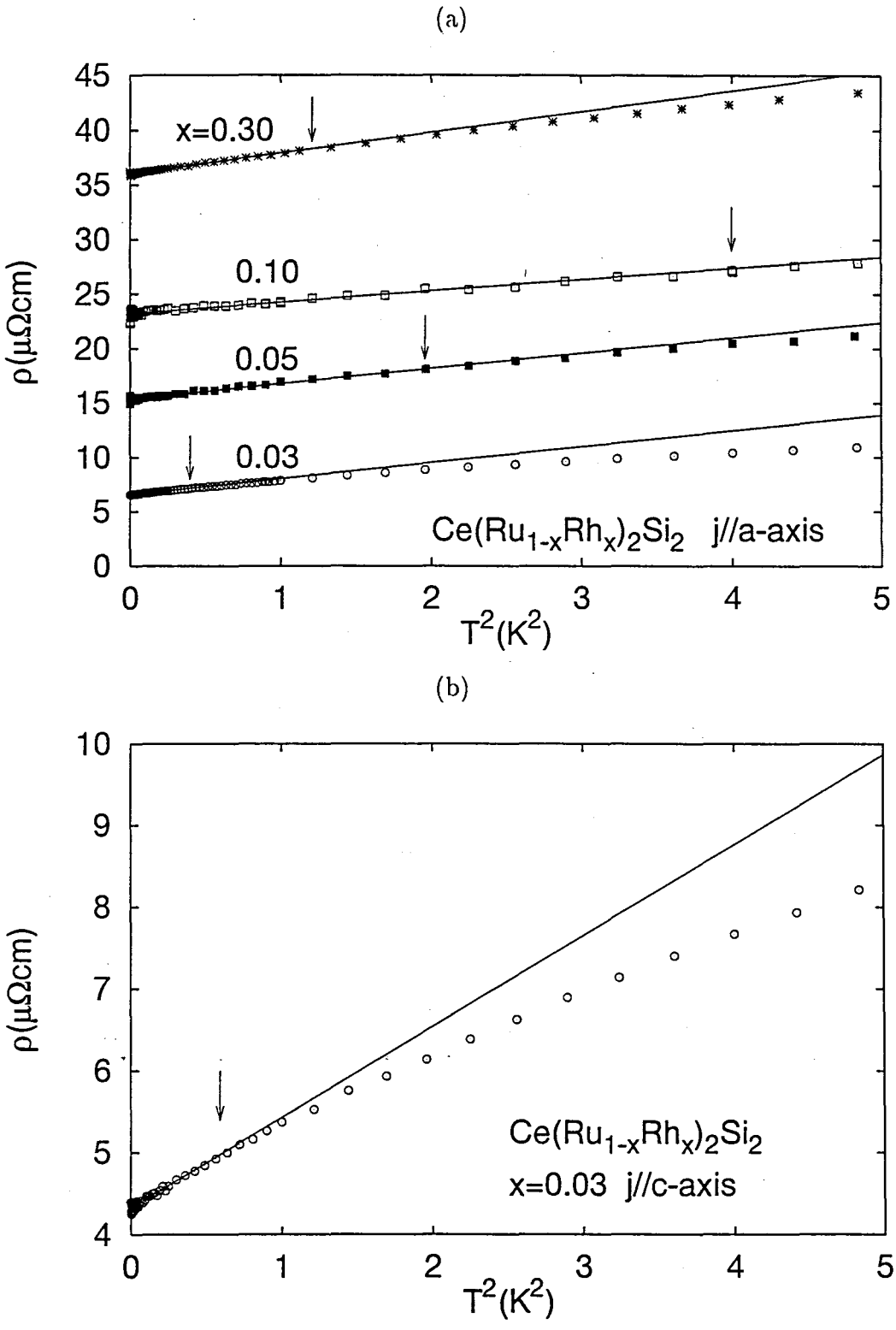

Figure 3.10: The low temperature resistivities are shown in the form of ρ-T^2 plot, (a) along the a-axis and (b) along the c-axis. The arrows in the figure indicate the temperature where the resistivity deviate from a T^2 dependence, $T_{\rm coh}$ for each x

(a)

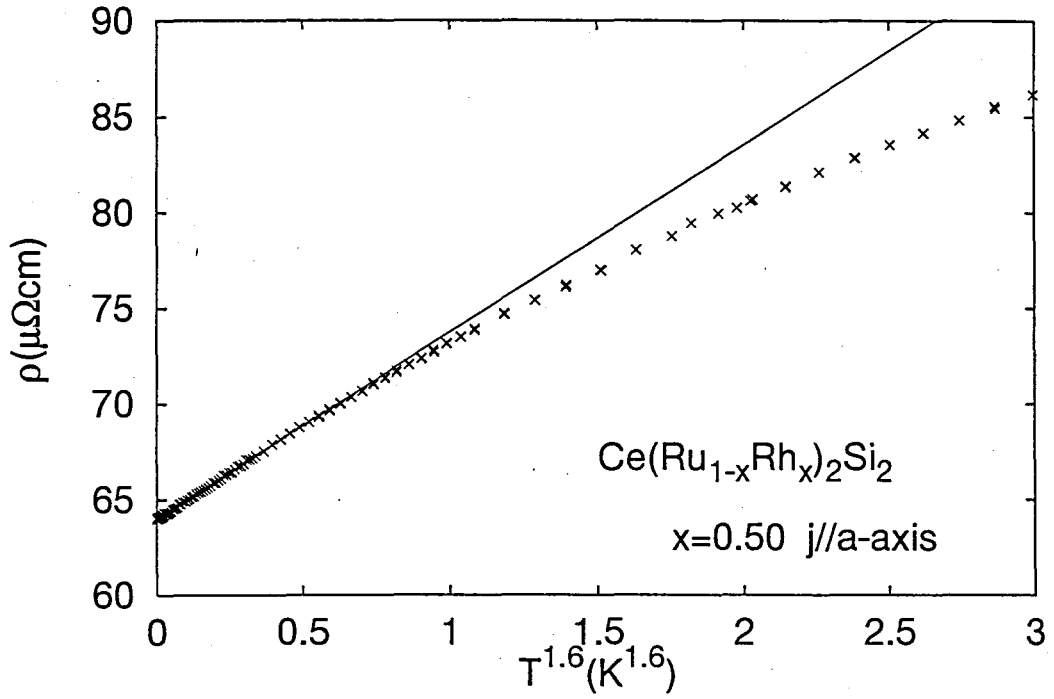

(b)

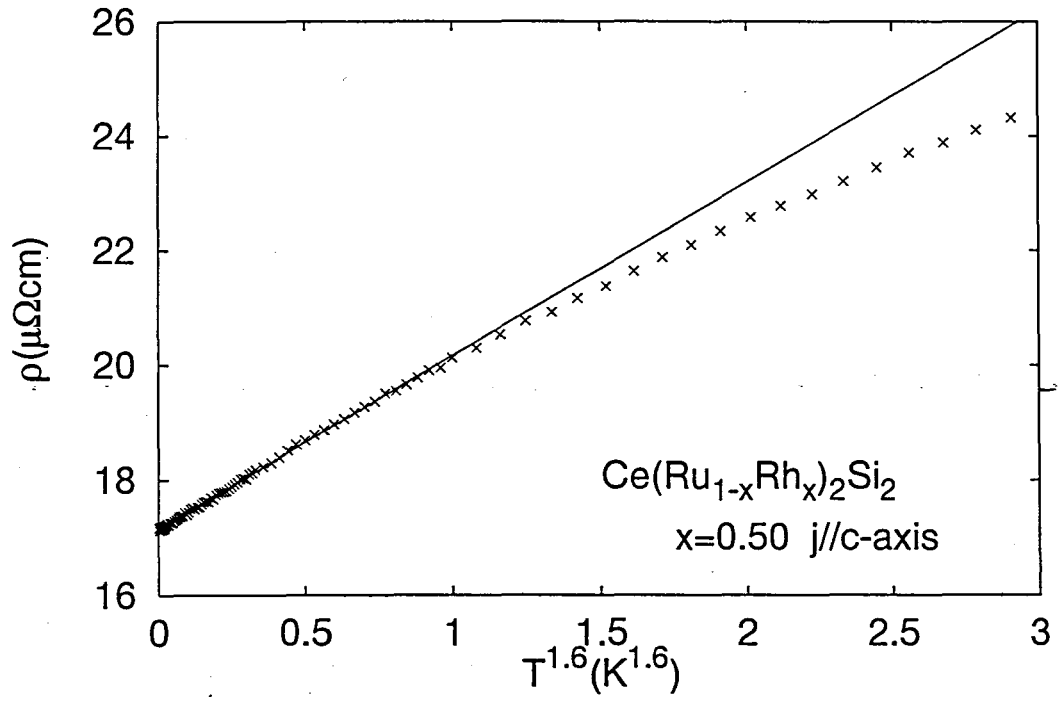

Figure 3.11: The low temperature resistivities of $x = 0.5$ are shown in the form of ρ-$T^{1.6}$ plot, (a) along the a-axis and (b) along the c-axis. Below 0.8 K the data along both axes show a $T^{1.6}$ dependence.

3.2 Discussions

3.2.1 Phase diagram of $Ce(Ru_{1-x}Rh_x)_2Si_2$

In this subsection I discuss on the phase diagram of $Ce(Ru_{1-x}Rh_x)_2Si_2$ obtained from our present results. In Fig. 3.12 I show the whole of the phase diagram. The solid lines in the figure represent the phase transition line and the broken lines represent the a kind of crossover line. Because the variation of $T_{\rho max}$ is very simlar to that of T_K , as I mentioned in the previous section, hereafter I use $T_{\rho max}$ as T_K . As Rh-concentration x increasing from $CeRu_2Si_2$, T_K drops rather steeply in small x region and reaches to the lowest value around $x = 0.15$, where T_N of SDW transition is maximum, then rises slightly and keep the value as large as that for $x < 0.05$ in the intermediate Rh-concentration region, about 20 K. For $x \leq 0.5$ the variation of T_K is rather small, comparing with the variation of their ground states. On the other hand in $CeRh_2Si_2$ the resistivity did not show the maximum in the temperature range between 1.5 K and 300 K [44]. It means that the T_K of $CeRh_2Si_2$ is much higher than 300 K or lower than its T_N (= 36 K). According to the large magnitude of its ordered moment, which is about 1.4 μ_B at 1.5 K [41], we expect the low value of T_K , however Y. Kawasaki *et al.* obtained much higher T_K , about 100 K, from NMR measurement [45]. It has been an open question where $CeRh_2Si_2$ locate in the Doniach phase diagram, in the region for $T_K \gg T_{RKKY}$, $T_K \ll T_{RKKY}$ or $T_K \sim T_{RKKY}$, and how to join to the Rh-intermediate concentration region, where the crossover from the single-site Kondo regime to the coherent regime can be found evidently.

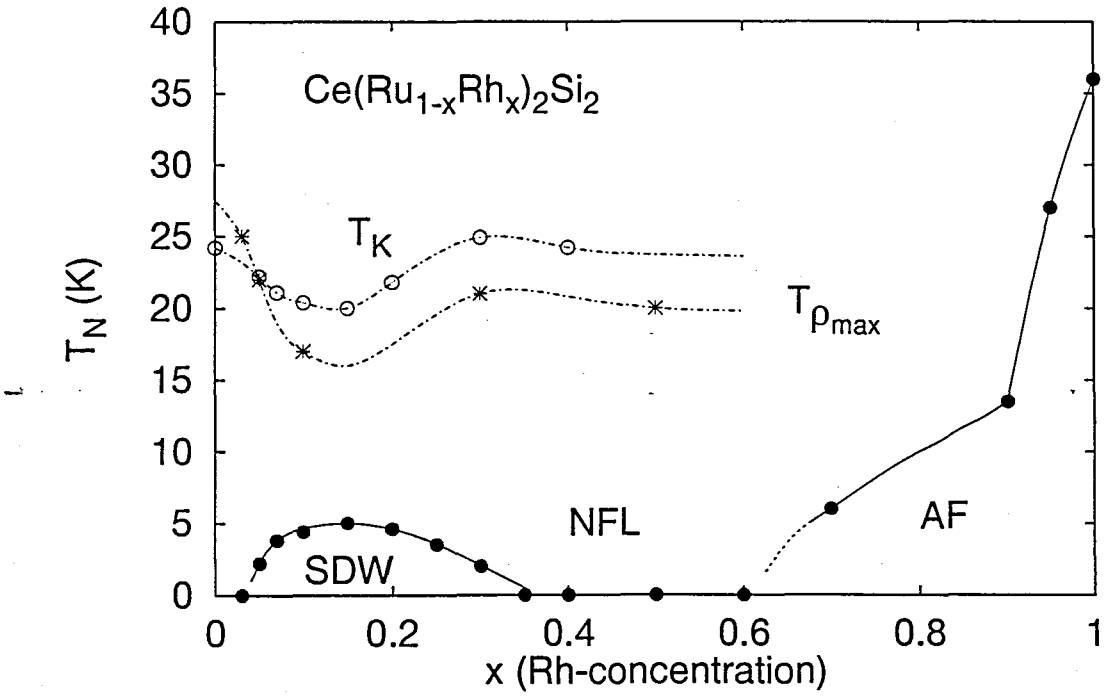

Figure 3.12: The phase diagram of $Ce(Ru_{1-x}Rh_x)_2Si_2$. The solid and broken lines are guides to eyes. T_K in the figure are sited from Ref. [34].

Figure 3.13 shows an enlarge-scaled phase diagram in the low Rh-concentration region. The most striking results of the study for low Rh-concentration region in $Ce(Ru_{1-x}$-

$Rh_x)_2Si_2$ is an absence of the NFL behavior near the QCP of the SDW phase, $x = 0.03$. The Neel line of SDW transition can be extrapolated to 0 around $x = 0.03$. It means that the QPT is occurred at $x \sim 0.03$ on the zero-temperature line. According to the inelastic neutron scattering experiment performed by Sato *et al.* [29], for $x = 0.03$ the antiferromagnetic correlation is strongly enhanced from $x = 0$, where the characteristic energy is reduced by the factor of 2. It is the microscopic evidence of the approaching to the QCP as x increasing from 0 to 0.03.

On the zero-temperature line it is a quantum fluctuation that collapses the magnetic order. In nonmagnetic region the magnetic moments does not fluctuate thermally but form a 'quantum' coherent state in which the 'up'-spin state and 'down'-spin state are combined. In the case of the HF systems the 'quantum' state is a coherent FL state which is formed through the hybridization between the conduction electrons and 'magnetic' f-electrons. In general description of the QPT, the coherent state should be unstable down to $T = 0$ as well as the magnetic ordered state at the QCP. Therefore the coherent line, which is the crossover line between the thermal fluctuating state and the coherent FL state, should vanish and the NFL behavior is expected to be observed down to 0 K at the QCP (See Fig.1.4). However in Fig. 3.13 the coherent line seems to connect from nonmagnetic side ($x \leq 0.03$) to magnetic side ($x > 0.03$) continuously. The coherent temperature $T_{\rm coh}$ is defined as the temperature where the resistivity starts to deviate from a T^2 behavior (See Fig. 3.10). We can expect two reasons why the NFL behavior did not observed near this QCP, which are

1. The region where the NFL behavior can be observed is very narrow. We has never reached that region in the experiment.

2. There is no region the NFL behavior is kept down to $T = 0$. In this case the phase transition occurs from the coherent FL state to the SDW state, like a superconducting phase transition, near the QCP.

In the first senario, the coherence line vanished at the QCP between $x = 0.03$ and 0.05, although we did not observe in the experiment. On the other hand, because the magnetic ordered state for $x > 0.03$ is the SDW state, the second scenario can be applicable. The SDW phase transition can be occurred from the coherent FL state because it caused by the nesting of the Fermi surface. It is very interesting what leads the QPT at this QCP. It may be the first order phase transition. However it has been a quite open question. It is a future subject.

In Fig. 3.14 I shows the enlarge scaled phase diagram in the intermediate Rh-concentration region. As I mentioned in Sec 3.1, the NFL behavior in the specific heat and the susceptibility was observed in a very wide range of this concentration region, for $0.3 \leq x \leq 0.5$. In the region of the SDW ground state, below $T_{\rm N}$, a finite $T_{\rm coh}$ exists. The coherent line seems to vanish in the intermediate region of the nonmagnetic ground state. Because we did not perfome the resistivity measurement for either $x = 0.35$ or 0.4, we cannot say about either how or where the coherent line vanishes. However the fact of that the specific heat keep the NFL behavior, logarithmic divergent behavior in C/T, down to 0.1 K indicates $T_{\rm coh}$ in the resistivity is also 0, not finite, over the intermediate nonmagnetic region. If it is true, there should be other origin besides the QPT of the NFL behavior. The coherent line should rise up as leaving from the QCP in the nonmagnetic region in the case of the QPT. The situation in this region is very complicated. This nonmagnetic region locate between two different QCP, therefore it is not so easy how the coherent line lies. Furthermore the effect of disorder cannot be negligible because of high substitution

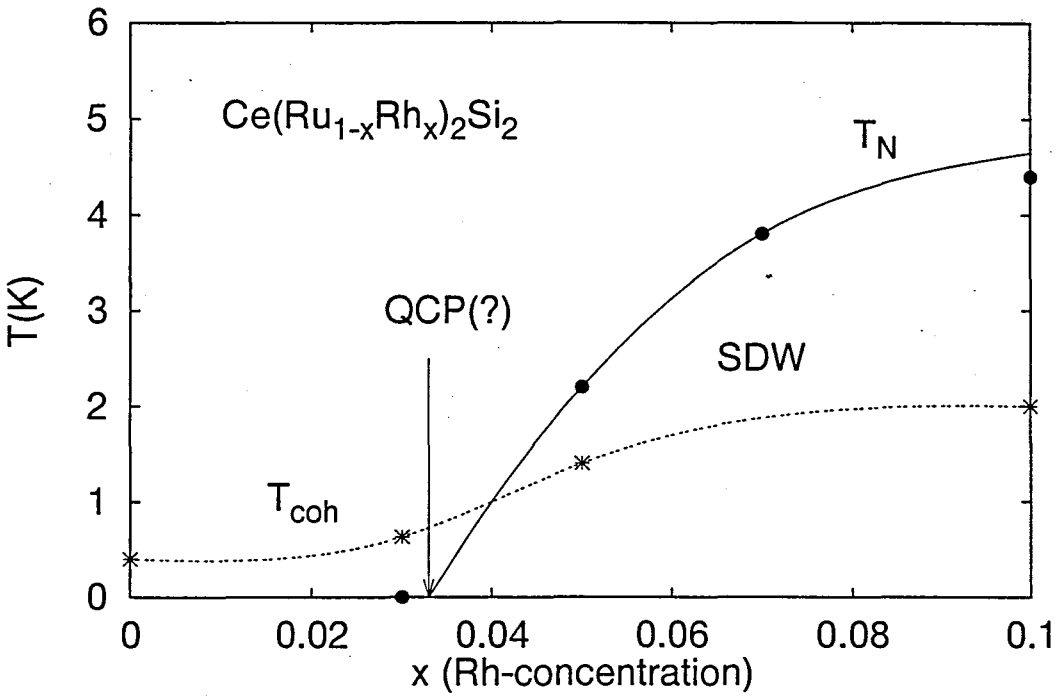

Figure 3.13: The enlarge-scaled phase diagram of $Ce(Ru_{1-x}Rh_x)_2Si_2$ ($x \leq 0.1$). The definition of T_{coh} is described in the text. T_{coh} for $x = 0$ is cited from Ref. [23].

of Ru for Rh. I will mention the further experimental study of the NFL in this region in Sec. 3.3.

3.2.2 CEF level of $Ce(Ru_{1-x}Rh_x)_2Si_2$

As I showed in Sec. 3.1, the magnetic susceptibilities of $Ce(Ru_{1-x}Rh_x)_2Si_2$ have almost no x-dependence in the high temperature, above 100 K, which show the Curie-Weiss law. I analyze the high temperature susceptibilities by the CEF model in the low and intermediate Rh-concentration region respectively. $Ce(Ru_{1-x}Rh_x)_2Si_2$ has a tetragonal crystal structure and the valence of Ce-ion is +3, whose total angular momentum $J = 5/2$, therefore whose CEF level can be drawn as Fig.3.15. Considering to the interaction between the Ce moment, we calculate the susceptibility with 4 parameter, Δ_1, Δ_2, a and the molecular field parameter λ. When the CEF parameters are determined, the magnetization within the first order of H is given by,

$$M = \frac{N_A(g_J\mu_B)^2 H}{Z^0} \sum_n \left[\sum_{m(lf)} \frac{|< m \mid J_\alpha \mid n >|^2}{k_B T} + 2 \sum_{m(hf)} \frac{|< m \mid J_\alpha \mid n >|^2}{E_m^0 - E_n^0} \right] e^{-E_n^0/k_B T} \tag{3.1}$$

where

$$Z^0 = \sum_n e^{-E_n^0/k_B T}$$

$$E_m^0 = E_n^0 \qquad \text{in the summation of } \sum_{m(lf)}$$

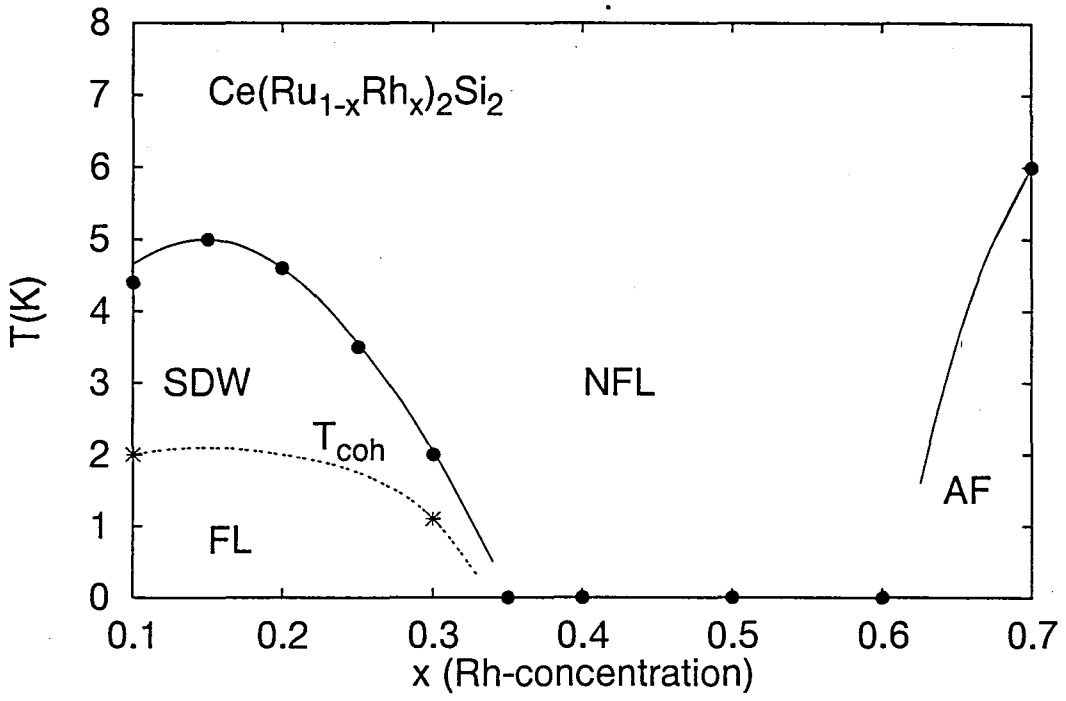

Figure 3.14: The enlarge-scaled phase diagram of $Ce(Ru_{1-x}Rh_x)_2Si_2$ ($0.1 \leq x \leq 0.7$).

$$E_m^0 \neq E_n^0 \qquad \text{in the summation of } \sum_{m(hf)} \tag{3.2}$$

$| n >$ is a wave function of an eigen state under the certain CEF and E_n^0 is its eigen energy. $\Delta_i = E_i^0 - E_0^0$ is a splitting energy between the excitation and ground level. Considering the molecular filed, H in Eqn. 3.1 is replaced with $H + \lambda M$, and we obtain the susceptibility $\chi = M/H$.

In Fig. 3.16 I show the results of the calculations and the comparison it with the experimental results and the parameters used for the calculation in Table 3.1. Above 50 K the both results has a good agreement, however below 50 K the experimental results are reduced from the calculation ones in both Rh-concentration regions. It is the result by the reduction of the freedom of the magnetic moments due to the Kondo effect.

Table 3.1: The CEF and the molecular field parameters of $Ce(Ru_{1-x}Rh_x)_2Si_2$ system.

	Δ_1	Δ_2	a	λ
$Ce(Ru_{1-x}Rh_x)_2Si_2$ ($x \leq 0.15$)	180	1000	0.96	-10
$Ce(Ru_{1-x}Rh_x)_2Si_2$ ($0.30 \leq x \leq 0.50$)	170	1500	0.945	-14
$CeRu_2Si_2$ [22]	220	1000	–	–
$CeRu_2Si_2$ [46]	280	1000	0.96	–
$CeRh_2Si_2$ [44]	680	310	0.975	-40

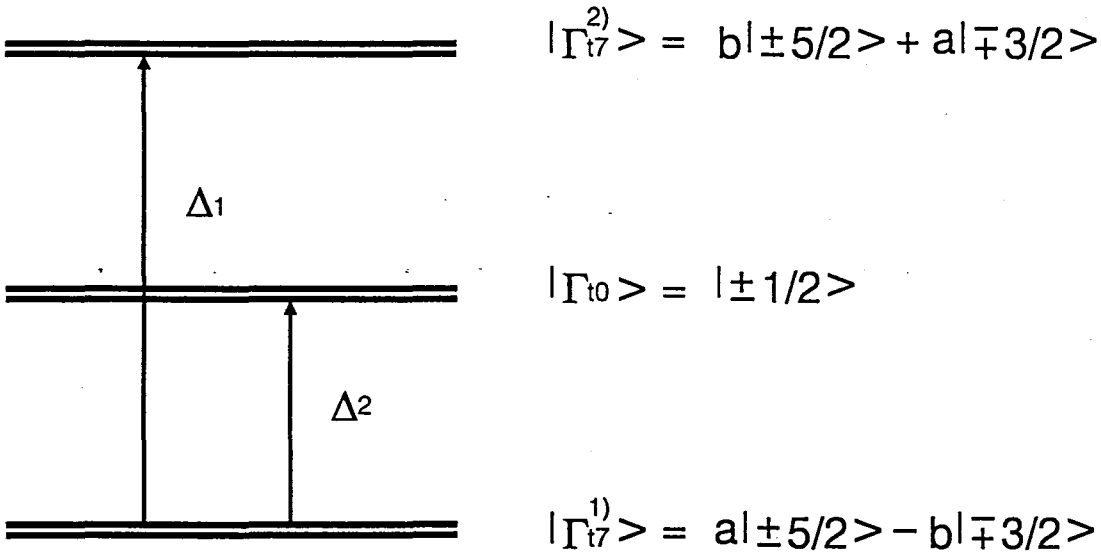

Figure 3.15: The energy level under the tetragonal CEF for $J = 5/2$.

(a)

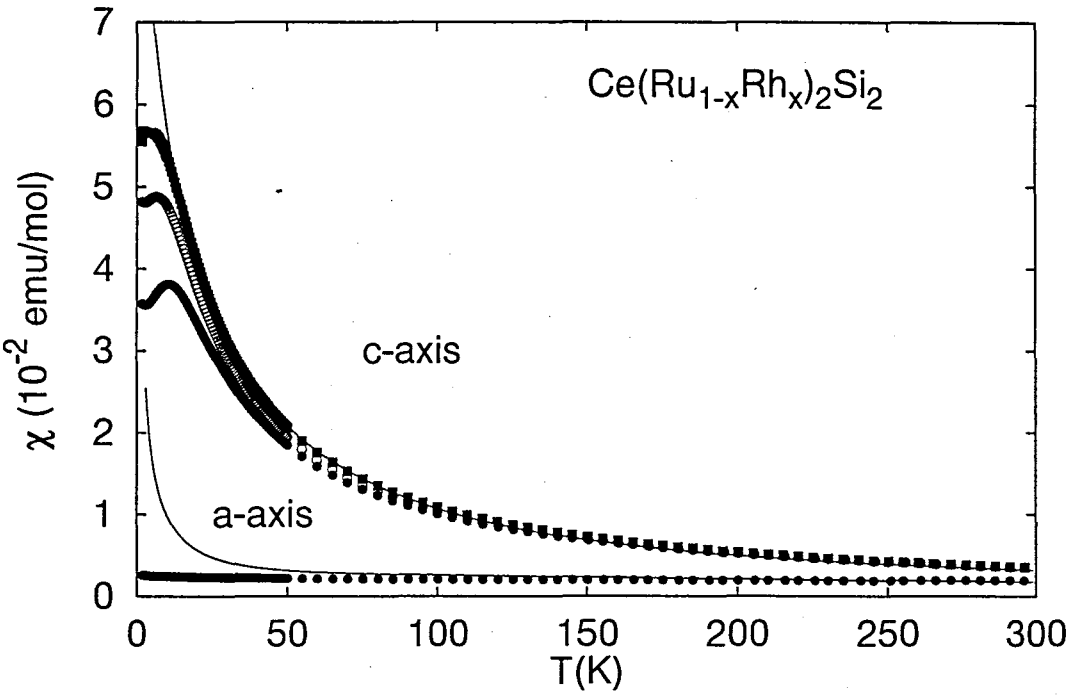

(b)

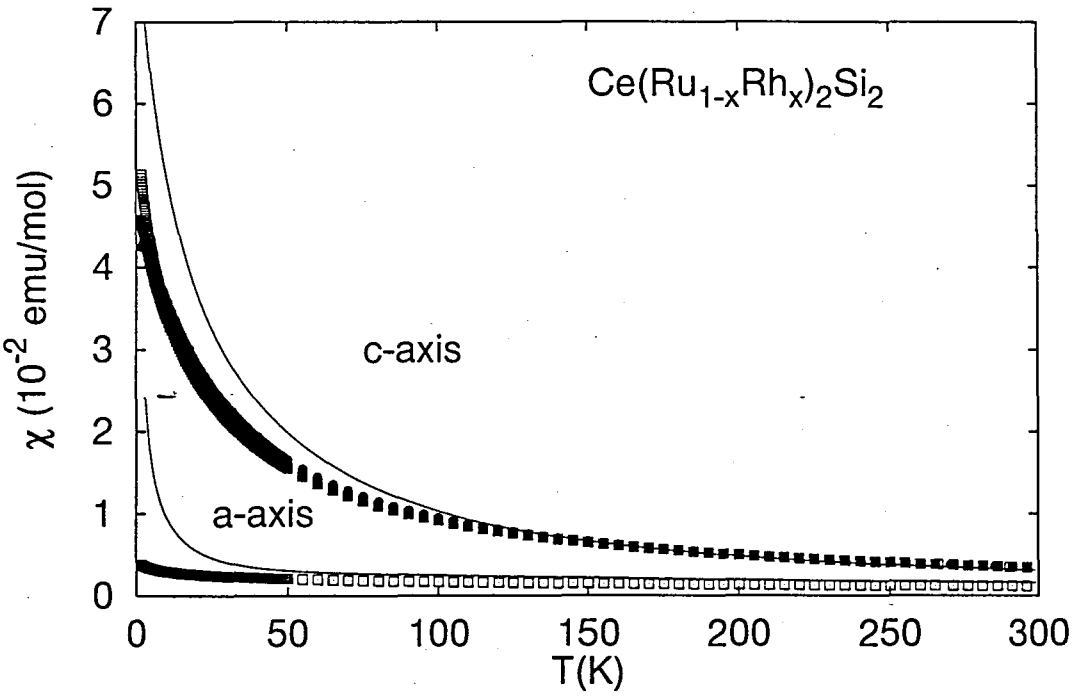

Figure 3.16: The calculation result of the susceptibilities by the CEF model in the (a) low Rh-concentration region and (b) intermediate Rh-concentration region. The solid lines are the calculation results. The CEF parameters used for the calculation are shown in Table 3.1.

3.2.3 The application of the SCR theory for the low and intermediate Rh-concentration region

As I discussed in the previous subsection, in the low Rh-concentration region the ground state is FL and the coherent temperature $T_{\rm coh}$ seems to not vanish at the QCP of the SDW phase, in spite of that the NFL behavior is expected to appear near the QCP. Recently S. Kambe *et al.* succeeded to explain the FL behavior of $Ce_{1-x}La_xRu_2Si_2$ and the NFL behavior of $CeCu_{6-x}Au_x$ near the each QCP by analyzing them based on the SCR theory [23]. Here, I also try to analyze the experimental results of $Ce(Ru_{1-x}Rh_x)_2Si_2$ based on this theory.

The SCR theory has established to describe the effect of the spin fluctuation of the itinerant electrons in narrow bands for the thermodynamic and transport properties in $3d$-transition metal compounds. Moriya and Takimoto recently predicted that the SCR theory can be applied also to describe the low temperature properties in HF systems [13]. The difference between $3d$-systems and HF systems is only their energy scale, which are correspond to their band width, $\sim 10^3$ K for $3d$-systems and ~ 10 K for HF systems, respectively. The theory describe their properties both in nonmagnetic, in magnetic region and near the QCP between both region because it treats not only the thermal but also the quantum spin fluctuations. According to the theory, the dynamical susceptibility $\chi(\boldsymbol{Q}+\boldsymbol{q},\omega)$ is parameterized as following,

$$\chi(\boldsymbol{Q}+\boldsymbol{q},\omega) \propto \frac{1}{\eta + Aq^2 - iC\omega/q^{z-2}} \tag{3.3}$$

where η is the reduced inverse staggered susceptibility, A and C are dimensionful constants reflecting the band structure of heavy quasi-particles and z is a dynamical exponent which represent the class of the spin fluctuation, which is 2 in a 3-dimensonal ($d = 3$) antiferrmomagnetic case. The third term in the numerator in Eq. 3.3 contains a contribution from the mode-mode coupling of the antiferromagnetic spin fluctuations. The theory neglect the higher order term of the coupling and determine the couping constant of the second term in a self-consistent fashion.

In the theory all thermodynamic and transport properties are driven from the dimenssionless inverse staggered susceptibility y ($= 1/(2T_{\rm A}\chi_{\boldsymbol{Q}})$), which is calculated in self-consistent from the sum-rule; the sum of the square local amplitude of the zero point and thermal spin fluctuation is constant. The self-consistent equation of y is given by,

$$y - y_0 = \frac{3}{2} y_1 \int_0^{x_c} {\rm d}x x^z \left[\ln(u) - \frac{1}{2u} - \Psi(u) \right] \tag{3.4}$$

with

$$u = x^{z-2}\frac{y + x^2}{t}, \qquad t = \frac{T}{T_0}, \qquad x = \frac{q}{q_{\rm B}} \tag{3.5}$$

where $q_{\rm B}$ is the cut-off wave number representing the effective zone boundary and x_c is the cut-off scaled wave number of the mode-mode coupling. T_0 and T_A are the energy scale of spin fluctuations characterizing the excitation of the frequency and wave number space, respectively. y_1 represent the mode-mode coupling constant for small q and y_0 represent the distance from the QCP at $T = 0$. The specific heat and the resistivity are given by the following equations from the value of y calculated by Eqn. 3.4 in the antiferromagnetic case.

$$C = 9R \int_0^{x_c} {\rm d}x x^2 \left\{ \left[u^2 - 2u\frac{{\rm d}y}{{\rm d}t} + (\frac{{\rm d}y}{{\rm d}t})^2 \right] \left[-\frac{1}{u} - \frac{1}{2u^2} + \Psi'(u) \right] \right.$$

$$-t\frac{\mathrm{d}^2 y}{\mathrm{d}t^2}\left[\ln(u)-\frac{1}{2u}-\Psi(u)\right]\Bigg\} \tag{3.6}$$

$$\rho = rR(t)$$

$$R(t) = 3\int_0^{x_c}\mathrm{d}x x^2\left[-1-\frac{1}{2u}+u\Psi'(u)\right] \tag{3.7}$$

where r is the rescaled factor of the resistivity, which is related with the coupling the conduction electrons and the localized moments of f-electrons. These expression is cited from Ref. [13]. M. Hatatani *et al.* obtained the uniform susceptibility at the QCP by considering the magnetic field dependence of y at low field [47]. I show the temperature dependences of some thermodynamic and transport quantities at the QCP in various classes of spin fluctuations in Table 3.2.

Table 3.2: Critical behavior at the QCP in various classes of spin fluctuations in the SCR theory

	η	$C(T)/T$	$\chi(T)$	$\rho(T)$
Ferro ($d=3,\ z=3$)	$T^{4/3}$	$-\ln T$	$T^{-4/3}$	$T^{5/3}$
Antiferro ($d=3,\ z=3$)	$T^{3/2}$	$1-T^{1/2}$	$1-T^{1/4}$	$T^{3/2}$

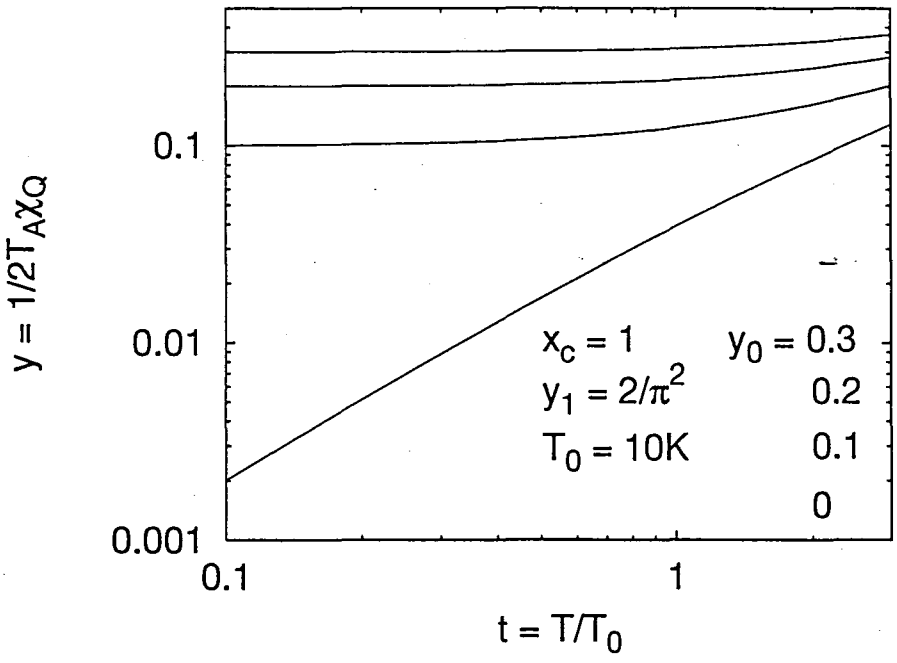

Figure 3.17: Calculated $y(T)$ by SCR theory using Eq. 3.4.

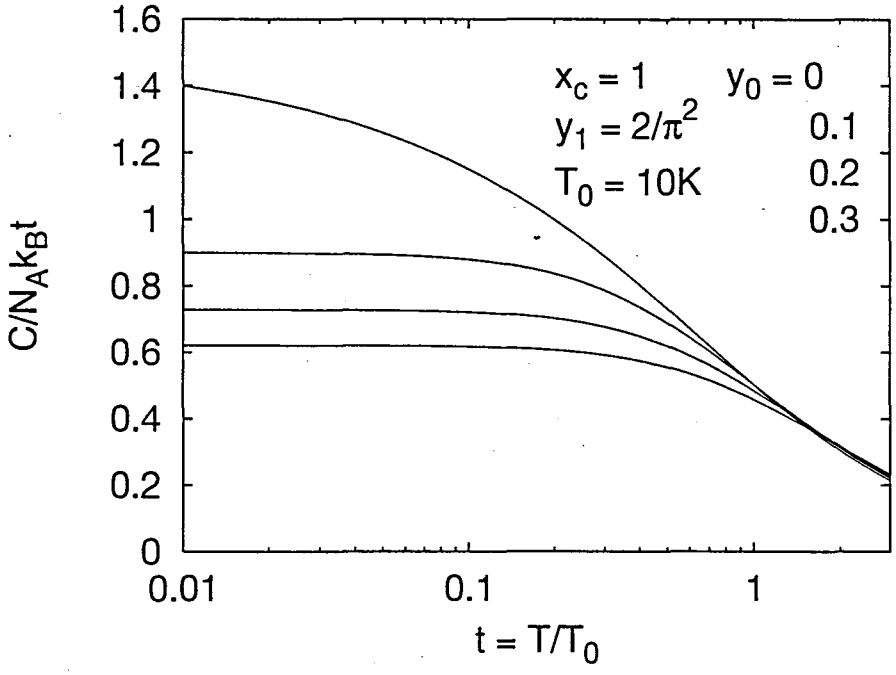

Figure 3.18: Calculated specific heat by SCR theory using Eq. 3.4.

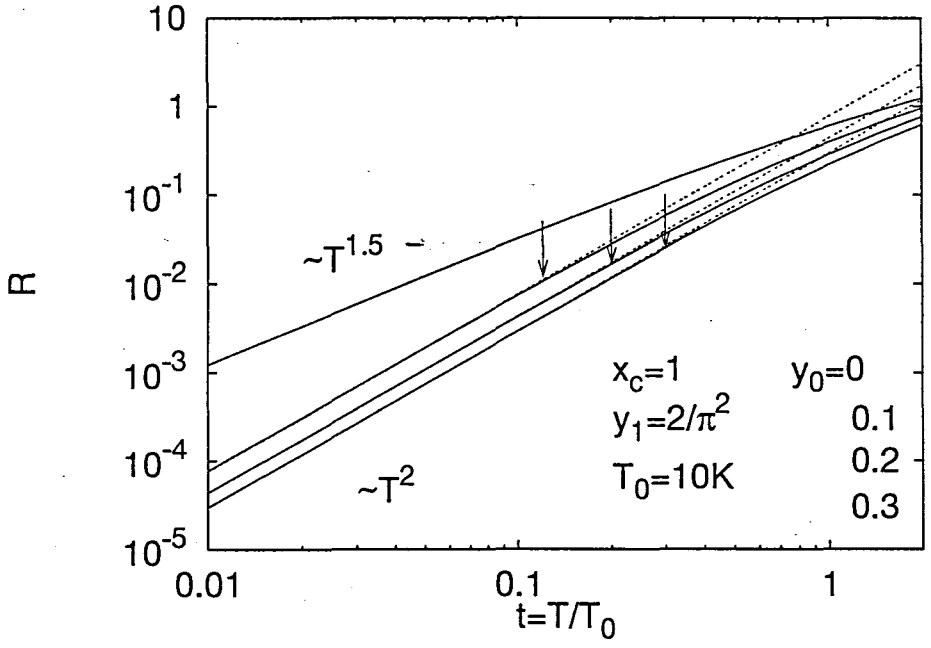

Figure 3.19: Calculated $R(T)$ by SCR theory using Eq. 3.4.

As leaving from the QCP, the FL-like temperature dependences recover in any physical quantities below $T_{\rm coh}$, which vanishes at the QCP. They can be calculated with 5 parameters $x_{\rm c}$, y_0, y_1, T_0 and $T_{\rm A}$. For the simplicity of the analysis, the value of $x_{\rm c}$ is fixed to 1. I show the calculating $y(T)$, $C(T)/T$ and $\rho(T)$ in the antiferromagnetic case in Fig. 3.17, 3.18 and 3.19, respectively. In Fig. 3.18 we can find the logarithmic divergent behavior of C/T in the intermediate temperature range $0.2T_0 \leq T \leq 2.0T_0$ with $y_0 = 0$, however at lower temperature C/T deviate from the $-\log T$-line and saturate to the finite value at $T = 0$. These results reproduce the NFL behavior in experiments well, $C/T \sim -\log T$, $\rho \sim T^n$ with $n < 2$ and $\chi \sim 1 - T^a$ with $a \sim 1/2$. In this framework the typical NFL behavior, $C/T \sim -\log T$, is the intermediate behavior. When T_0, which is roughly $T_{\rm K}$, is very small, $-\log T$ dependence of C/T may continue down to the lowest temperature in experiment, as in $CeCu_{5.9}Au_{0.1}$.

I show the calculation and experimental results of C/T of $x = 0$ and 0.03 in Fig. 3.20. There is a good agreement between both results. The parameters used in the calculations are listed in Table 3.3. Figure 3.21 shows the calculation and experimental results of the rescaled resistivity R of $x = 0.03$ along both axes with the same parameters used in the calculation of C/T. The poorer agreement is found in the resistivity at high temperature as compared with that of C/T. The susceptibility at $T = 0$ is given in the SCR description by,

$$\frac{1}{\chi(0)} = 2(1 + y_0)T_{\rm A} \tag{3.8}$$

$T_{\rm A}$ obtained from the experimental value of $\chi(0)$ for each concentration are listed in Table 3.3. In the table I also show the the parameters obtained from the spin-lattice relaxation rate $1/T_1$ in the NMR measurement [48], which agree with the parameters obtained from the specific heat.

The dynamical susceptibility $\chi(\boldsymbol{Q}+\boldsymbol{q}, \omega)$ is a complex number and their imaginary part ${\rm Im}\chi(\boldsymbol{Q} + \boldsymbol{q}, \omega)$ is related with the magnetic excitation spectrum, which can be obtained from the inelastic neutron scattering experiment. In the framework of the SCR theory, ${\rm Im}\chi(\boldsymbol{Q} + \boldsymbol{q}, \omega)$ is parameterized as,

$${\rm Im}\chi(\boldsymbol{Q} + \boldsymbol{q}, \omega) = \frac{\chi_{\boldsymbol{Q}+\boldsymbol{q}}(\omega/\Gamma_{\boldsymbol{Q}+\boldsymbol{q}})}{1 + (\omega/\Gamma_{\boldsymbol{Q}+\boldsymbol{q}})^2} \tag{3.9}$$

where

$$\Gamma_{\boldsymbol{Q}+\boldsymbol{q}} = 2\pi T_0(y + x^2), \qquad \frac{1}{\chi_{\boldsymbol{Q}+\boldsymbol{q}}} = 2T_{\rm A}(y + x^2) \tag{3.10}$$

I show the calculation results of $\Gamma_{\boldsymbol{Q}+\boldsymbol{q}}$ and $1/\chi_{\boldsymbol{Q}+\boldsymbol{q}}$ with $\boldsymbol{Q} = (0\ 0\ 0.35)$ comparing with the experimental results, which were obtained by Sato *et al.* [29], in Fig. 3.22. The parameters are also listed in Table 3.3. Comparing with the parameters obtained from other experiments, they have a good agreement with each other except for $T_{\rm A}$. The value of $T_{\rm A}$ obtained from $1/\chi_{\boldsymbol{Q}+\boldsymbol{q}}$ is much larger than that obtained from the uniform susceptibility or the NMR measurements. $T_{\rm A}$ is the parameter which represents the strength of the dispersion of spin fluctuations and is linked to the dispersion relation around the antiferrmagnetic wave vector $\boldsymbol{Q}$, $\Gamma_{\boldsymbol{Q}} - \Gamma_{\boldsymbol{Q}+\boldsymbol{q}} \propto Aq^2$ by $T_{\rm A} = Aq_{\rm B}^2/2$. However, far from $\boldsymbol{Q}$, this approximation of the dispersion relation is not valid because of an effect of the higher-order terms of $\boldsymbol{q}$ which are neglected near $\boldsymbol{Q}$. (See Fig. 3.23). We may estimate the small value of $T_{\rm A}$ from the uniform susceptibility on account of this.

Next I discuss on the x-dependence of the parameters obtained from the experiments. y_0, is the value represent the distance from the QCP at $T = 0$, decreases as x increasing.

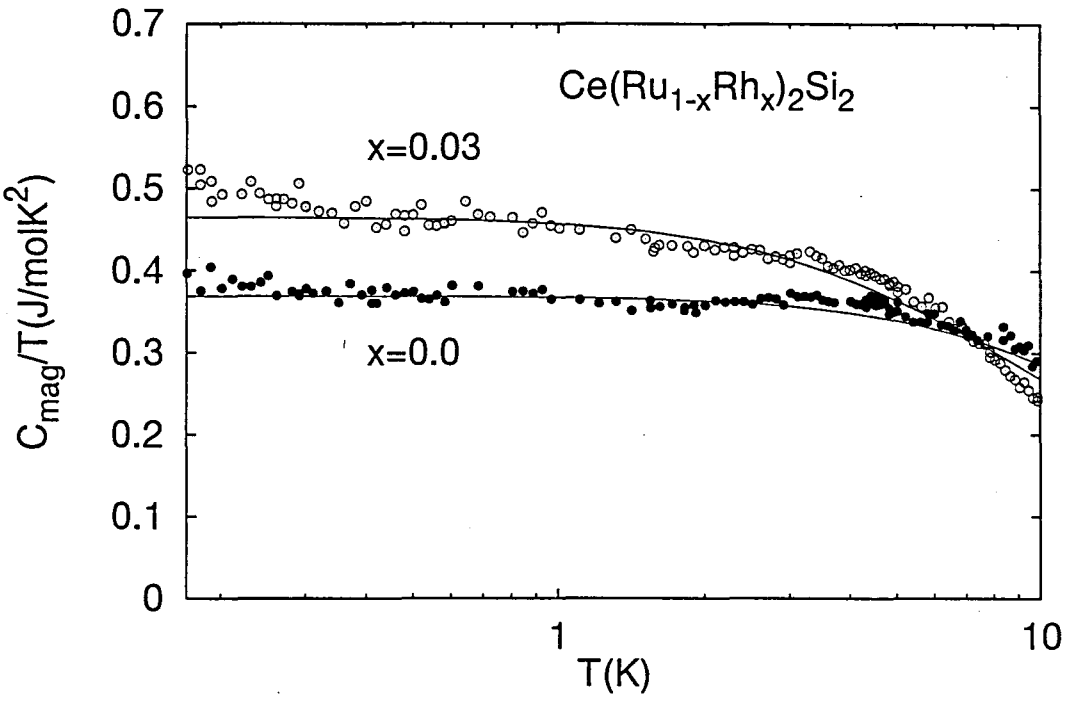

Figure 3.20: The calculation results of the specific heats of $x = 0$ and 0.03 by SCR theory using the parameters listed in Table 3.3 with comparing with the experimental results. The solid lines represent the calculation results.

It is consistent with the experimental fact that the system approaches to the QCP as x increasing. On the other hand T_0 slightly increases as x increasing in contrast with the decreasing of T_K estimated from the experiment, for example T_{max} of the resistivity. Assuming $T_0 \approx T_K$, we estimate the almost x-independent value of y_0. The calculation has too much parameters to determine them without ambiguity from one expeiment. We try to analyze some experiments and obtain the same tendency of the variation of the parameters with x. Therefore I conclude that the low temperature properties in the low Rh-concentration region can be explained by the SCR theory well. However there still remains the problem of the variation of T_{coh}. As I stress in Sec. 3.2.1, T_{coh} seems not to vanishes at the QCP but to slightly increase. In the framework of the SCR theory the crossover temperature T_{cr} from the classical regime to the quantum regime in the paramagnetic state, which is related with T_{coh}, is given by $T_{cr} \sim y_0 T_0$. T_{cr} calculated from the parameters listed in Table 3.3 decreases to 0 approaching to the QCP in contrast with T_{coh}. Further experiment for much closer concentration to the QCP is needed.

In the intermediate Rh-concentration region the NFL behavior is observed for $x = 0.4$ and 0.5. I show the calculation results of C/T in Fig. 3.24. In the calculation I fixed the value of y_0 at 0 because of their wide temperature range where the $-\log T$ dependence of C/T were observed. The parameters used for the calculation is also listed in Table 3.3. The agreement between the calculation and experimental results is not so bad. And other physical quantities, the resistivity and the susceptibility, for $x = 0.5$ has very similar temperature dependence predicted at the QCP by the SCR theory. However it is unreasonable that y_0 is 0 in the wide x-region, which should be 0 only at the QCP. I will discuss on the NFL behavior in the intermediate Rh-concentration region, especially

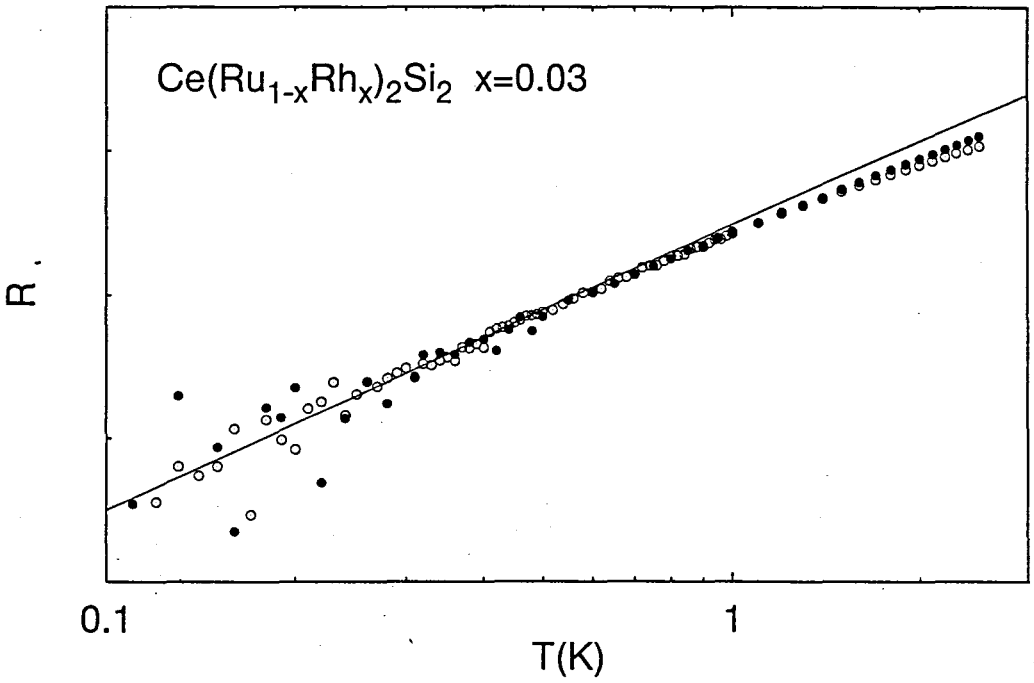

Figure 3.21: The calculation results of the rescaled resistivities of $x = 0.03$ by SCR theory using the parameters listed in Table 3.3 with comparing with the experimental results along a- (open circle) and c-axis (filled circle). The solid lines represent the calculation results.

for $x = 0.5$ and 0.6, in Sec. 3.3, including the crossover from the NFL to the FL by applying a magnetic field. There seems to be the interplay between the disorder effect caused by alloying and the quantum critical fluctuation.

Table 3.3: The parameters of the SCR theory obtained from the experiments in $Ce(Ru_{1-x}Rh_x)_2Si_2$, $Ce_{1-x}La_xRu_2Si_2$ and $CeCu_{6-x}Au_x$ system. The parameters for $Ce(Ru_{1-x}Rh_x)_2Si_2$ with $x = 0.03$ obtained from $1/T_1$ are referred from Ref. [48] and the parameters for $Ce_{1-x}La_xRu_2Si_2$ and $CeCu_{6-x}Au_x$ are referred from Ref. [23].

	y_0	y_1	T_0	T_A
$Ce(Ru_{1-x}Rh_x)_2Si_2$				
$x = 0$ (C, χ_0)	0.30	0.50	14.0	16.5
$x = 0.03$ (C, χ_0)	0.08	0.70	17.0	14.6
$x = 0$ (Γ_Q, χ_Q)	0.15	1.0	10.0	34.0
$x = 0.03$ (Γ_Q, χ_Q)	0.03	1.0	17.0	62.0
$x = 0.03$ ($1/T_1$)	0.025	0.3	15.0	12.0
$x = 0.4$ (C, χ_0)	0.0	3.0	13.0	13.9
$x = 0.5$ (C, χ_0)	0.0	5.5	10.0	10.3
$Ce_{1-x}La_xRu_2Si_2$				
$x = 0$ (C, χ_0)	0.31	1.6	14.1	16
$x = 0.05$ (C, χ_0)	0.10	1.33	14.7	14
$x = 0.075$ (C, χ_0)	0.05	0.77	14.2	11
$CeCu_{6-x}Au_x$				
$x = 0$ (C)	0.40	10.0	3.0	–
$x = 0.1$ (C)	0.003	16.7	3.4	–

(a)

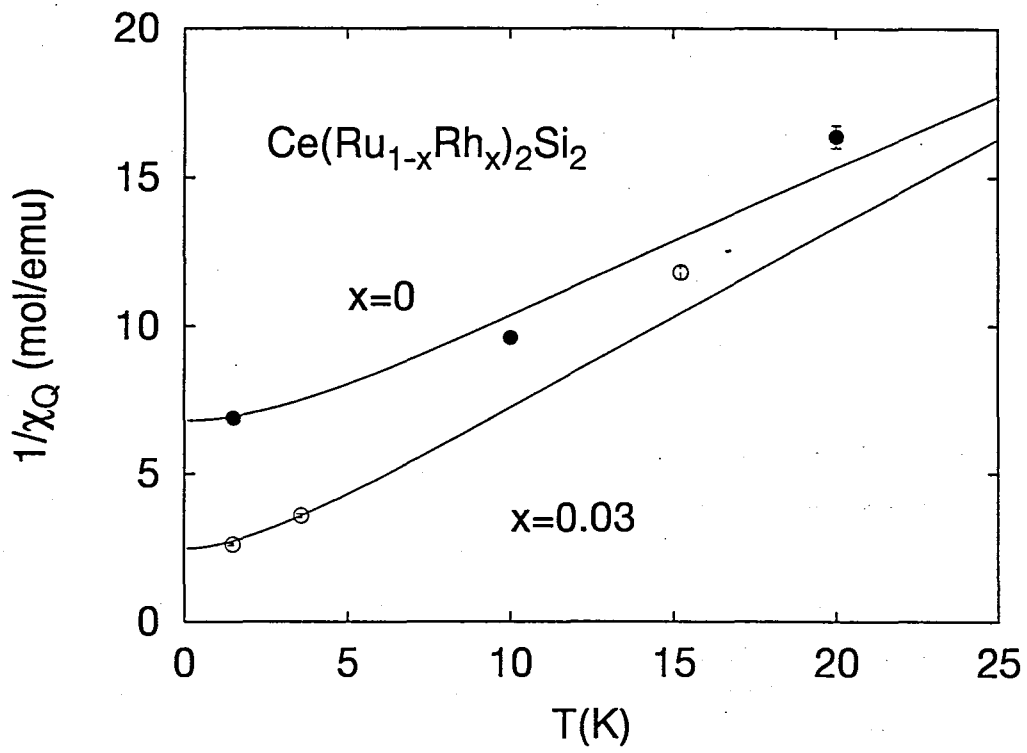

(b)

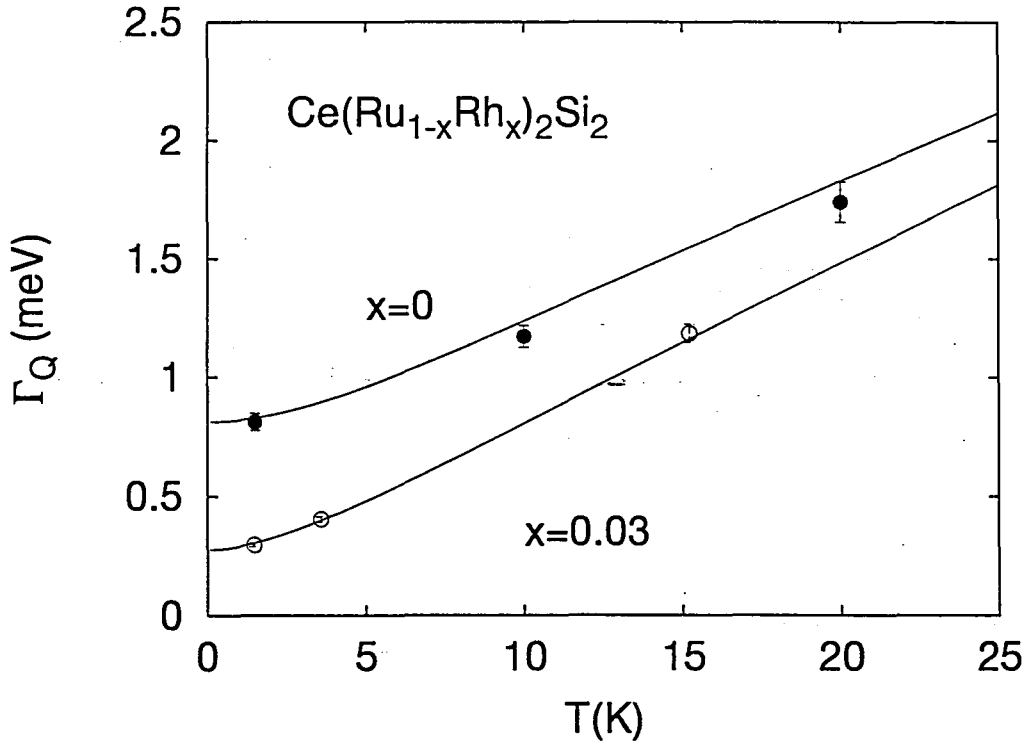

Figure 3.22: The staggered susceptibility (a) and the energy line width of spin fluctuation with $\boldsymbol{Q} = (0\ 0\ 0.35)$ of $x = 0$ and 0.03. The solid line represent the calculating results for each concentrations by SCR theory. using the parameters listed in Table. 3.3.

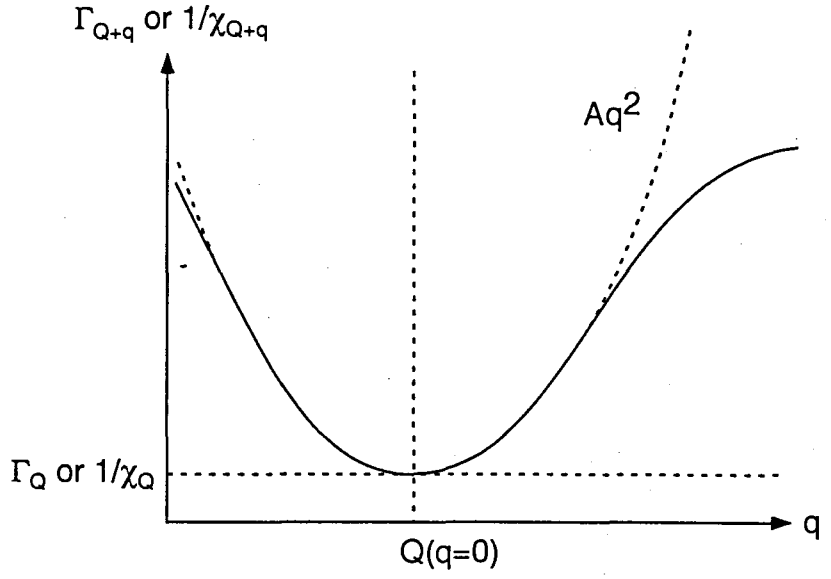

Figure 3.23: The schematics of the dispersion relation of Γ_{Q+q} or $1/\chi_{Q+q}$. The dashed line is an extrapolating curve from the small q approximation. The solid line is an expected curve with higher-order terms of q.

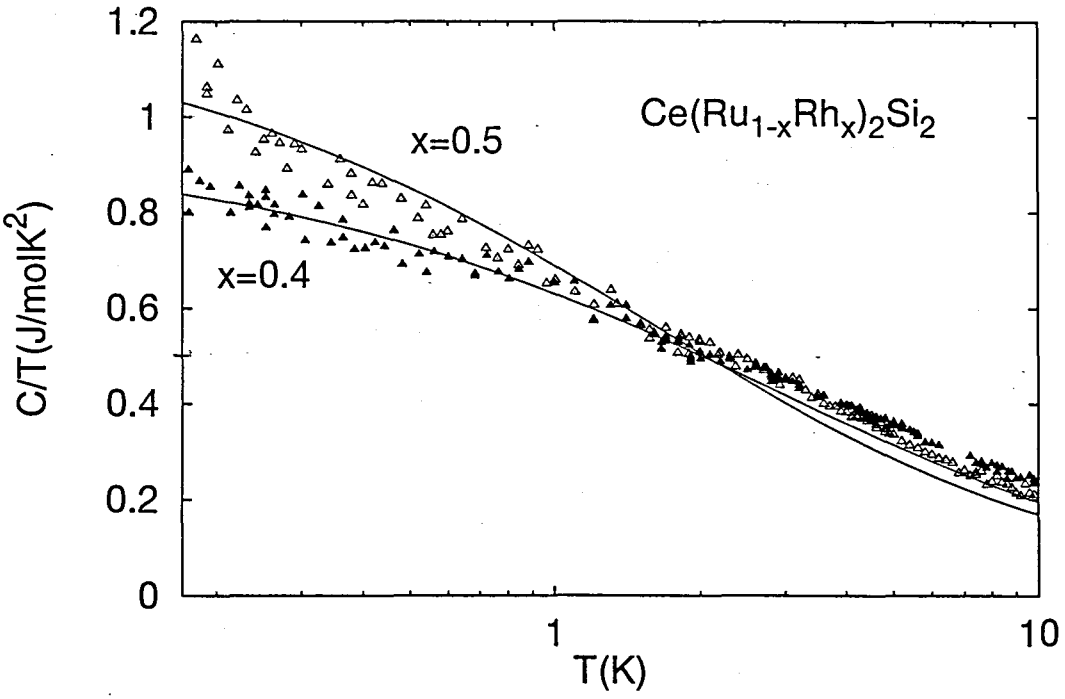

Figure 3.24: The calculation results of the specific heats of $x = 0.4$ and 0.5 by SCR theory using the parameters listed in Table 3.3 with comparing with the experimental results. The solid lines represent the calculation results.

3.2.4 Discussion on the disorder effect in the intermediate Rh-concentration region – The distribution of the Kondo temperature

In this subsection I argue the effect of the disorder due to the substitution Ru for Rh for the thermodynamic properties in the intermediate Rh-concentration region. The crystallographic disorder or the frustration of the magnetic interaction, which are expected in this region, may influence to the physical properties in complex. As a first step to understand the effect of disorder I try to analyze the specific heat and the susceptibility by considering the distribution of the Kondo temperature. It is the most simple approximation of the influence of the disorder. The crystallographic disorder leads the distribution of the local density of the conduction electron $\rho_{\rm F}^i$ or the strength of the local Kondo interaction $J_{\rm K}^i$, which cause the distribution of the local Kondo temperature $T_{\rm K}^i$. In this model, Kondo disorder model, the interactions between the remaining local moments at a temperature are neglected. Only the competition between the thermal fluctuation of the remaining local moments and the local Kondo effect is considered independently at each Ce-site. In this sense the Kondo disorder model is the single-site model. The low temperature anomalous behavior, the NFL behavior, comes from the 'living' local moments which is uncompensated by the Kondo effect because of their low $T_{\rm K}$.

In a recent paper O. O. Bernal *et al.* have reported the results of the analyzing the specific heat, the uniform susceptibility and the local susceptibility measured by NMR of $UCu_{5-x}Pd_x$ for $x = 0.1$ and 0.15 based on the Kondo disorder model [16]. The model successfully explain the experimental results. Therefore we try to analyze the data by the same means. For the first time we assume the Gaussian distribution of $\lambda = \rho_{\rm F} J_{\rm K}$ with the average value $< \lambda >$ and the rms width w.

$$P(\lambda) = \frac{1}{\sqrt{2\pi}w} \exp(-\frac{(\lambda - < \lambda >)^2}{2w^2}) \tag{3.11}$$

$T_{\rm K}$ is given by using λ as $T_{\rm K} = \varepsilon_{\rm F} \exp(-1/\lambda)$, where $\varepsilon_{\rm F}$ is the Fermi energy of the conduction electron band. The distribution of $T_{\rm K}$ is given by,

$$P(T_{\rm K}) = \mid \frac{{\rm d}\lambda}{{\rm d}T_{\rm K}} \mid P(\lambda(T_{\rm K})) \tag{3.12}$$

When we denote the specific heat and the magnetization with one unique $T_{\rm K}$ as $C(T_{\rm K};T)$ and $M(T_{\rm K};T,H)$ respectively, we can calculate the specific heat and the susceptibility as followings.

$$C(T) = \int_0^\infty {\rm d}T_{\rm K}\, P(T_{\rm K}) C(T_{\rm K};T) \tag{3.13}$$

$$M(T,H) = \int_0^\infty {\rm d}T_{\rm K}\, P(T_{\rm K}) M(T_{\rm K};T,H) \tag{3.14}$$

Here we use the expression of the resonant level model (RLM) [24], which is the phenomenological model for the explanation of the temperature dependence of thermodynamic quantities in the impurity Kondo system, as $C(T_{\rm K};T)$ and $M(T_{\rm K};T,H)$. Both expressions are

$$C(T_{\rm K};T) = \frac{\Delta}{\pi T}\left\{1 - \frac{\Delta}{2\pi k_{\rm B} T}\Psi'\left(\frac{1}{2} + \frac{\Delta}{2\pi k_{\rm B} T}\right)\right\} \tag{3.15}$$

$$M(T_{\rm K};T,H) = g\mu_{\rm B}\,{\rm Im}\left\{\frac{2}{\pi}\Psi\left(1+\frac{\Delta+ig\mu_{\rm B}\,H}{\pi{\rm kB}T}\right)\right.$$
$$\left.-\frac{1}{\pi}\Psi\left(1+\frac{\Delta+ig\mu_{\rm B}\,H}{2\pi k_{\rm B}\,T}\right)\right\} \tag{3.16}$$

Δ is the width of the DOS with Lorentzian shape at the Fermi energy and is roughly the size of the Kondo temperature. In Fig. 3.25 and 3.26 I show the calculation results of the specific heats, the susceptibilities by using the parameters listed in Table 3.4. The distribution functions with each parameters are shown in Fig. 3.27. When the distribution at $T_{\rm K}=0$ is finite, the thermodynamic quantities diverge down to $T=0$. From the distribution function we can calculate the mean value and the standard deviation of $T_{\rm K}$, $<T_{\rm K}>$ and $\sigma_{\rm K}$, in numerical,

$$<T_{\rm K}> = \int_0^\infty {\rm d}T_{\rm K}\,T_{\rm K}\,P(T_{\rm K}) \tag{3.17}$$

$$\sigma_{\rm K} = \int_0^\infty {\rm d}T_{\rm K}\,(T_{\rm K}-<T_{\rm K}>)^2P(T_{\rm K}) \tag{3.18}$$

which are also lited in Table 3.4.

Table 3.4: The parameters used for the calculations which are shown in Fig. 3.25 $\sim$ 3.27 are listed.

	$<\lambda>$	w	$\varepsilon_{\rm F}$ (K)	$<T_{\rm K}>$ (K)	$\sigma_{\rm K}$ (K)
(a)	0.2	0.001	10000	20.22	0.505
(b)	0.2	0.02	10000	21.71	10.37
(c)	0.2	0.05	10000	28.87	28.67

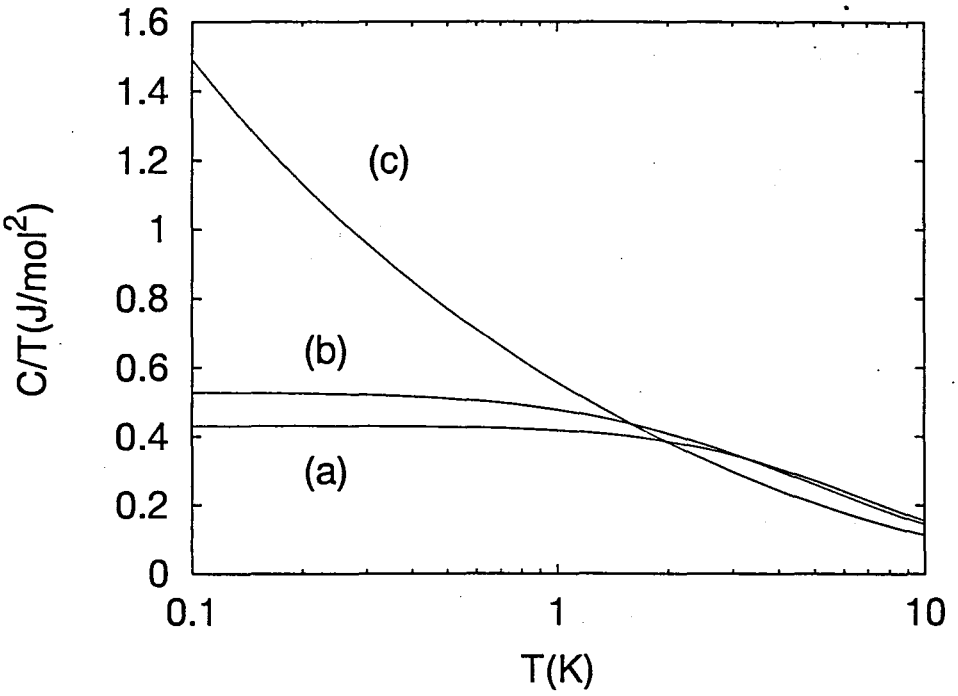

Figure 3.25: The calculation of the specific heats by the Kondo disorder model using the parameters listed in Table 3.4.

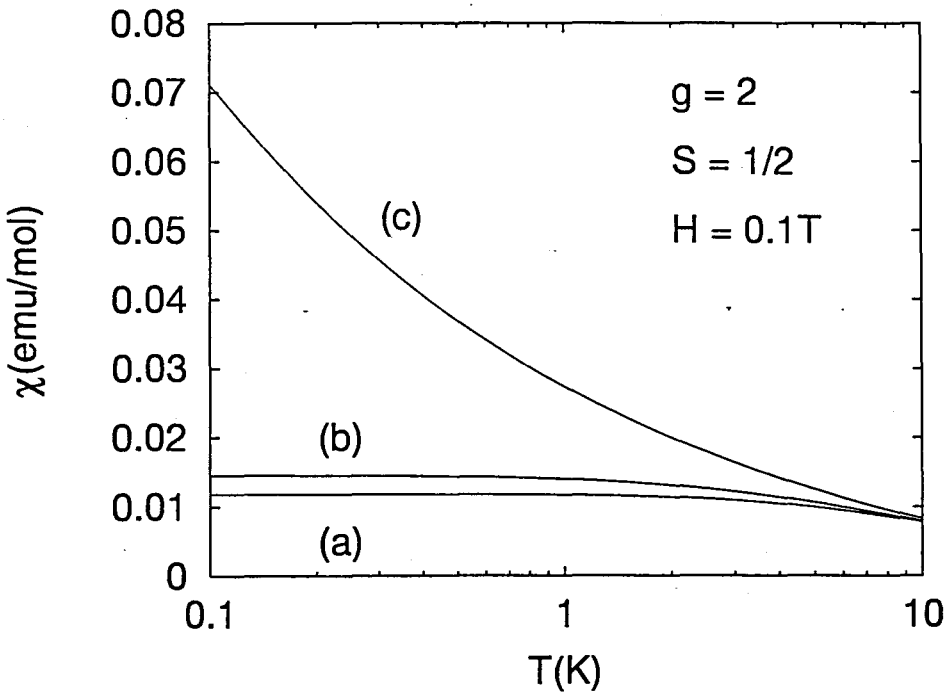

Figure 3.26: The calculation of the susceptibility by the Kondo disorder model using the parameters listed in Table 3.4.

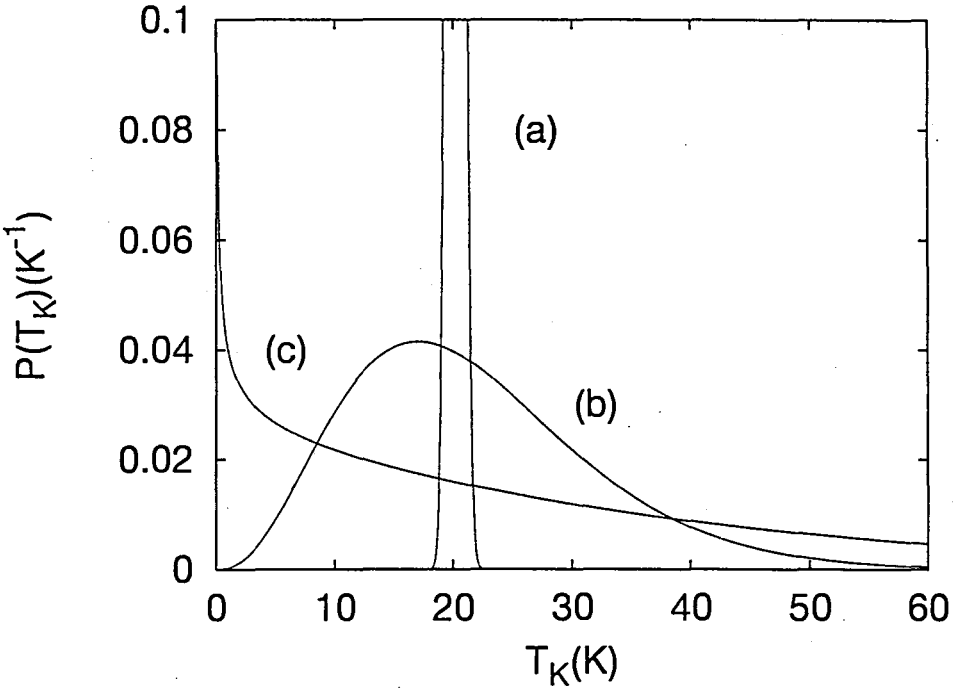

Figure 3.27: The distribution function of T_K with parameters listed in Table 3.4.

Figure 3.28 and 3.29 show the calculation results of the specific heats and the susceptibilities for $x = 0.4$ and 0.5 with comparing the experimental results, respectively. The agreements between the calculation and the experimental results of the susceptibilities are very good in the whole temperature range, while those of the specific heats are much poorer. The parameters used for the calculation of the specific heat and the susceptibility are different (listed in Table 3.5). I used the same parameters in the distribution function of λ and assumed the different Fermi energy, $\varepsilon_F = 3500$ K and 10000 K in the calculation of the specific heat and the susceptibility respectively. This disagreement may comes from the problem of the Wilson's ratio $(\pi^2 {k_B}^2/3{\mu_B}^2)(\chi(0)/\gamma(0))$ which is 1 in the RLM, however 2 in the numerical solution by K. Wilson [49] of the impurity Kondo problem. In the perturbation by U of the Anderson hamiltonian (see Eq. 1.3) the Wilson's ratio varies from 1 to 2 continuously. The RLM assumes the free electron without considering the correlation between electrons, therefore the Wiloson's ratio should be 1. In general the ratio in the HF system deviate from 1 by corresponding to the strong correlation between the quasi-particles. The lower Wilson's ratio leads naturally the lower T_K in the calculation of the specific heat than that of the susceptibility. In Fig 3.30 I show the distribution of T_K obtained from the calculation of the specific heats and the susceptibilities for $x = 0.4$ and 0.5. In this figure we can find that the distribution at $T_K = 0$ is almost 0 for both concentrations, which means the thermodynamic quantities must be going to saturate down to $T = 0$. C/T diverges logarithmically in the whole experimental temperature range, while the susceptibility seems to start to saturate. It is worth much while making sure whether the susceptibility saturate to the finite value or diverge down to $T = 0$.

The Kondo disorder model seems to explain the physical properties in the intermediate Rh-concentration region. Especially in this framework we can understand the appearance of the NFL behavior in the wide x region. However there are still something difficulty. One of them is the temperature dependence of the resistivity. As I mentioned above this model consider only the single-site effect. When the T_K merge to one unique value, the resistivity goes to the finite value ρ_0 with the temperature dependence $1 - AT^2$, which is the description of the local FL theory. The distribution of T_K modifies it as $1 - A'T$, which is predicted theoretically by Miranda *et al.* [15] and observed in $UCu_{5-x}Pd_x$ by R. Chau *et al.* [50]. On the other hand the resistivity in our system has a temperature dependence like $\rho_0 + AT^{1.6}$, which seems to be the modification of the coherent FL state. There is another difficulty in the magnetization process. I show the comparison the calculation results with the experimental ones of the magnetization by using the same parameters for the susceptibility in Fig. 3.31. The results roughly agree with the experimental ones, however the non-linearity in the low field cannot explain by this model.

Table 3.5: The parameters used for the calculations of the specific heats and the susceptibilities for $x = 0.4$ and 0.5 are listed.

	$<\lambda>$	w	ε_F (K)	$<T_K>$ (K)	σ_K (K)
$x = 0.4$ (C)	0.18	0.0215	3800	16.7	10.4
$x = 0.5$ (C)	0.18	0.025	3400	15.6	11.0
$x = 0.4$ (χ)	0.18	0.0215	10000	44.0	27.3
$x = 0.5$ (χ)	0.18	0.025	10000	45.8	32.4

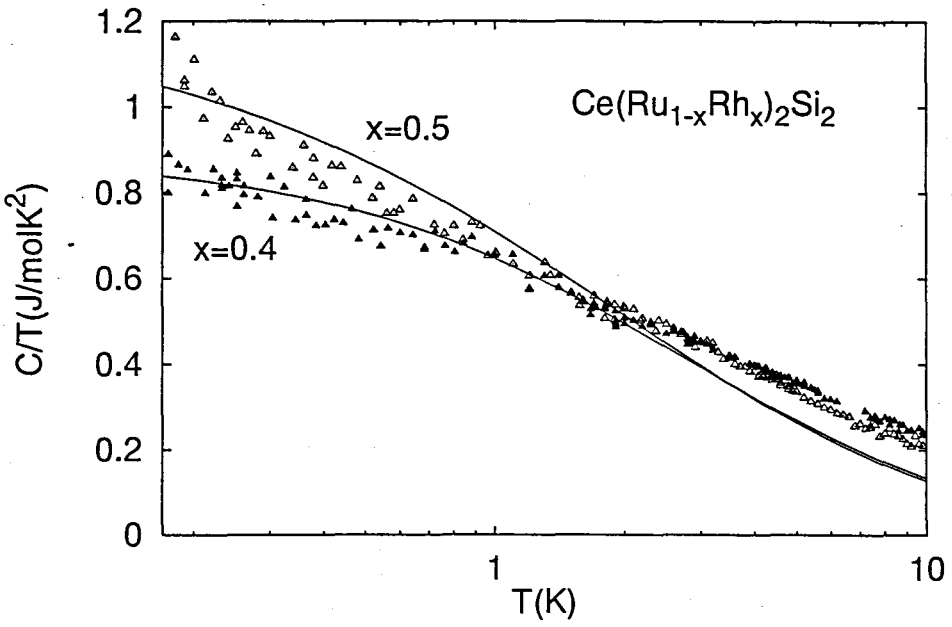

Figure 3.28: The calculation results of the specific heats for $x = 0.4$ and 0.5 based on the Kondo disorder model with comparing to the experimental results. The parameters used for the calculation are listed in Table 3.5.

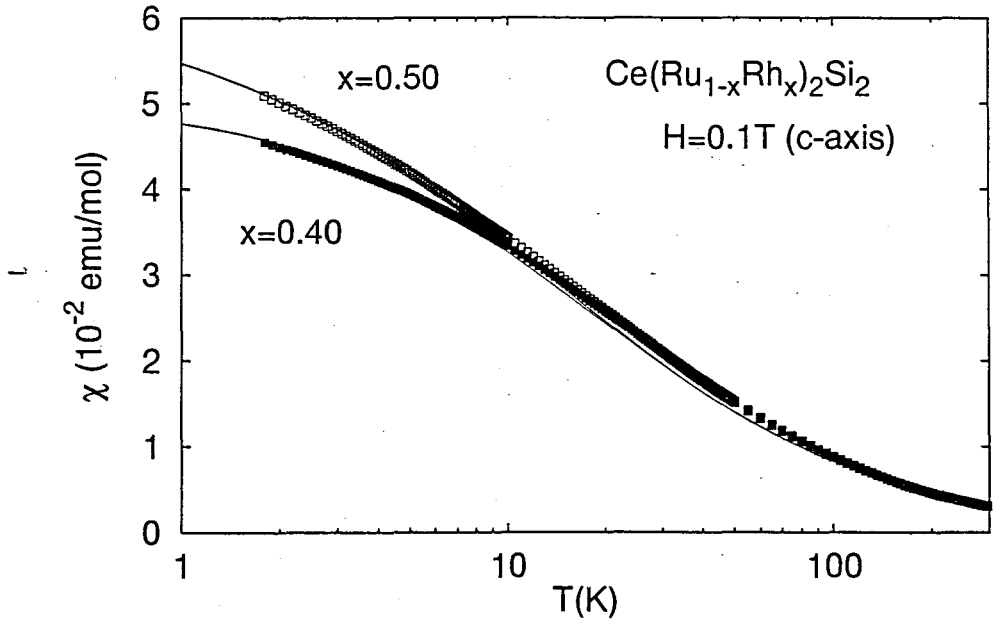

Figure 3.29: The calculation results of the susceptibilities for $x = 0.4$ and 0.5 based on the Kondo disorder model with comparing to the experimental results. The parameters used for the calculation are listed in Table 3.5.

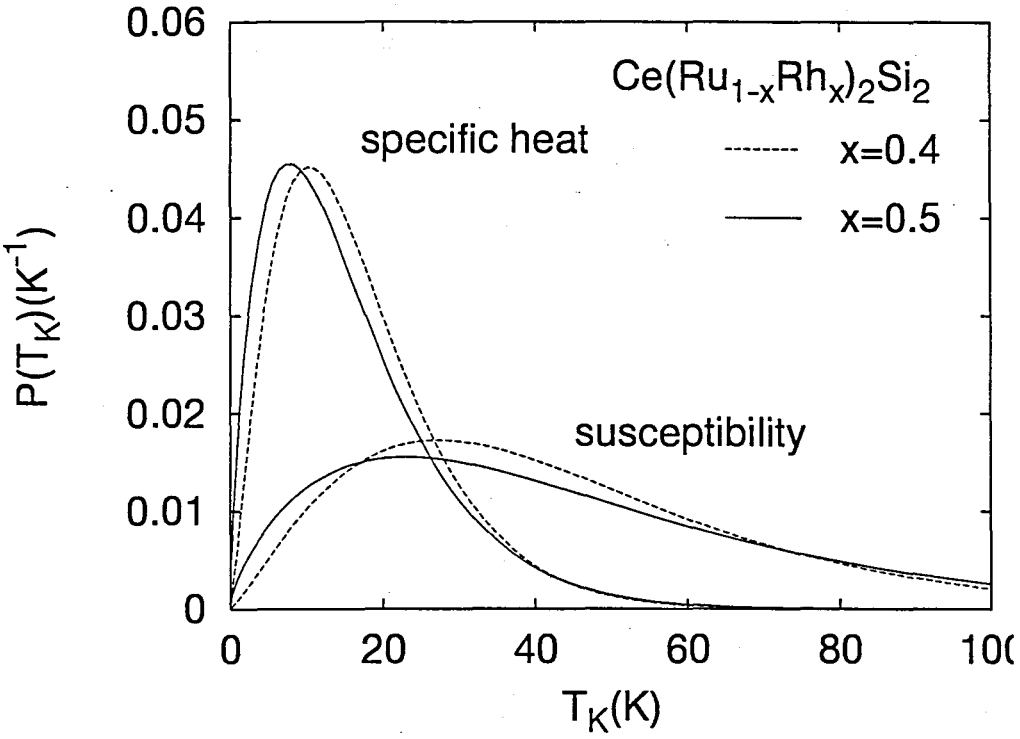

Figure 3.30: The distribution function of T_K obtained from the calculations of the specific heats and the susceptibilities for $x = 0.4$ and 0.5.

(a)

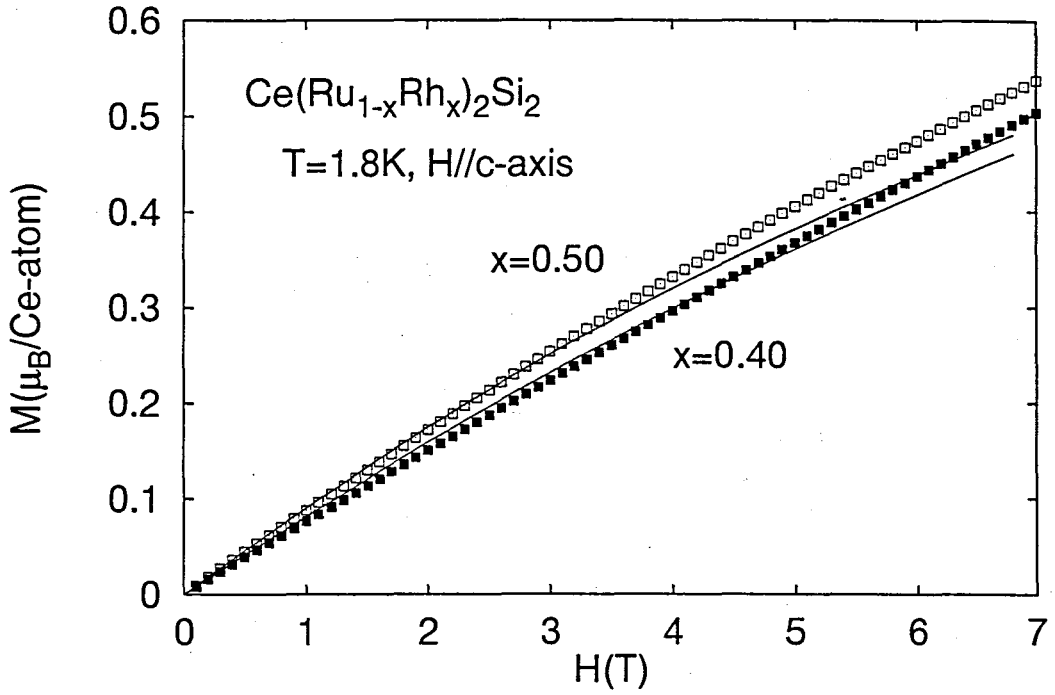

(b)

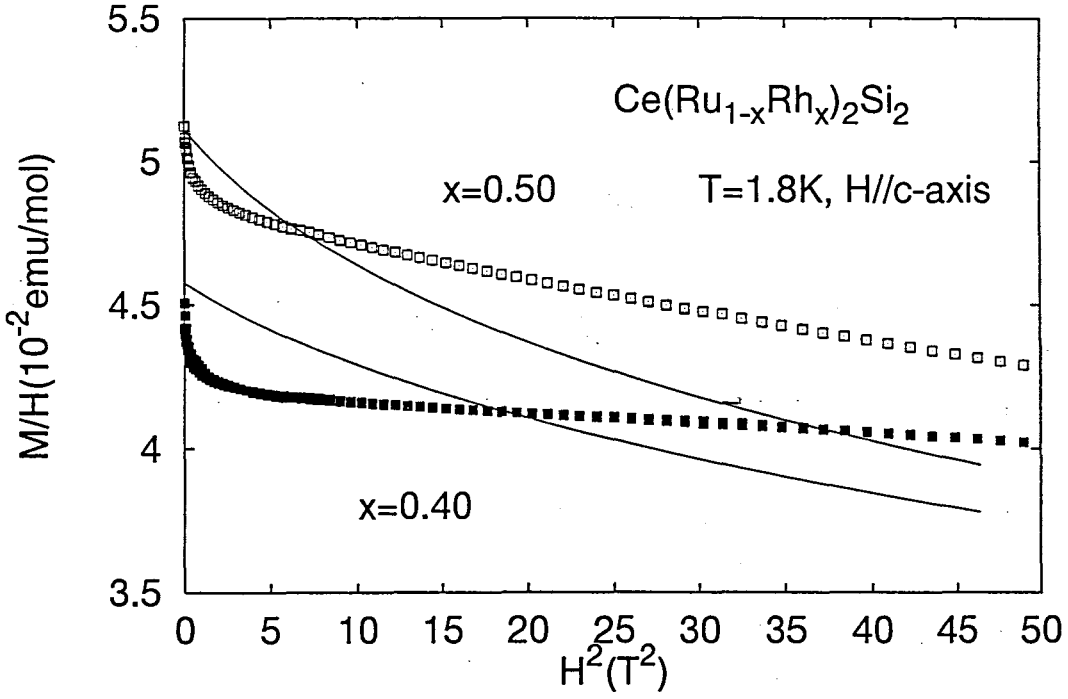

Figure 3.31: The calculation results of the magnetization for $x = 0.4$ and 0.5 based on the Kondo disorder model with comparing to the experimental results in the form of (a) M vs H and (b) M/H vs H^2. The parameters is the same for the calculation of the susceptibility.

3.3 The detailed study of the NFL behavior in the intermediate Rh-concentration region

In the preceding section I reported the NFL behavior ($C/T \sim -\log T$, $\chi \sim 1 - T^a$ $a = 1/3 \sim 3/4$, $\rho \sim T^{1.6}$) in the intermediate Rh-concentration region of $Ce(Ru_{1-x}Rh_x)_2Si_2$ system. In this section I will discuss on this anomalous behavior in more detail, especially for $x = 0.5$ and 0.6. In order to obtain further information of the NFL behavior, I performed the low temperature susceptibility measurement and the resistivity measurement under an external magnetic field. Then I obtained the interesting phase diagram near QCP in this concentration region, where the crossover line between the NFL regime to the FL regime was found in the resistivity measurement in rather high field region ($H \geq 1$ T). Furthermore in the smaller field region we discovered another crossover line, observed in the low temperature susceptibility measurement, which can be correspond to the interplay between the disorder and the QCP.

3.3.1 Field effect on the NFL behavior in the resistivity – Crossover from NFL to FL by applying an external magnetic field

One of the evidences for which the NFL behavior can be considered as the effect of the QPT is the experimental fact that the NFL easily collapses by varying the external parameter, for example applying a pressure or an external magnetic field. It is naturally led from the description of the QPT, because the variation of an external parameter cause the leaving from the QCP. By applying a pressure the strength of the hybridization (J/W) is enhanced, which leads the enhancedment of the quantum fluctuation and reducement the critical fluctuation of the order parameters, which is an antiferromagnetic fluctuation in most of cases. Therefore the recovery of the FL is observed by applying a pressure [51]. The similar behavior is observed when applying an external magnetic field [9, 19], which is also considered to be due to the suppression of the antiferromagnetic critical fluctuation. Therefore it is very useful way to study the field effect on the NFL.

Figure 3.32 shows the experimental results of the resistivity under magnetic field, plotted as a function of T^2, in which we can clearly find the T^2 behavior in the high field region ($H \geq 1$ T). I also show the recovery of the FL in another way. When the resistivity varies as $\rho_0 + A'T^n$, we can obtain the value of the power n from the slope of $\log(T\mathrm{d}\rho/\mathrm{d}T)$ vs $\log T$ plot without an ambiguity of the residual resistivity, ρ_0.

$$\log(T\frac{\mathrm{d}\rho}{\mathrm{d}T}) = \log(nA') + n\log T \tag{3.19}$$

Figure 3.33 shows the differential resistivity at zero filed in this plot, and Fig. 3.34 shows the field dependence of the power n. In this figure we can also find the recovery of the FL above 1 T.

In Fig. 3.35 I plot the T_{coh} obtained from the resistivity measurements as a function of H. In high field and low temperature region, the FL-regime exist. T_{coh} seems to be extrapolated to the finite value, around 0.2 K, down to zero field from high field region, however a T^2 behavior could not be found at zero field in any temperature range, where T_{coh} is at most 0.1 K. The T_{coh} line drops rapidly around 1 T, where the T_{coh} line seems to be divided into two regime, a 'low field' line and a 'high field' line.

The magnetoresistance also shows the existence of two regime for this concentration region in HT-plain. In Fig. 3.36 we can find the rapid increasing of the magnetoresistance

below 0.2 T, in contrast with that in high field a general quadratic dependence on field due to the orbital effects on non-standard band structure was observed. The anomaly in low field represents only a variation of few percent in the resistivity, but it is clearly observable, which disappear at high temperature. Such a sharp increasing of the magnetoresistance cannot be explained by the suppression of quantum critical fluctuation. F. J. Ohkawa pointed out the distribution of Kondo temperature can explain the linear field dependence of the resistivity [52]. In our system, $Ce(Ru_{1-x}Rh_x)_2Si_2$ for $x = 0.5$ (intermediate Rh-concentration region), the low field regime may be the 'disorder' regime. Here I use the disorder regime as the meaning including quantum Griffiths phase, not a simple model of distribution of T_K .For $x = 0.03$ the magnetoresistance at 60 mK, which not shown in Fig. 3.37, shows not a sharp increasing at low field but a quadratic field dependence, in contrast for $x = 0.5$, because of less disorder.

The scaling analysis of the resistivity based on the dynamical mean-field theory for the Kondo alloy system

In the framework of the QPT, the thermodynamic properties can be scaled by the parameter Δ represent the distance from the QCP, which is indicated y in the SCR theory. Roughly speaking, when Δ is smaller than T the system behave as FL. Here I describe the scaling analysis of the resistivity based on the recent dynamical mean-field (DMF) theory for the Kondo alloy system developed by D. R. Grempel [53] for the explanation of the crossover from the NFL to FL.

The Kondo alloy model is described as a system of localized spins interacting with conduction electrons via a local Kondo coupling. The localized spins interact among themselves through an exchange coupling that may be approximated by an Ising-like term that most experimental systems, our system also, exhibit strong uniaxial anisotropy. The hamiltonian of the model is given by,

$$\mathcal{H} = -\sum_{i,j,\sigma} t_{ij} c^{\dagger}_{i\sigma} c_{j\sigma} + J_K \sum_i \boldsymbol{S}_i \boldsymbol{s}_i + \frac{1}{2} \sum_{i,j} J_{i,j} \boldsymbol{S}_i \boldsymbol{S}_j \tag{3.20}$$

where $\boldsymbol{S}_i$ and $\boldsymbol{s}_i$ denote a localized spin operators and a local electronic spin density at site i, and $c^{\dagger}_{i\sigma}$ and $c_{i\sigma}$ are the creation and annihilation operators for the conduction electrons in a tight-binding conduction band with nearest-neighbor hopping integral t_{ij}. J_K and J_{ij} represent the local Kondo coupling and the exchange coupling respectively. The second term of the hamiltonian favors the screening of the localized moments below a characteristic temperature T_K and the last term favors the appearance of a magnetic order below a temperature $T_m = \mathcal{O}(\mid J_{ij} \mid)$. The nonmagnetic-magnetic QPT is occurred at the QCP at $T = 0$ around $J\ (= \mid J_{ij} \mid) \sim T_K$.

In the Ref [53] they investigated the case of a random exchange interaction with zero mean, which describes a QCP of a metallic spin glass. The antiferromagnetic case is likely to be more relevant for our system, however we cannot exclude the possibility of the case of spin galss because of a high degree of disorder and the competition of different type of antiferromagnetic phase in this concentration region. In the DMF approach, the hamiltonian 3.20 is reduced to an effective impurity model by integrating out the electronic and spin degrees of freedom of all but one of the lattice sites. The integrated degrees of freedom provide a bath to which the 'impurity' site is coupled. According to D. R. Grempel [54], in the 'extended' DMF approach [55] the both antiferromagnetic and spin glass cases are precisely the same in the paramagnetic region. The DMF theory is exact when the lattice coordination z is infinite. The reduced hamiltonian is a single

impurity model in a time-dependent magnetic field, as

$$\mathcal{H}(\tau) = -[h^z(\tau) + H]S^z(\tau) - J_K S^x(\tau) \tag{3.21}$$

where $h^z(\tau)$ is a dynamic field, which is the result integrating out the degrees of freedom of electrons and spins, and H is an applied external magnetic field. And $h^z(\tau)$ is given by

$$h^z(\tau) = \int_0^\tau d\tau' Q(\tau - \tau') S^z(\tau) \tag{3.22}$$

$$Q(\tau - \tau') = J^2 < S^z(\tau) S^z(\tau') > + \frac{2 - \alpha(J_K/D)}{|\tau - \tau'|^2} \tag{3.23}$$

$Q(\tau - \tau')$ is a retarded interaction. The first term in Eq. 3.23 is a feedback from the spins and the second term is that from the electrons. Near the QCP the first term is dominant, which leads the NFL behavior, while far from the QCP as temperature decreasing finally the second term becomes dominant and the FL behavior appears.

Monte-Calro simulations of the DMF Kondo alloy model show that its low energy properties are very well described by an effective strong-coupling model [53, 56]. Near the QCP the spectrum of local magnetic excitation is given by,

$$J_c \chi''(\omega) = \sqrt{\Delta} \Phi(\frac{\omega}{J_c \Delta}) \tag{3.24}$$

with the universal function $\Phi(x)$,

$$\Phi(x) = \frac{1}{\sqrt{2}} x \left[(1 + x^2)^{1/2} + 1\right]^{-1/2} \tag{3.25}$$

At $J = J_c$ the QPT occurs. The distance from the QCP Δ is obtained from its self-consistent equation,

$$\Delta = \Delta_0 + 2\sqrt{\Delta} \frac{T}{T_0} \left[\sqrt{1 + \frac{T}{2\sqrt{3} T_0 \Delta}} - 1\right] \tag{3.26}$$

where the scale temperature T_0 is roughly the Kondo temperature and Δ_0 is Δ at $T = 0$, given by in the presence of a magnetic field,

$$\Delta_0 = \left(1 - \frac{J}{J_c}\right) + \frac{H^2}{H_0} \tag{3.27}$$

Here, $H_0 = J_c/(g\mu_B)^2$ and we assume $T \ll T_0$ and $H \ll H_0$. The first term $r = (1 - J/J_c)$ represent the distance from the QCP at zero field and zero temperature, which can be tuned by alloying or applying a pressure. The self-consistent equation of Δ cannot be solved in closed form but its behavior in limiting cases can be easily found;

$$\Delta = \begin{cases} \Delta_0 + (\frac{3}{4})^{1/4} (\frac{T}{T_0})^{3/2} & \text{for } T/T_0 \gg \Delta_0 \\ \Delta_0 + \frac{1}{2\sqrt{3\Delta}} (\frac{T}{T_0})^2 & \text{for } T/T_0 \ll \Delta_0 \end{cases} \tag{3.28}$$

In the DMF formalism, the temperature dependent term of the resistivity is written as, $\delta\rho \propto 1/(D(0)\tau)$ where $D(0)$ is the DOS of the conduction electron at Fermi energy and τ is the scattering time [57]. In the present case the latter is given by [14],

$$\frac{1}{\tau} = \frac{D(0) J_K^2}{4} \int_0^\infty d\omega \frac{\chi''(\omega)}{\sinh \beta\omega} \tag{3.29}$$

Combining Eqs. 3.24 and 3.29, the temperature dependent term is found to obey the scaling form,

$$\rho(T) - \rho(0) \propto T^{3/2}\Psi(\frac{(T/T_0)}{\Delta}) \tag{3.30}$$

with the universal scaling function $\Psi(x)$ determined by $\Phi(x)$,

$$\Psi(x) = x^{-1/2}\int_0^\infty du \frac{\Phi(ux)}{\sinh u} \tag{3.31}$$

The asymptotic behavior of physical quantities follows from the above equation. The disipative part of the dynamical susceptibility $\chi''(\omega)$ behaves as $\chi''(\omega) \propto \sqrt{\omega}$ for $\omega \gg \Delta$ and $\chi''(\omega) \propto \omega/\sqrt{\Delta}$ otherwise. Inserting these asymptotic results in Eq. 3.29, we obtain the resistivity $\delta\rho \propto T^{3/2}$ for $T/T_0 \gg \Delta_0$ and $\delta\rho \propto T^2/\sqrt{\Delta}$ for $T/T_0 \ll \Delta_0$, and also obtain the asymptotic limits of the scaling function of the resistivity $\Psi(x)$ as,

$$\Psi(x) \propto \begin{cases} x^{1/2} & \text{for x}\to 0 \quad \text{(FL-regime)} \\ \text{const.} & \text{for x}\to\infty \quad \text{(NFL-regime)} \end{cases} \tag{3.32}$$

The shape of $\Psi(x)$ that interpolates between these asymptotic limits is shown in Fig. 3.38.

The theory also predict the behavior of the uniform susceptibility,

$$J\chi(T) = \sqrt{1+\Delta} - \sqrt{\Delta} \tag{3.33}$$

by assuming the similarity to the local susceptibility [53]. The fact of that ferromagnetic fluctuations do not develop into long-range correlation near an antiferromagnetic or a spin glass QCP justifies this assumption. At $r = 0$ has a dependence $\chi(T) - \chi(0) \propto T^{3/4}$, more generally in the temperature region $T/T_0 \gg \Delta_0$. This prediction is different from that by SCR theory, which is $\chi(T) - \chi(0) \propto T^{1/4}$ near the antiferromagnetic QCP (see in Sec. 3.2.3). Supposedly this difference comes from the neglecting the mode-mode coupling in the DMF theory. Here I follow the guidance of the DMF theory for the analysis the experimental data in a magnetic field.

In a real analysis we must determine three parameters r, T_0 and H_0. At the critical concentration r must vanish. From the phase diagram of $Ce(Ru_{1-x}Rh_x)_2Si_2$ (Fig. 3.12) and several experimental results we expected $x_c = 0.5$, however we cannot exclude the possibility of that r is very small but finite for $x = 0.5$. The scale temperature T_0 and field H_0 are related with the Kondo temperature. In order to determine the value of T_0 we fit the susceptibility at 1kG by using the Eqs. 3.33 and 3.26 with $\Delta_0 = 0$. This condition is justified in a temperature region $r \ll T$ and in a field region $H \ll H_0$. I show the experimental result of the susceptibility at 1 kG down to 100 mK in Fig. 3.39 with theoretical result. The best fit of the experimental data is obtained for $T_0 = 24$ K. Once T_0 is known, r and H_0 can be determined from the scaling plot of the T- and H-dependent resistivity using the scaling form Eq. 3.30. In Fig. 3.40 I show the results of the analysis for the resistivity along a- and c-axis. The data points represent the values of the scaled resistance $(\rho(T) - \rho(0))/t^{3/2}$ as a function of the reduced variables t/Δ, where $t = T/T_0$, in the temperature range $T \leq 0.9$ K. We can make all the data merge on a single curve by choosing the values $r = 8 \times 10^{-3}$ and $H_0 = 13$ T. The solid curves in Fig. 3.40 are the theoretical results. Except the data at zero field, represented by the empty squares in the figure, the scaling works satisfactory for all experimental data.

The characteristic temperature $T_0 = 24$ K is of the same order of magnitude as the Kondo temperature of this system. The theoretical value of the characteristic field $H_0 = J_c/g^2\mu_B$ can also be expressed in terms of the zero temperature limit of the susceptibility

per Ce-atom ($\chi(0) = (g\mu_B)^2/J_c$). From the experimental value at 1 kG $\chi(0) \approx 5 \times 10^{-2}$ emu/mol and taking $g = 2$, we can estimate $H_0 \approx 11$ T, which compares rather well with the value determined from the scaling analysis of the resistivity. The value of r is a measure of the 'chemical' distance from the true critical concentration $r \propto (x - x_c)/x_c$. Alternatively we can write $r = \delta J/J_c$, where $\delta J = J - J_c$, giving $\delta J \approx 200$ mK. This is a very small energy compared with all other energy scale, therefore we can conclude this concentration is very close to the critical concentration and the NFL behavior, at least in the field region higher than 1 T, can be considered as the quantum critical phenomena. And this value is surprisingly consistent with the value of T_{coh} extrapolated from high field T_{coh}-line (I had discussed with Fig. 3.35 already).

In conclusion of this subsection, I have shown the scaling analysis of the resistivity under a magnetic field and found that the experimental results, especially the crossover from the NFL to FL by applying a magnetic field, are well explained by the description of the QPT based on the DMF theory. However in low field region, below a few kG, we must search for another physics with considering the presence of the disorder and interplay between the disorder and the quantum critical phenomena, probably. I will discuss on the low field, including a zero field limit, properties with the experimental results of the susceptibility in a following sections.

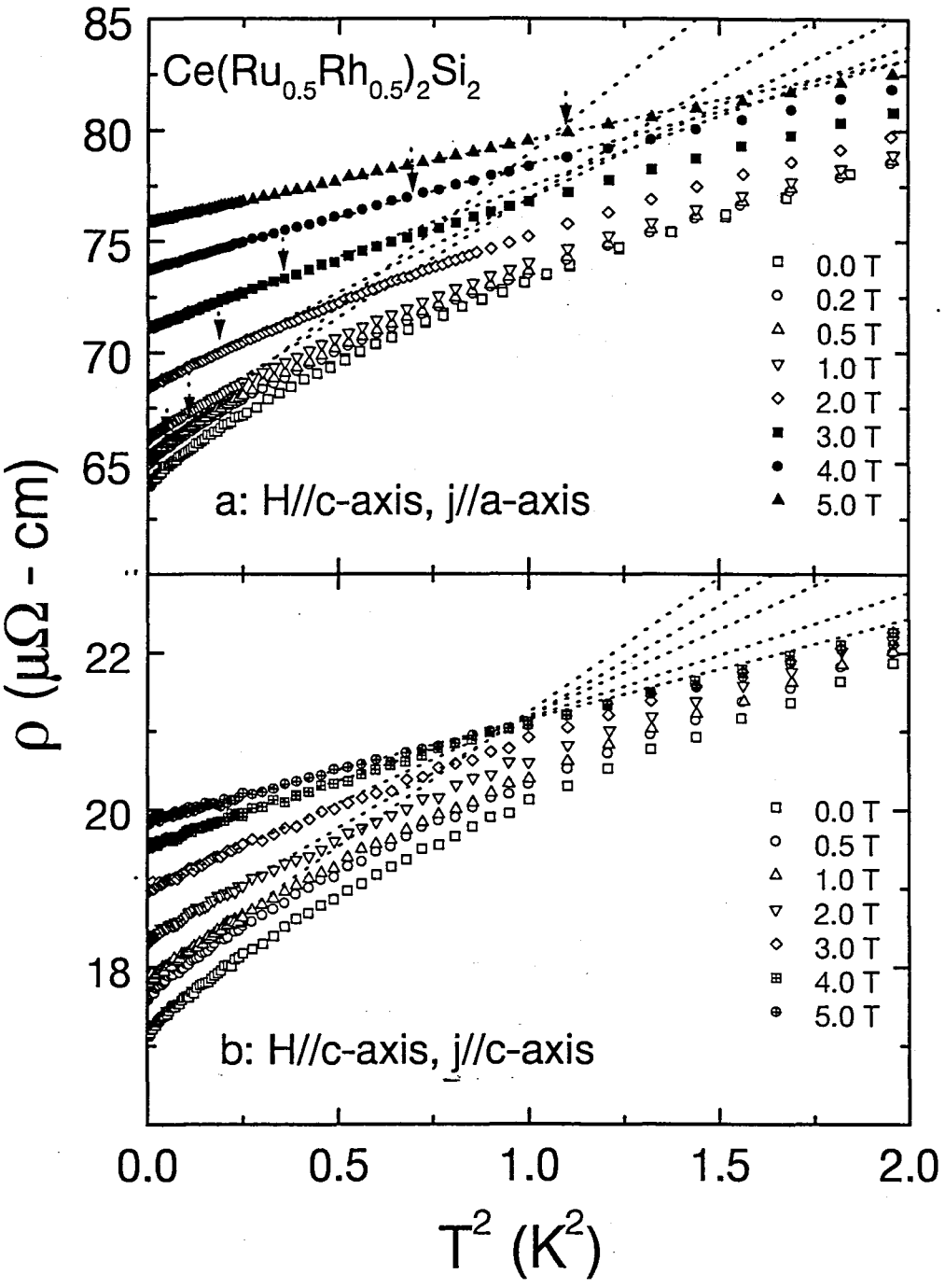

Figure 3.32: The resistivity of $x = 0.5$ under an external magnetic field along c-axis up to 5 T; the excitation current along (a) a-xis and (b) c-axis. The dashed lines represent a T^2 behavior. The arrows indicates the range of the temperature where a T^2 behavior was observed.

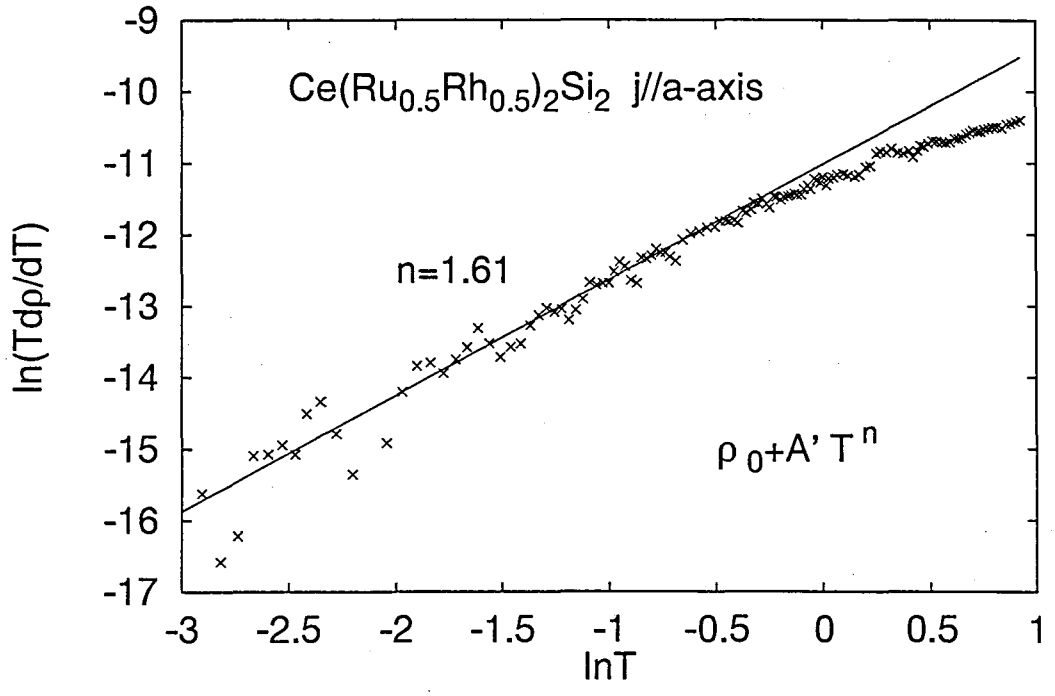

Figure 3.33: The differential resistivity of $x = 0.5$ along a-axis at zero filed is shown in the form of $\log(T\mathrm{d}\rho/\mathrm{d}T)$ vs $\log T$.

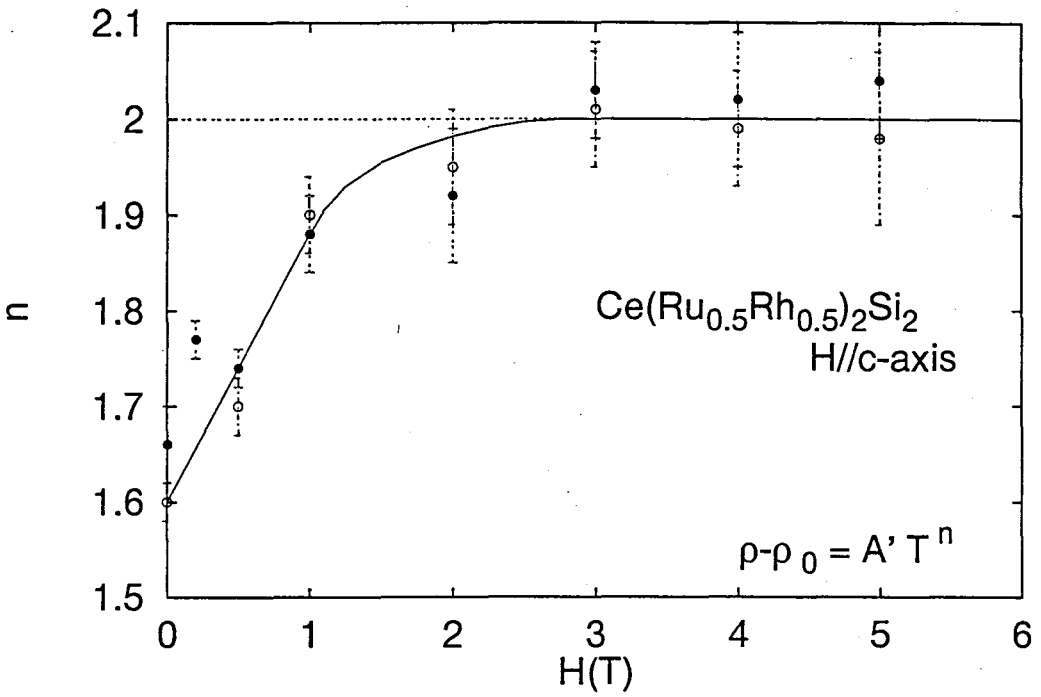

Figure 3.34: The power of the resistivity n is shown as a function of a magnetic field H. In this figure the open circles represent that along c-axis and the closed circles represent that along a-axis.

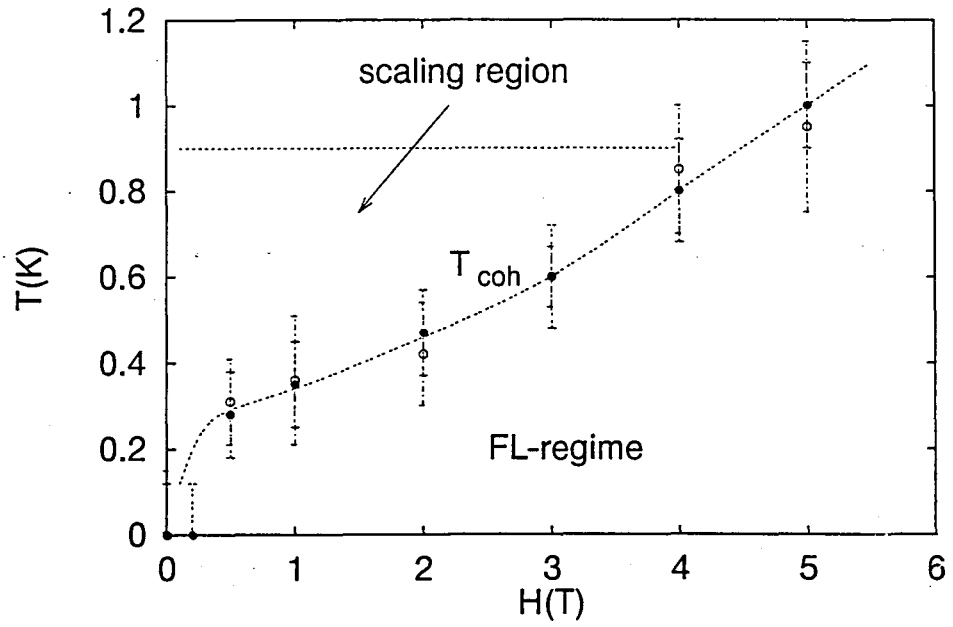

Figure 3.35: T_{coh} at various field are plotted. Below 0.9 K, indicating as 'scaling region' in the figure, the resistivity can be scaled on one universal curve (described in the text in detail).

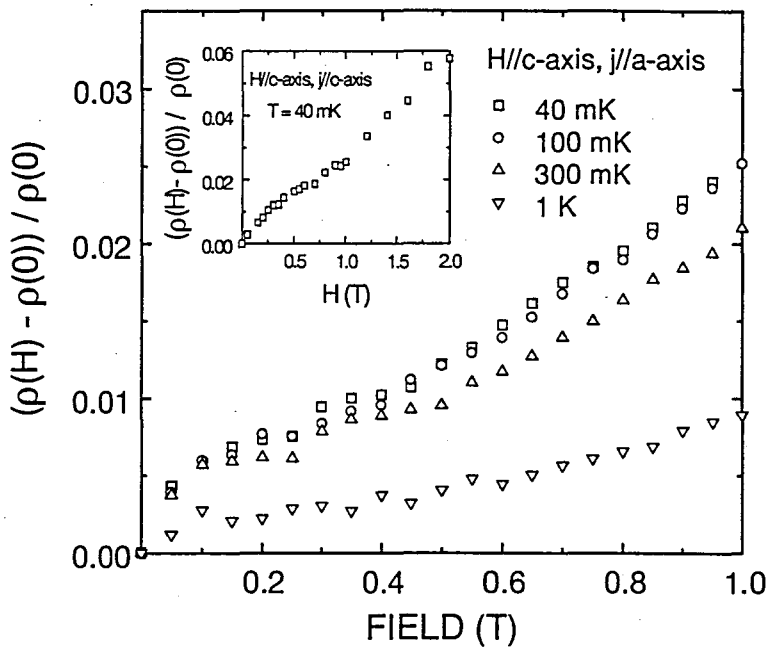

Figure 3.36: The magnetoresistance $(\rho(H) - \rho(0))/\rho(0)$ measured along the a-axis at several temperatures are plotted as a function of an applied field along c-axis. In the inset figure the same plot for the current along c-axis at 40 mK is shown.

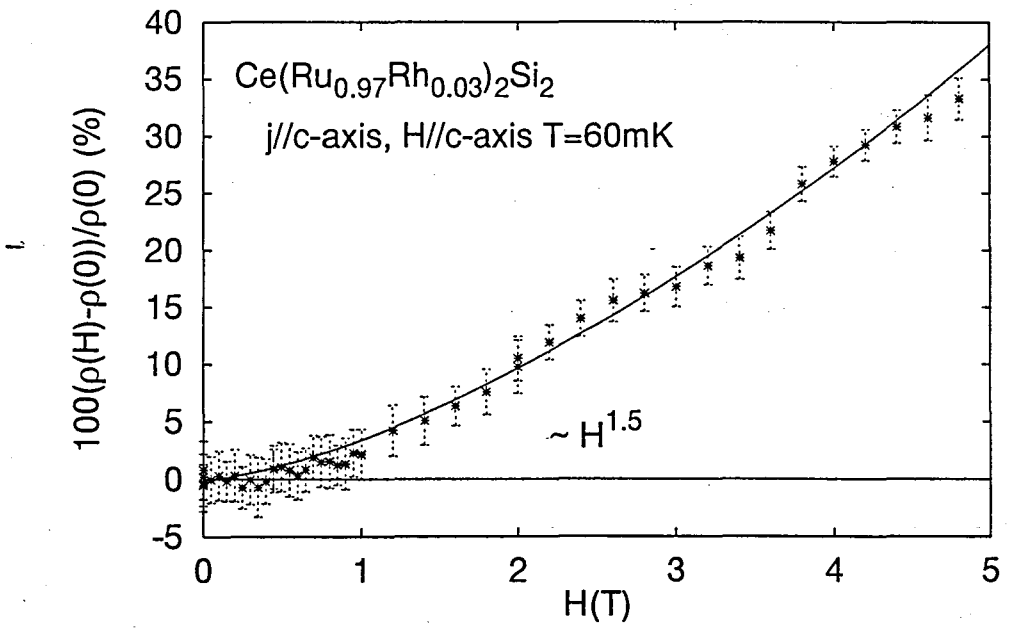

Figure 3.37: The magnetoresistance $(\rho(H) - \rho(0))/\rho(0)$ for $x = 0.03$ measured along the c-axis at 60 mK is shown. The solid line represents the $H^{1.5}$ dependence.

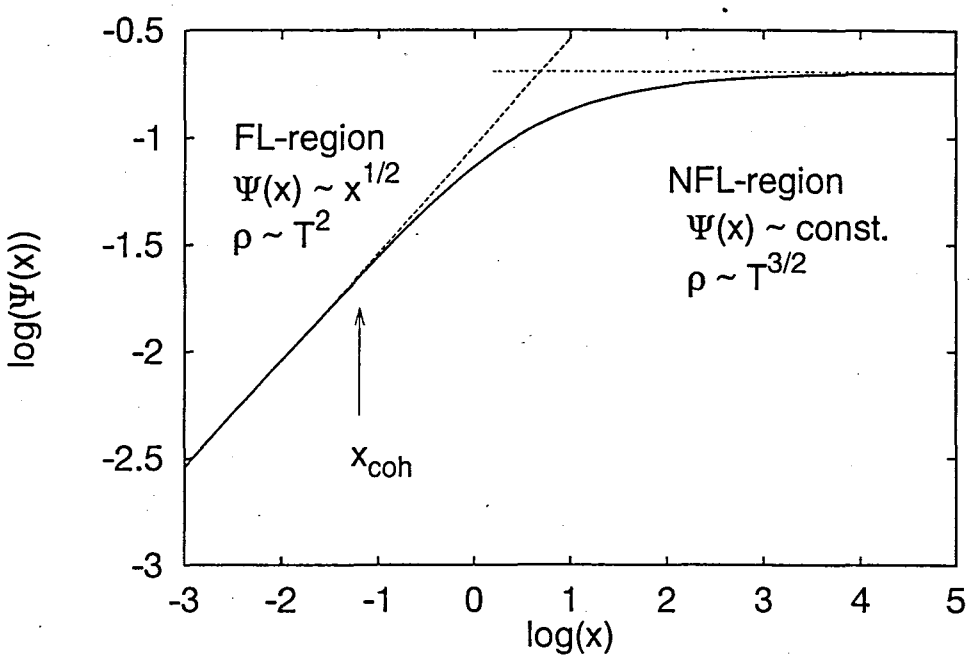

Figure 3.38: The shape of the scaling function of the resistivity $\Psi(x)$ (represented by the solid line in the figure) is shown. The dashed lines represent the behavior in the limiting region.

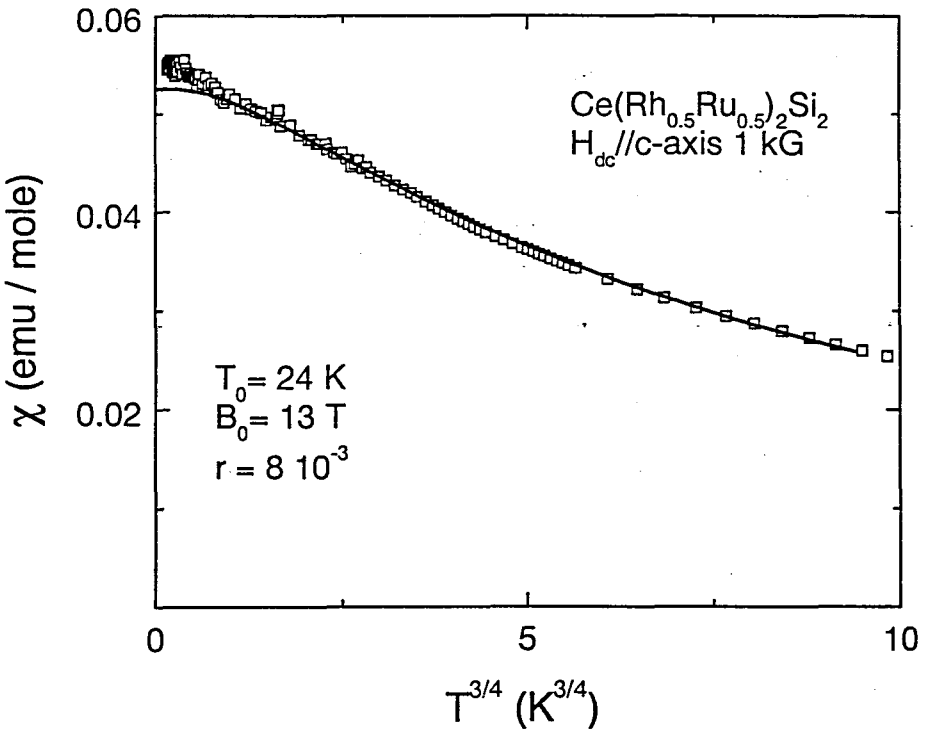

Figure 3.39: The DC susceptibility at 1kG down to 100 mK along c-axis is shown. The solid line represents the theoretical result computed as described in the text.

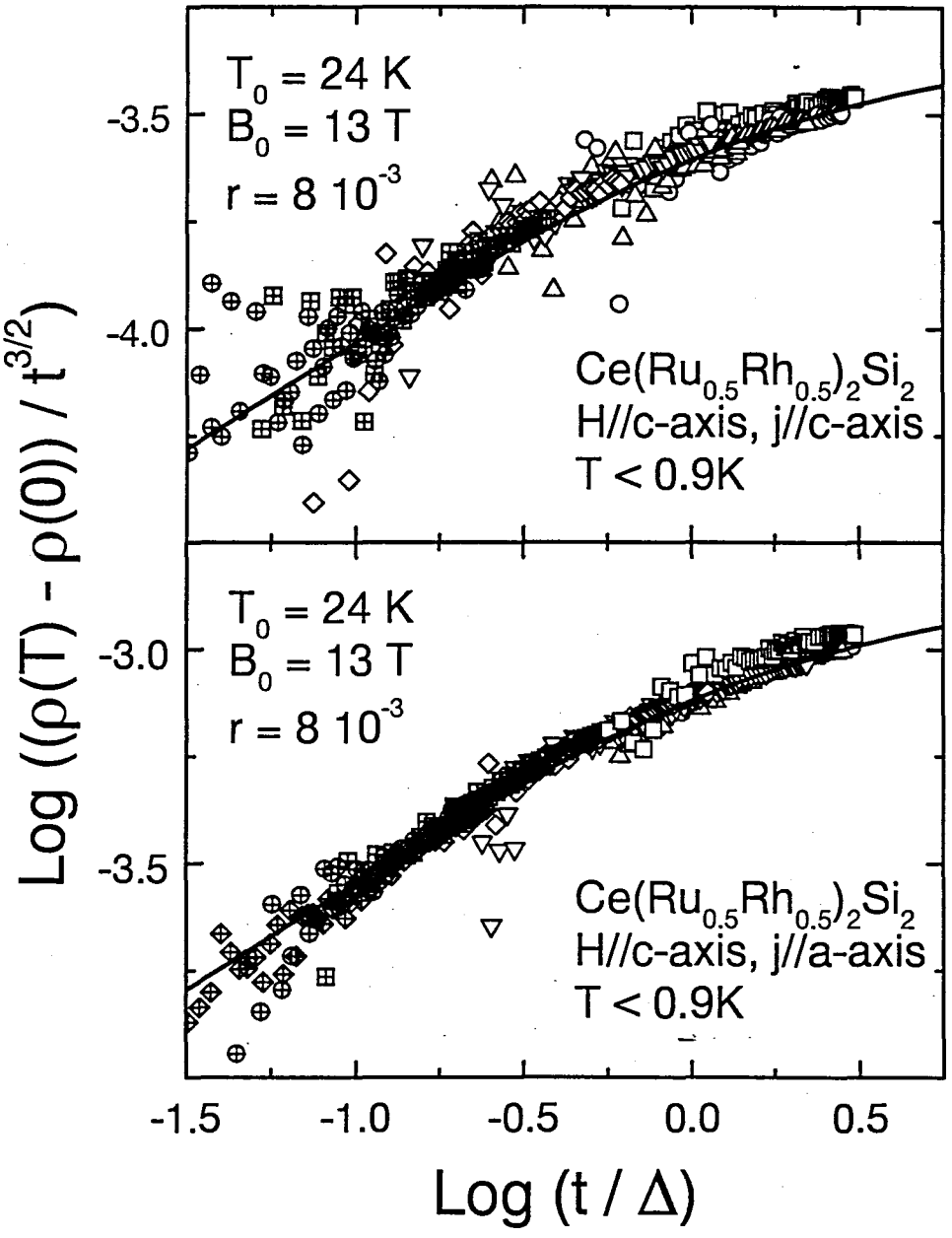

Figure 3.40: Scaling plots of the resistivity along a- and c-axis. The solid line is the theoretical scaling curve.

3.3.2 Susceptibility in a low and high magnetic field

In Sec. 3.3.1, I discuss on the scaling analysis of the resistivity under an external magnetic field and the description of the QPT for the explanation of the NFL behavior. In conclusion the description can be applicable for the high field region. On the other hand in a low field region there is another physics, which can be seen in a deviation of the experimental data at zero field from the scaling function and the magnetic field dependence of $T_{\rm coh}$. Here, I show the results of the magnetic field dependence of the susceptibility for $x = 0.5$ and 0.6, and report the discovery of a scaling of the susceptibility in a low field and temperature region, which has different character from that found in the resistivity under rather higher field.

High temperature region

First, I discuss on the variation of the temperature dependences of the susceptibilities in the intermedite Rh-concentration at various magnetic field. As I showed in Fig. 3.6 (b), the susceptibilities at 1 kG below 10 K in this concentration region have a temperature dependence like,

$$\chi(T) = \chi_0 - BT^a \tag{3.34}$$

with $a = 3/4$, $1/2$, $1/3$ and $1/2$ for $x = 0.35$, 0.4, 0.5 and 0.6 respectively, which indicates the system approaches to the FL regime, where the value of a is 2, as leaving from the QCP of the Rh-rich antiferromagnetic phase. If the susceptibility can be written as Eq. 3.34, the exponent a is determined from the slope of the $\log(-T{\rm d}\chi/{\rm d}T)$ vs $\log T$ plot as I did for the resistivity data (Sec. 3.3.1).

$$\log\left(-T\frac{{\rm d}\chi}{{\rm d}T}\right) = \log(aB) + a\log T \tag{3.35}$$

In the resistivity under a magnetic field we found the recovery of the FL behavior for $x = 0.5$, therefore I have examined the field dependence of the susceptibility at high temperature, $T \geq 1.8$ K, up to 4 T for $x = 0.35$, 0.4, 0.5 and 0.6.

I show the susceptibility of $x = 0.5$ in a various field applied along the c-axis in Fig. 3.41, where we can see the strong non-linearity of the magnetization below 10 K. I will discuss on this non-linearity just later, and here I focus on only the temperature dependence of the susceptibility in a magnetic field. Figure 3.42 shows the differential susceptibility in the form of $\log(T{\rm d}\chi/{\rm d}T)$ vs $\log T$. The figure represents that the exponent a repidly increases as increasing a field up to 1 T, then the enhancedment of a becomes rather slowly and a reaches to around 3/4 at 4 T. Such a field dependence of a was found also for $x = 0.35$, 0.4 and 0.6. I show the field dependence of a in Fig. 3.43. The value of a at the lowest field is different from that predicted by theories, which is 1/4 by the SCR theory and 3/4 by the DMF theory. In a low field, below 1 T, the temperature dependence of the susceptibility becomes stronger rapidly for each concentration. And the variation of the susceptibility becomes steeper as temperature decreasing. Therefore the measurement in much lower temperature and field region is needed to see the 'true' behavior of the susceptibility.

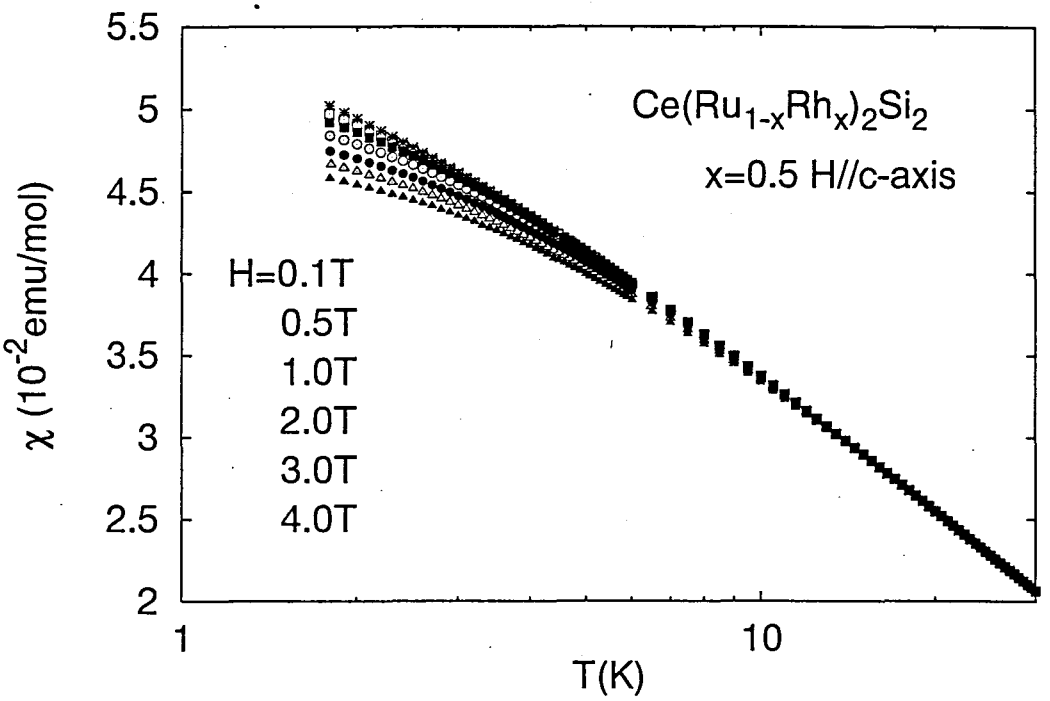

Figure 3.41: The susceptibility of $x = 0.5$ in a various field applied along the c-axis are shown.

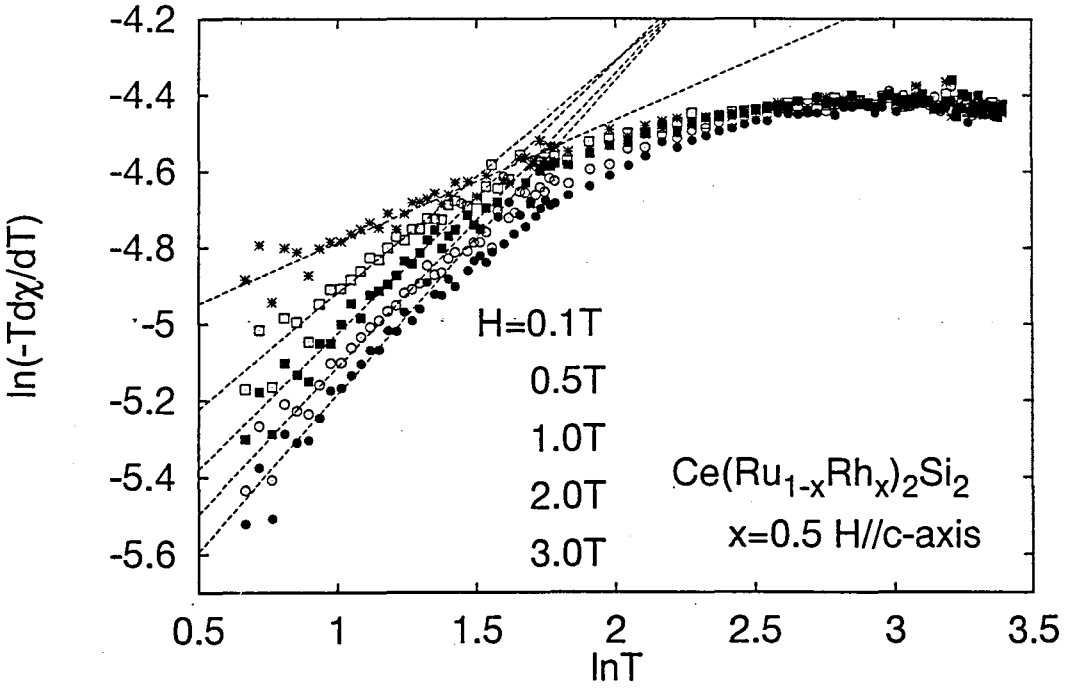

Figure 3.42: The differential susceptibility of $x = 0.5$ in a various field applied along the c-axis are shown in the form of $\log(T\mathrm{d}\chi/\mathrm{d}T)$ vs $\log T$. The dashed line represent the slope of the curve at low temperature.

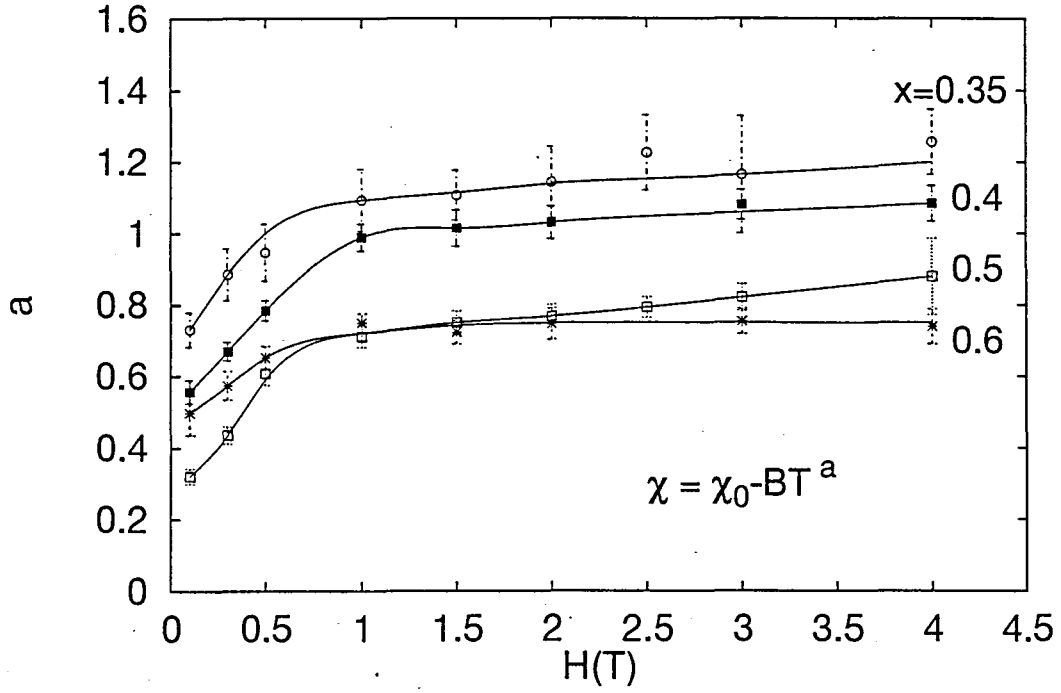

Figure 3.43: The variation of the temperature dependence of the susceptibility in Rh-concentration x.

Non-linear susceptibility

The magnetic field dependence of the susceptibility shown in Fig. 3.41 suggests the strong non-linear susceptibility χ_2 which is diverging down to $T = 0$. The magnetization in a paramagnetic state can be expanded by the odd power of the magnetic field H as follows.

$$M = \chi_0 H + \chi_2 H^3 + \cdots \tag{3.36}$$

Thus the non-linear susceptibility χ_2 can be obtained as the slope in the M/H vs H^2 plot.

$$M/H = \chi_0 + \chi_2 H^2 + \cdots \tag{3.37}$$

Figure 3.44 shows the magnetization in the form of M/H vs H^2 for various Rh-concentrations at 1.8 K. In the intermediate concentration region, the 'NFL' region, χ_2 is negative and very large in a low field region. The field dependence of M/H for these concentrations is not monotonic, but changes around 1 T into more gentle slope. On the other hand in the low concentration region, the FL region, χ_2 is much smaller than that for $x = 0.4$ or 0.5, which can be seen almost zero. In fact χ_2 for $x = 0$ or 0.03 has a small negative value. The large non-linearity at higher field is due to the metamagnetic transition. In the SDW state, for $x = 0.05$ and 0.15 χ_2 is positive and for $x = 0.3$ χ_2 is negative at first, which is much smaller than that for $x = 0.4$ or 0.5, and changes to positive as increasing a field, up to a few kG. A positive χ_2 is expected in an antiferromagnetic ordered state. For $x = 0.3$ we observed the NFL behavior in the specific heat above T_N at zero field, thus the negative χ_2 for $x = 0.3$ in a low field can be considered to have a same origin with the NFL. These results show that the magnetic field dependence of M/H at 1.8 K of $Ce(Ru_{1-x}Rh_x)_2Si_2$ systematically changes, depending on the magnetic ground state.

In Fig. 3.45 (a) I show χ_2 obtained from the fitting the magnetization data by Eq. 3.37 below 1 T for $x = 0.4$ and 0.5, and 0.03 for the comparison, as a function of a temperature. χ_2 for $x = 0.03$ is much smaller than that for $x = 0.4$ or 0.5. The temperature dependences of χ_2 for $x = 0.4$ and 0.5 are almost same. I also show the χ_2 in the form of the $\log(-\chi_2)$ vs $\log T$ plot for $x = 0.5$. Clearly we can see the divergence of χ_2 down to $T = 0$ negatively with the exponent -1.5. For $x = 0.4$ the same temperature dependence is observed, which is not shown in Fig. 3.45 (b). The strong negative non-linearity of the magnetization was also observed in the typical NFL system $CeCu_{5.9}Au_{0.1}$ by H. v. Löhneysen *et al.* at 0.15 K [9]. However, they did not measure the temperature dependence of χ_2. We have measured the magnetization of $CeCu_{5.9}Au_{0.1}$ at various temperature and obtained the non-linear susceptibility as a function of a temperature by the mean above mentioned. The single-crystalline and the poly-crystalline sample used for the measurements were grown by A. A. Menovsky in University of Amsterdam. I show the temperature dependence of χ_2 of $CeCu_{5.9}Au_{0.1}$ in Fig. 3.46. Surprisingly the temperature dependences of χ_2 for $Ce(Ru_{1-x}Rh_x)_2Si_2$ and $CeCu_{5.9}Au_{0.1}$ are quite same, in both system $\chi_2 \propto T^{-1.5}$. It suggests the divergence of χ_2 is the characteristic behavior of the NFL, which has an universality as well as the logarithmic divergent behavior of C/T.

How can we interpret about this divergence of χ_2? It is difficult to understand it in the description of the antiferromagnetic QPT. In the case of a classical antiferromagnetic phase transition, χ_2 never diverge and supposedly neither does in the case of the QPT. In the case of spin glass, χ_2 must diverge as approaching to the phase transition temperature T_g, and in the case of the QPT the mean-field theory expects $\chi_2 \propto T^{-3/2}$ [14], which is the same temperature dependence as our experimental results. Thus, is $Ce(Ru_{1-x}Rh_x)_2Si_2$ for

(a)

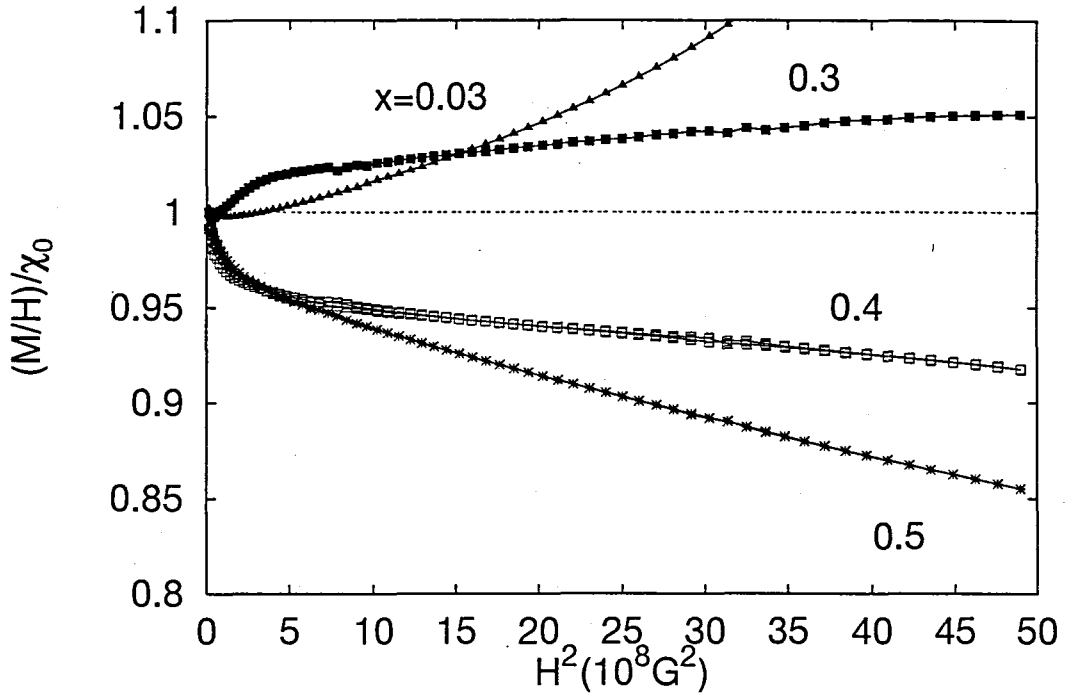

(b)

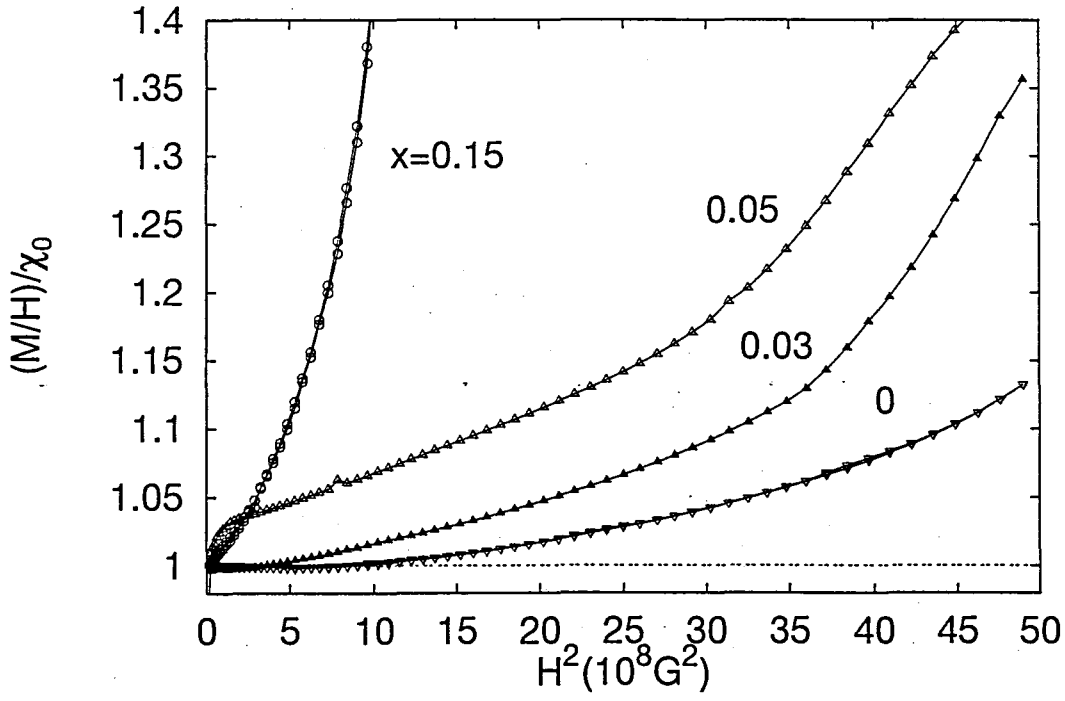

Figure 3.44: $(M/H)/\chi_0$ vs H^2 plot at 1.8 K for (a) the intermediate Rh-concentration region, and (b) the low Rh-concentration region. For the comparison I show the data for $x = 0.03$ also in (a).

(a)

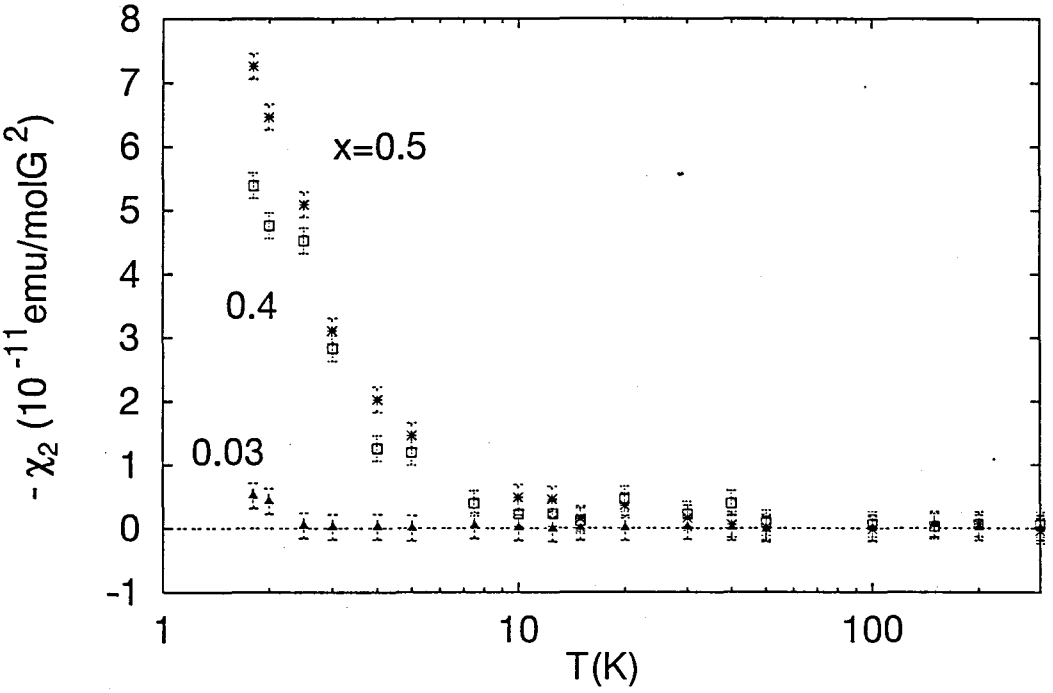

(b)

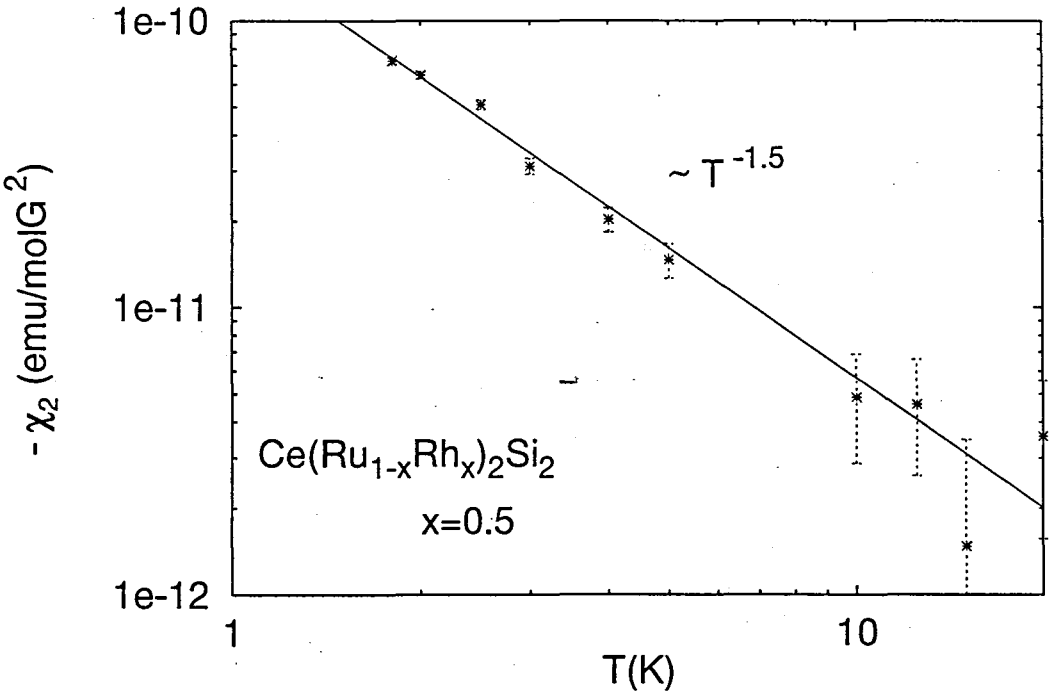

Figure 3.45: (a) χ_2 as a function of a temperature for $x = 0.03$, 0.4 and 0.5 are shown. (b) $\log(-\chi_2)$ vs $\log T$ plot for $x = 0.5$ is shown. The solid line in (b) represent the temperature dependence as $\sim T^{-1.5}$.

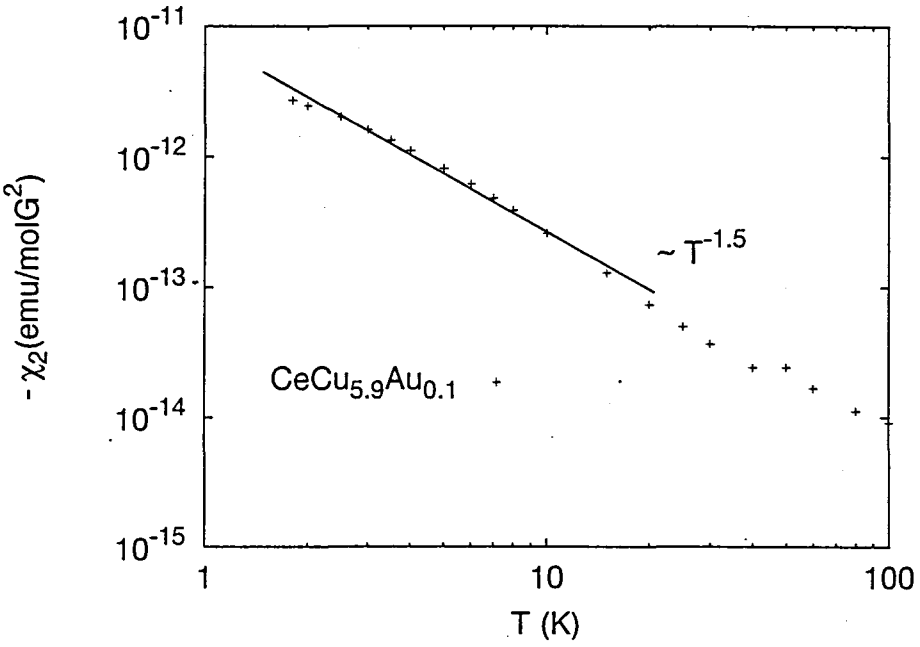

Figure 3.46: χ_2 of $CeCu_{5.9}Au_{0.1}$ is shown in the form of $\log(-\chi_2)$ vs $\log T$.

$x = 0.4$ and 0.5 and $CeCu_{5.9}Au_{0.1}$ near the QCP of spin glass? It can be in the $Ce(Ru_{1-x}Rh_x)_2Si_2$ system, because in the intermediate Rh-concentration region there should be a competition between two different antiferromagnetic correlation with chemical disorder. It is noted that in the similar system, $U(Ru_{1-x}Rh_x)_2Si_2$ system, for around $x = 0.4$ the spin glass phase was found [58]. However in the $CeCu_{5.9}Au_{0.1}$ it is very doubtful the QPT of spin glass occurs, considering its small substitution of Cu for Au. The Kondo disorder model also may explain the divergence of χ_2 by assuming the valid distribution of T_K , however this model seems not to be applicable for $CeCu_{5.9}Au_{0.1}$ for the same reason.

Recently A. H. Castro-Neto *et al.* have tried to treat the both effect of quantum critical fluctuations near an (antiferro)magnetic QCP and a distribution of the Kondo temperature introduced by a chemical disorder for the explanation of the NFL behavior [17]. In this theory they suggested the similarity between the NFL system and the 'quantum Griffiths phase' can appear near the QCP of the spin glass [59]. Originally, 'Griffiths phase' was proposed by R. B. Griffiths for a diluted ferromagnet [60]. In a diluted system, or disordered system more generally, the phase transition temperature T_c decreases from its clean value T_c^0. In the temperature region $T_c < T < T_c^0$ the system does not display a global order, however in an infinite system an arbitrarily large regions show local orders, with a small but nonzero probability that usually decreases exponentially with the size of the region. These 'static' fluctuations, introduced by chemical disorder for example, are known as 'rare region' and the order parameter fluctuates induced by them. Since they are weakly coupled, and flipping them requires changing the order parameter in a whole region, the system shows very slow dynamics. In a static feature, the free energy is non-analytic everywhere in the region $T_c < T < T_c^0$. In a classical case this 'Griffiths singularity' is very weak and there are only a few experimental evidences [61]. In the case of the QPT, Griffiths phase, or more appropriately Griffiths region, also appears in a certain region of a non-thermal parameter r at the zero-temperature. In a quantum case, Griffiths singularity is expected to be stronger than that in a classical case. In Ref. [59] the

Ising spin glass system in a transverse magnetic field has been studied. When a transverse field Γ is smaller than the critical value Γ_c, a spin glass state is realized, otherwise the ground state is paramagnetic. In a certain region 'quantum' Griffiths region is realized. I show the schematic phase diagram of quantum spin glass system in Fig. 3.47. Quantum Griffiths region must be connected smoothly to the QCP of the spin glass. The non-linear susceptibility χ_2 diverges to infinite in the quantum Griffiths region as well as at the QCP. Therefore the measurement of χ_2 is very important for the study on the quantum Griffiths phase.

In the disordered Kondo lattice system, local Kondo coupling plays a role of a transverse magnetic field, which is distributed randomly. Magnetic anisotropy is also important for the similarity between the disordered Kondo lattice system and the quantum spin glass system. In Ref. [17] several physical quantities are predicted as same in the quantum spin glass system, for example,

$$\begin{aligned} C/T &\propto T^{-1+\lambda} \\ \chi_0 &\propto T^{-1+\lambda} \\ \chi_2 &\propto T^{-3+\lambda} \end{aligned} \tag{3.38}$$

Our $Ce(Ru_{1-x}Rh_x)_2Si_2$ system satisfy the condition to realize the 'quantum Griffiths' description, however $CeCu_{6-x}Au_x$ system does not. In a strong disordered system, Griffiths region should be found. Thus, how about in a weak disordered system? In Griffiths region there is no universality, the value of λ can vary. At the end point of the Griffiths region, λ should be 1, outside here no singularity is found. In a weak disordered system the 'spread' of Griffiths region must be narrow or can vanish. In $CeCu_{5.9}Au_{0.1}$, is much weaker disordered system than $Ce(Ru_{1-x}Rh_x)_2Si_2$, χ_2 may saturate in a lower temperature. I will discuss on it in the following section again.

I try to apply this model for $Ce(Ru_{1-x}Rh_x)_2Si_2$ system. In this model the temperature dependences of several physical quantities can be expressed by using one prameter λ, which is related with the power decay of the autocorrelation function of the local moments in the rare region. Unfortunately, the value of λ obtained from the specific heat, susceptibility and non-linear susceptibility are different each other, which are 0, -1.5 (for $x = 0.4$) or -1.7 (for $x = 0.5$) and -1.5 respectively. The temperature ranges where these values are given are also different, in the specific heat between 0.1 K and 10 K, in the susceptibility between 1.8 K and 10 K and in the non-linear susceptibility between 1.8 K and 10 K. Precise measurements of χ_0 and χ_2 in a lower temperature should be required. In a following section I will discuss on it.

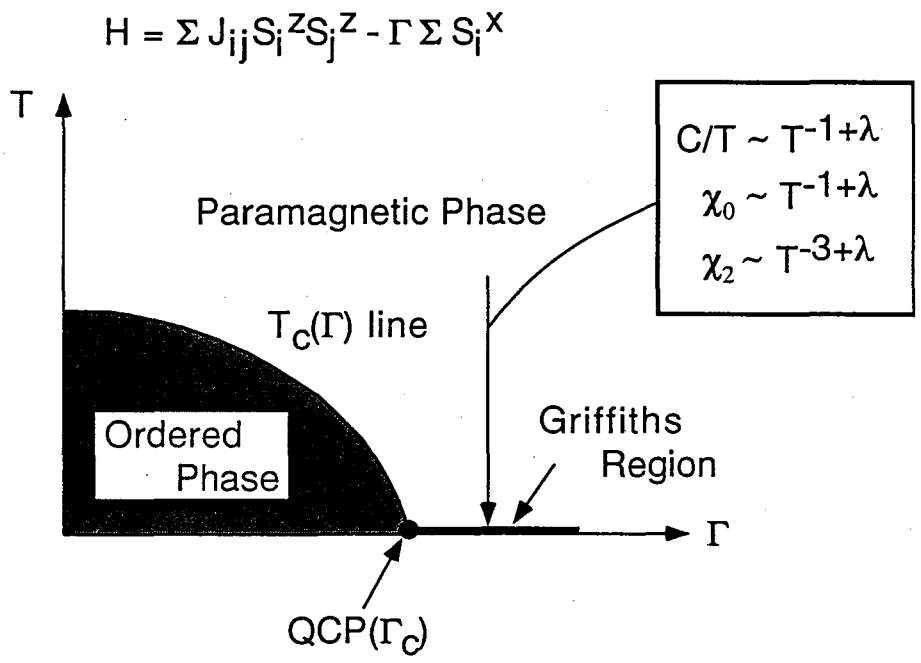

Figure 3.47: The schematic phase diagram of the transverse-field quantum spin glass is shown [62]. The thick portion along the horizontal axis ($T = 0$) indicates the quantum Griffiths region.

Low temperature susceptibility – the scaling of the susceptibility in a low field region $H < 1$ kG

From the measurement above 1.8 K the susceptibilities in the intermediate Rh-concentration region has a form of $1 - T^a$ with $a > 0$. We found the strong non-linearity of magnetization in a low field as a few kG, which suggest the existence of low scale energy as a few hundred mK. Therefore the measurement above 1.8 K may not guarantee a lower temperature behavior. The scaling analysis of the resistivity as functions of temperature and field also suggest that the low field region below a few kG is a different regime from the high field region. The logarithmic divergent behavior of C/T and the deviation from a T^2 law of the resistivity are found at zero field. These experimental results strongly requires a low temperature susceptibility measurement in a low field.

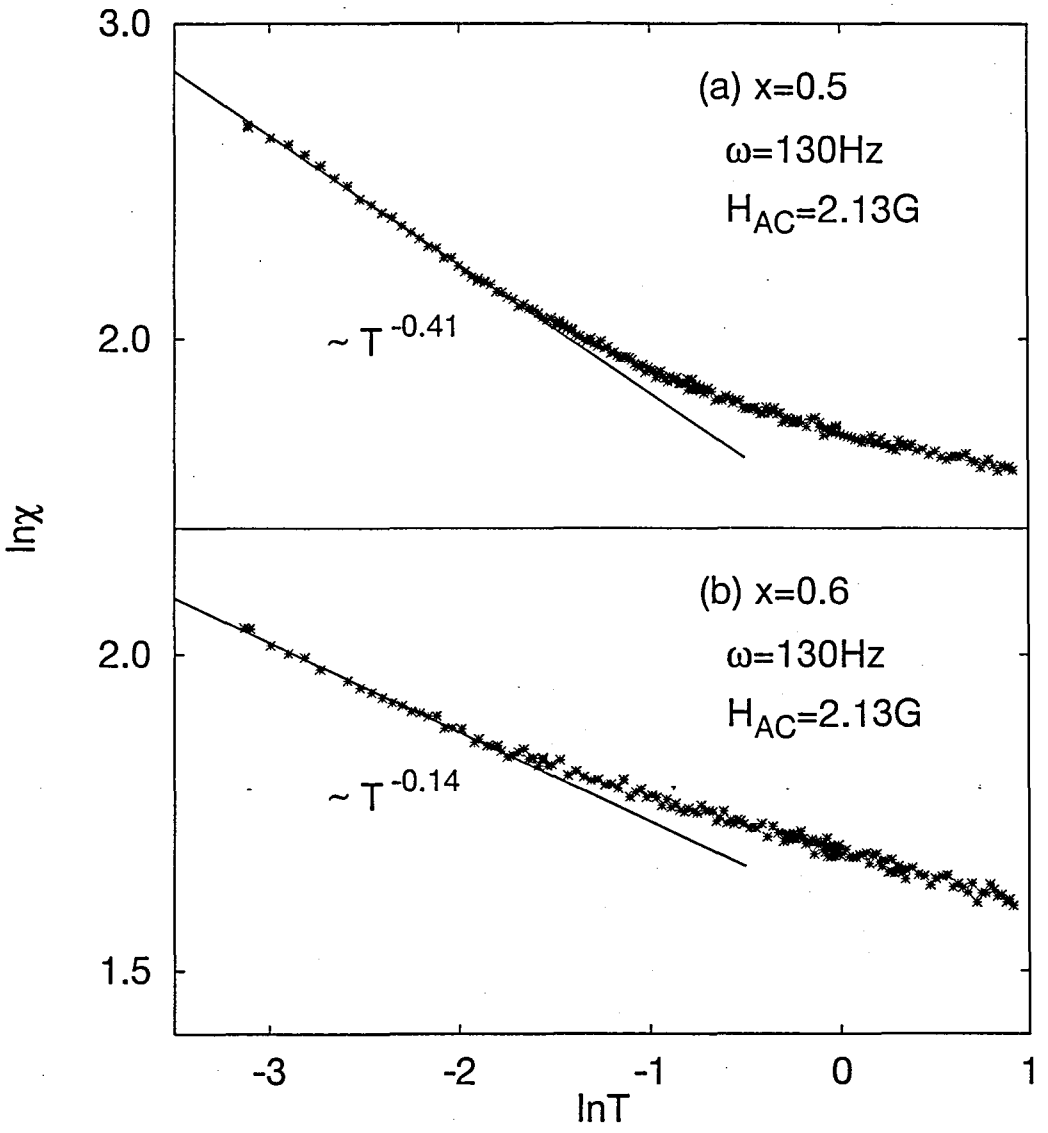

Figure 3.48: The AC-susceptibility down to 40 mK for (a) $x = 0.5$ and (b) 0.6.

Figure 3.48 shows the real part of the AC-susceptibility χ down to 40 mK with an AC-field $H_{AC} = 2.13$ G and a frequency $\omega = 130$ Hz. I tested the dependence of the

susceptibility on an amplitude of AC-field between 0.5 and 5 G, and any significant dependence was not observed. It means that the susceptibility above condition is the value at zero field limit. In this figure we can find that the susceptibility for each concentration diverge down to $T = 0$ with small exponent, as $\chi(T) \propto T^{-\gamma}$. These divergent behavior of $\chi(T)$ cannot be understood by antiferromagnetic or spin glass quantum critical description. However the DC-susceptibility at 1 kG shows a non-divergent behavior as $1 - T^{3/4}$ down to 100 mK. (See Fig. 3.39) It is the behavior at spin glass QCP.

In order to examine the crossover from divergent to non-divergent behavior in $\chi(T)$ by applying a magnetic field more detailed, I have measured the AC-susceptibilities in a DC-magnetic field for $x = 0.5$ and 0.6 and show in Fig. 3.49. AC-susceptibility in a DC-field can be recognized as a differential susceptibility $\chi(T, H) = \partial M/\partial H$ at $H = H_{\rm DC}$. In the figure strong field dependences of $\chi(T, H)$ can be found and the divergence of $\chi(T)$ are easily suppressed by applying a magnetic DC-field of 100 G for each concentration. $\chi(T, H)$ under a finite field also show the broad maximum at a certain temperature, T_m. The field dependence of $\chi(T, H)$ is too strong to be explained by the existence of fluctuating impurity spins individually. If we assume that, the size of such a fictuating spin is estimated at about 20 $\mu_{\rm B}$ from the position of T_m.

As I mentioned in Sec. 3.3.1 the resistivity for $x = 0.5$ under a magnetic field above 1 kG can be understood as a quantum critical phenomena near antiferromagentic or spin glass QCP. And the susceptibility at 1 kG is also explained by it. It means that the 'mean field' excitation near QCP dominates the physical properties in a low temperature and an appropriately high field (> 1 kG) region even in the intermediate concentration region. At $x = 0.5$ the system is a little way from the true critical concentration x_c, the 'chemical' distance is about 200 mK. $x = 0.6$ also locate in the non-magnetic region, and should be much nearer x_c than $x = 0.5$. However the system enters to another regime as decreasing a magnetic field where the energy scale of fluctuation should be much smaller than 200 mK. And the divrgence of $\chi(T)$ at $H = 0$ indicate that it may be to vanish as approaching to zero temperature at zero field. Hence we strongly conjecture the existence of a different singularity from that originated in the QCP over wide Rh-concentration region in the non-magnetic side. This can be understood by the "Quantum Griffiths" picture. Although it is expected from the high temperature (≥ 1.8 K) susceptibility and magnetization measurements as I discussed in last subsection, the low temperature susceptibility measurements have presenred it much more clearly. From our recent μSR experimental result for $x = 0.5$ such clustering of spins was expected [42]. The muon relaxation rate increases sharply below 2 K, and is to saturate below 0.7 K. This feature is taken as an indication of the existence of isolated cluster of unscreened localized moments of Ce-ions which continue to fluctuate even at very low temperature with very long decay time. It is estimated about 2 μsec. The finite size cluster seems to be the rare region in the quantum Griffiths phase. The large clusters fluctuating very slowly drive the divergence of $\chi(T)$. Furthermore the relaxation of muon spin can be suppressed easily by a magnetic field of 100 G, which is consistent with the AC-susceptibility results in a finite field. It can be recognized as the suppression of the slow fluctuation by a field because of its small characteristic energy.

Here I try to apply the quantum Griffiths model for $x = 0.5$ by using Eqn. 3.38 again. I show each λ obtained from $\chi_0(T)$, $\chi_2(T)$ and $C(T)/T$ in Table 3.6. Nonlinear susceptibility $\chi_2(T)$ at low temperature was obtained from the field dependence of $\chi(T, H) = \chi_0(T) + \chi_2(T)H^2 + \cdots$. (See in Fig. 3.50) Each quantity is plotted in the single- or double-logarithmic scale in Fig. 3.51. $\chi_0(T)$ and $\chi_2(T)$ can be reproduced by the divergence with small exponent better than the logarithmic divergence. On the Other

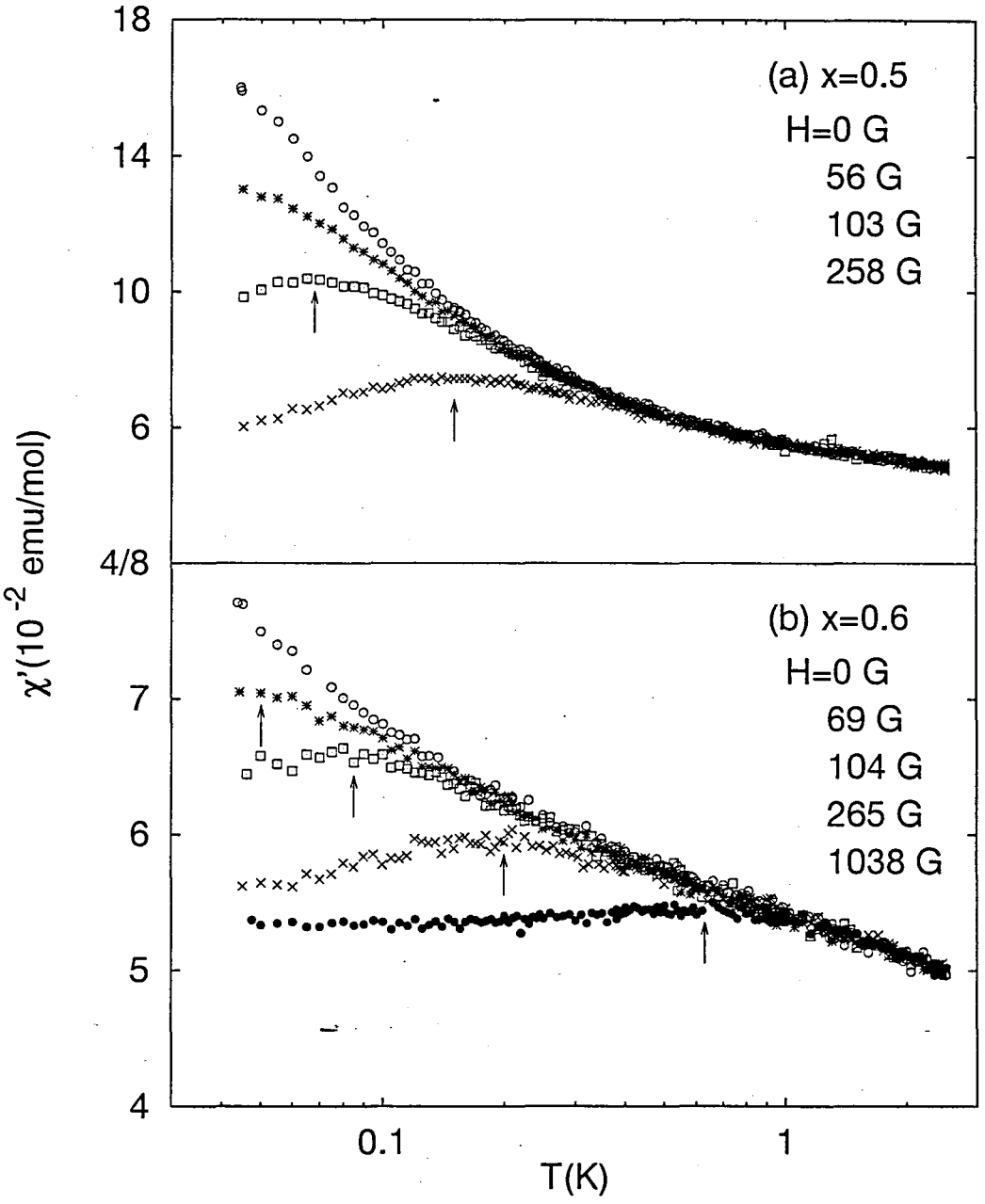

Figure 3.49: The AC-susceptibilities of $Ce(Ru_{1-x}Rh_x)_2Si_2$ for $x = 0.5$ (a) and 0.6 (b) measured in condition described in text under a DC-magnetic field up to 1 kGe are shown. The arrows indicate the temperature, $T_m(H)$, where the susceptibility shows a broad maximum.

hand $C(T)/T$ shows perfectly linear dependence in the form of $C(T)$ vs $-\log T$. Finally the value of λ for $x = 0.5$ obtained from experiment is not unique, which is $0.60 \pm 0{:}04$ from $\chi_0(T)$, 0.80 ± 0.16 from $\chi_2(T)$ and 1.0 from $C(T)/T$. The reason of the ununiqueness of λ may be caused by neglecting the other contibution to the physical quantities. Thus I have tried to reproduce the experimetal results of $\chi_0(T)$ and $C(T)/T$ by a divergent component with a mean field contribution, as $\chi_{\rm MF}(T) + T^{-\gamma}$ and $C_{\rm MF}(T)/T + T^{-\gamma}$. The mean field contribution has been calculated by parameters obtained in Sec. 3.3.1. The agreements between the experiments and calculations are good (not shown in any figure), and the value of γ is unique, 0.8.

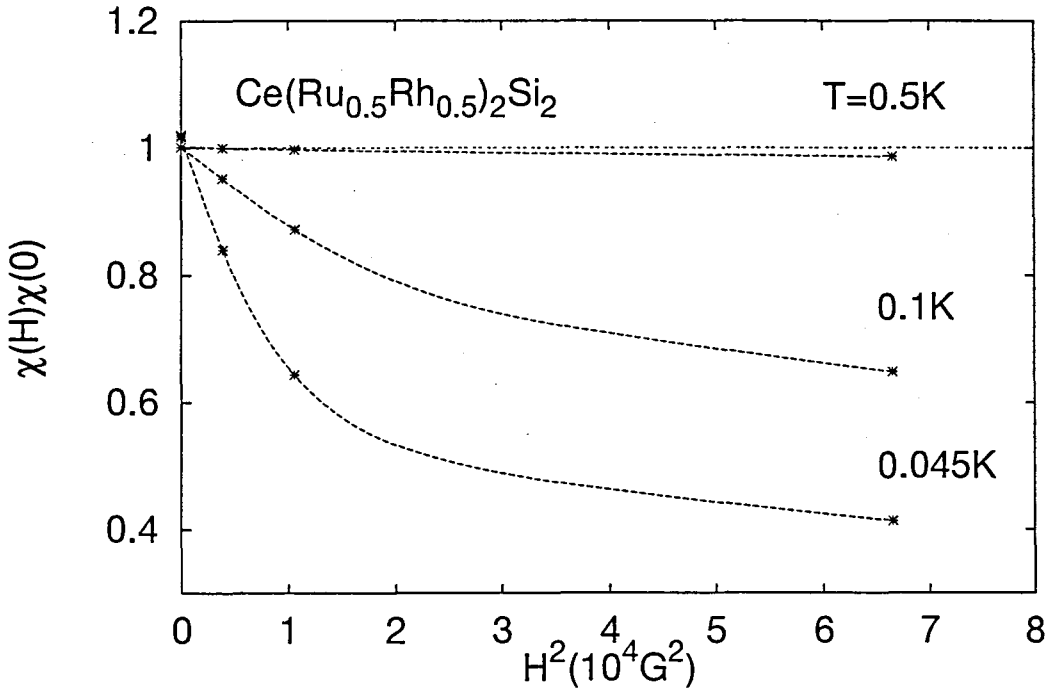

Figure 3.50: $\chi(H)/\chi(0)$ vs H^2 at each temperature are shown. The broken lines are drawn in a guide to eyes.

Table 3.6: The values of λ of $x = 0.5$ obtained from several experiments are listed with the temperature range in which a power law behavior is valid.

λ (C/T)	λ (χ_0)	λ (χ_2)
0.71 ± 0.08	0.60 ± 0.04	0.80 ± 0.16
0.1 K $\sim$ 1.0 K	0.04 K $\sim$ 0.2 K	0.04 K $\sim$ 1.0 K
$1.0(\log T)$	$1.0(\log T)$	$1.0(\log T)$
0.1 K $\sim$ 10 K	0.04 K $\sim$ 0.13 K	0.04 K $\sim$ 0.17 K

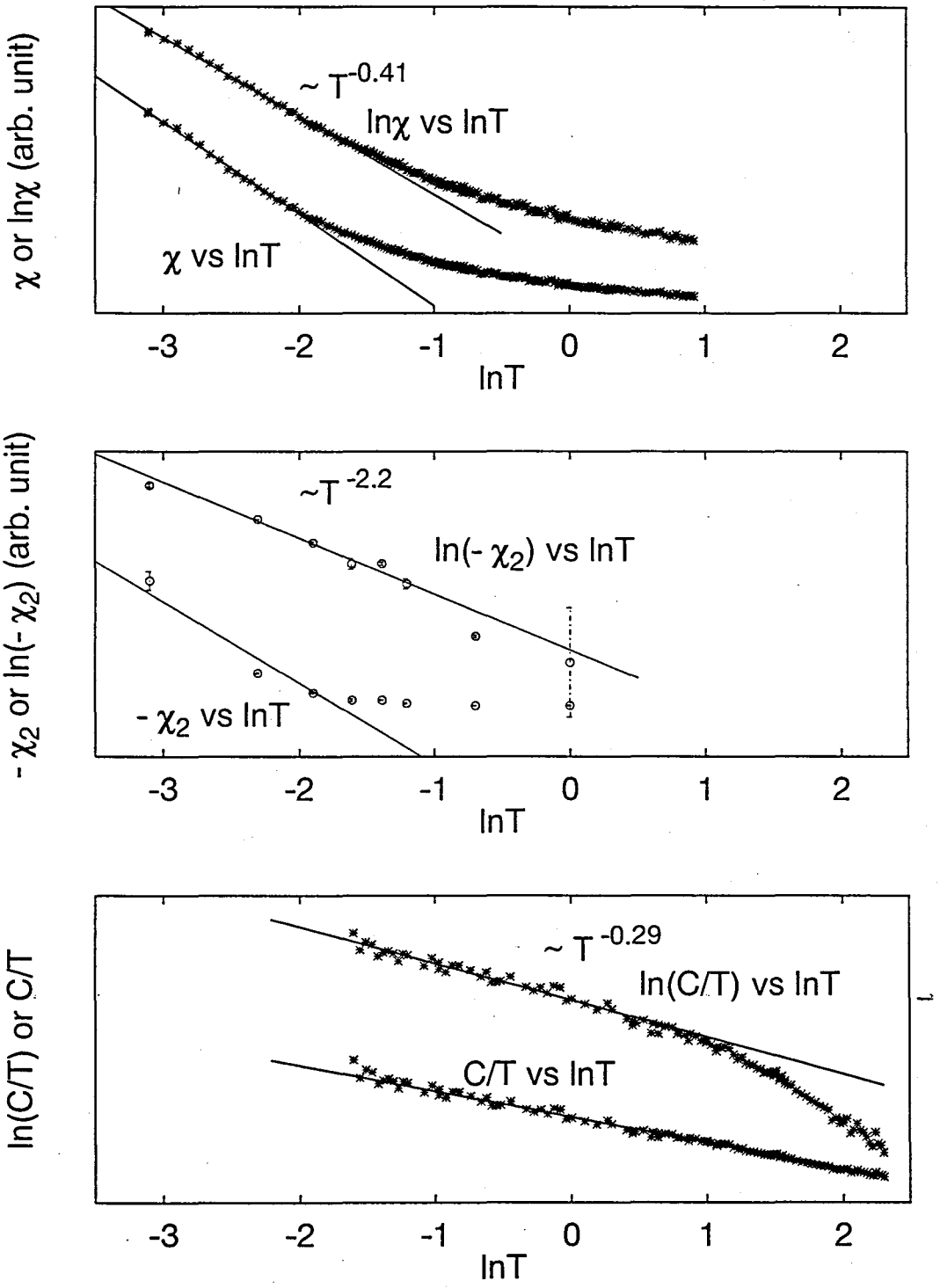

Figure 3.51: $\chi(T)$, $\chi_2(T)$ and $C(T)/T$ of $x = 0.5$ are shown.

Next I discuss on the scaling analysis of the susceptibility in order to investigate the excitation in a low field region detailed. For each concentration, $x = 0.5$ and 0.6, the energy scale should vanish at $T = 0$ and $H = 0$, hence I assume that the scaling form of $\chi(T, H)$ as

$$\chi(T, H) = T^{-\gamma} f(H/T^{\delta}) \tag{3.39}$$

Figure 3.52 shows the scaling plots of $\chi(T, H)$. The experimetal data for each concentration below an appropriate 'scaling' temperature $T_s(H)$ collapses on each scaling curve respectively, except for the data at 1038 G. The exponent γ for $x = 0.5$ and 0.6 are 0.41 ± 0.02 and 0.15 ± 0.03 respectively, which are same values as the exponent of the divergence of the susceptibility at zero field in margin of errors. It means that the asymptotic behaviors expected from the scaling analysis in a finite field are same as the experimental results at zero field. That is to say, we can define the scaling region up to the appropriate field, it sould be between 600 Oe and 1 kOe, including zero field. The values of γ and the scaling functions $f(t)$ for $x = 0.5$ and 0.6 are quite non-universal, however the exponent δ for each concentration are almost same, which are 1.21 ± 0.02 and 1.29 ± 0.04 for $x = 0.5$ and 0.6 respectively. In the "Quantum Griffiths" picture the exponent γ is related to the power in the distribution of cluster size [66], in which the spins are coupled strongly, and it should be composition dependent. On the other hand, the exponent δ may be related to the couple between the 'quantum' tunneling energy and the Zeeman energy of a cluster, which can be universal. In order to verify this scaling can explain the behaviors of other thermodynamic quantities, we examine that of specific heat, which also diverges down to 0 K as $C(T)/T \sim -\log T$ for $x = 0.5$. From the scaling form Eq. 3.39 we obtaine the singular part of $C(T)/T$ at zero field as $T^{-\alpha}$ with $\alpha = 2 + \gamma - 2\delta$. For $x = 0.5$ α is -0.01 ± 0.06, which is consistent with the experimental result. Hence we stress that in this region 'non-universal' equations of state exist for each concentration.

Figure 3.53 shows the phase diagram for $x = 0.5$ and 0.6, in what $T_s(H)$, $T_m(H)$ and a crossover temperature $T^*(H)$ are plotted. $T^*(H)$ is defined as the temperature where the susceptibility in a finite field separate from that at zero field. As reflecting the composition independent of δ, the curves of three characteristic temperatures for $x = 0.5$ and 0.6 are almost same. In the low field region (I), $T > T^*(H)$, the cluster should fluctuate in quantum or thermally, hence the susceptibility keeps on diverging. While in the high field region (III), $T < T_m(H)$, the fluctuation is suppressed and the susceptibility decreases to a fnite value down to 0 K. This region may connect to the higher field region, $H > 1$ kOe, the mean field (MF) 'quantum critical' region. The region (II), $T_m(H) < T < T^*(H)$, is the crossover area. The field dependences of T^* and T_m are $\sim H^{1/\delta}$ in the margin of errors, hence we represent their position as vertical lines in the scaling plot, Fig. 3.52.

A short while ago, I described the zero-field susceptibility by the MF result with an additional diverging contribution, $\chi(T) = \chi_{MF}(T) + aT^{-\gamma}$ with $\gamma = 0.8$, below 2.5 K. This expression means that there are two separate region; one is the MF region where spins interact weakly and are quenched below a crossover temperature T_{FL}. The other one is Griffiths region where spins coupled strongly and formed clusters. Such a strong coupled region appears due to the shift of the balance between the RKKY magnetic interaction and the Kondo effect to the ordered phase from the MF value locally in various places, which is caused by a 'chemical' disorder. The distribution of those shifts should be continuous, hence there is not evident phase separation above mentioned. We think that it is impossible to disentangle to two different components in susceptibility. It is indicated by the success of the scaling analysis of 'total' susceptibility in low field

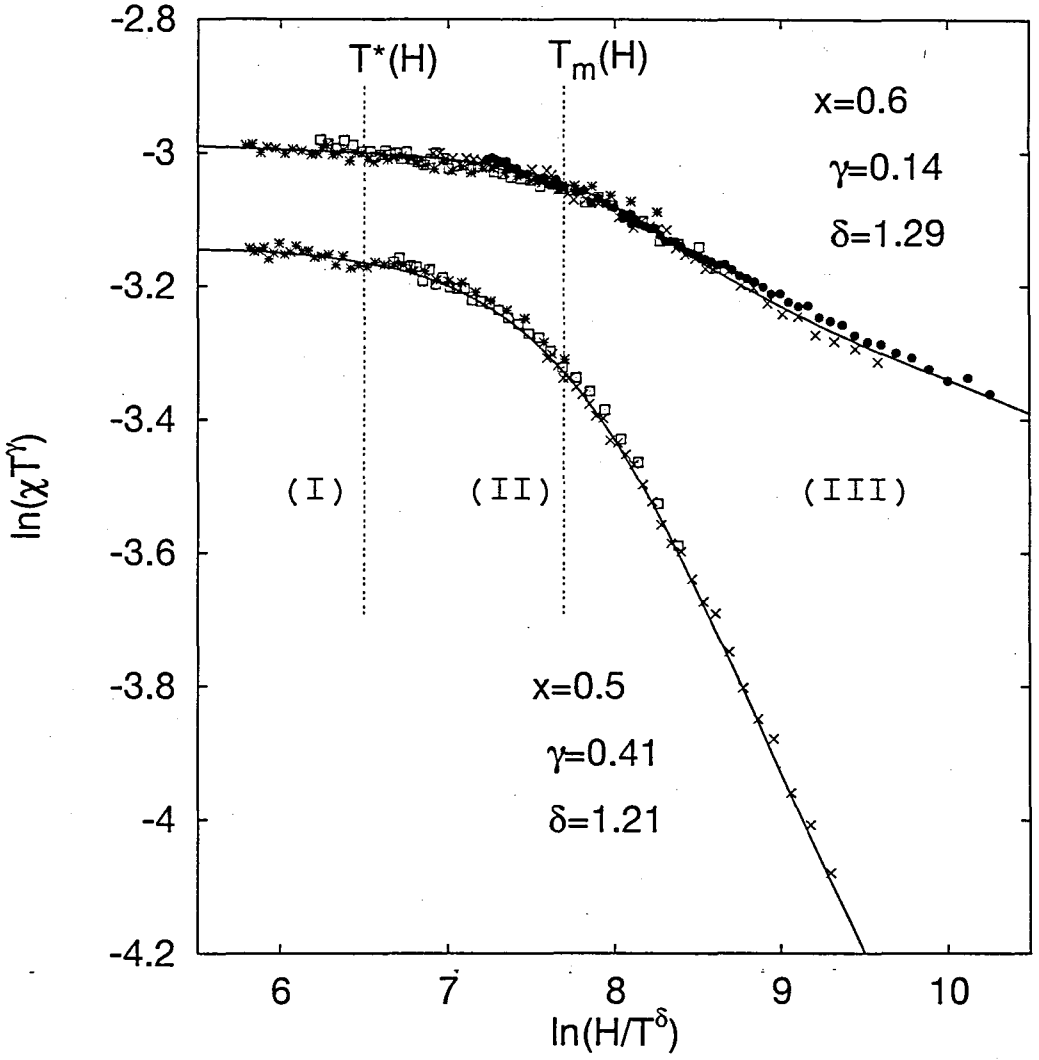

Figure 3.52: The scaling plots of $\chi(T,H)$ for $x = 0.5$ and 0.6 are shown. The two solid lines are the scaling function $f(t)$ for each concentrations, which are guides to eyes. The vertical dashed lines represent the position of $T^*(H)$ and $T_m(H)$ in this scaling plot.

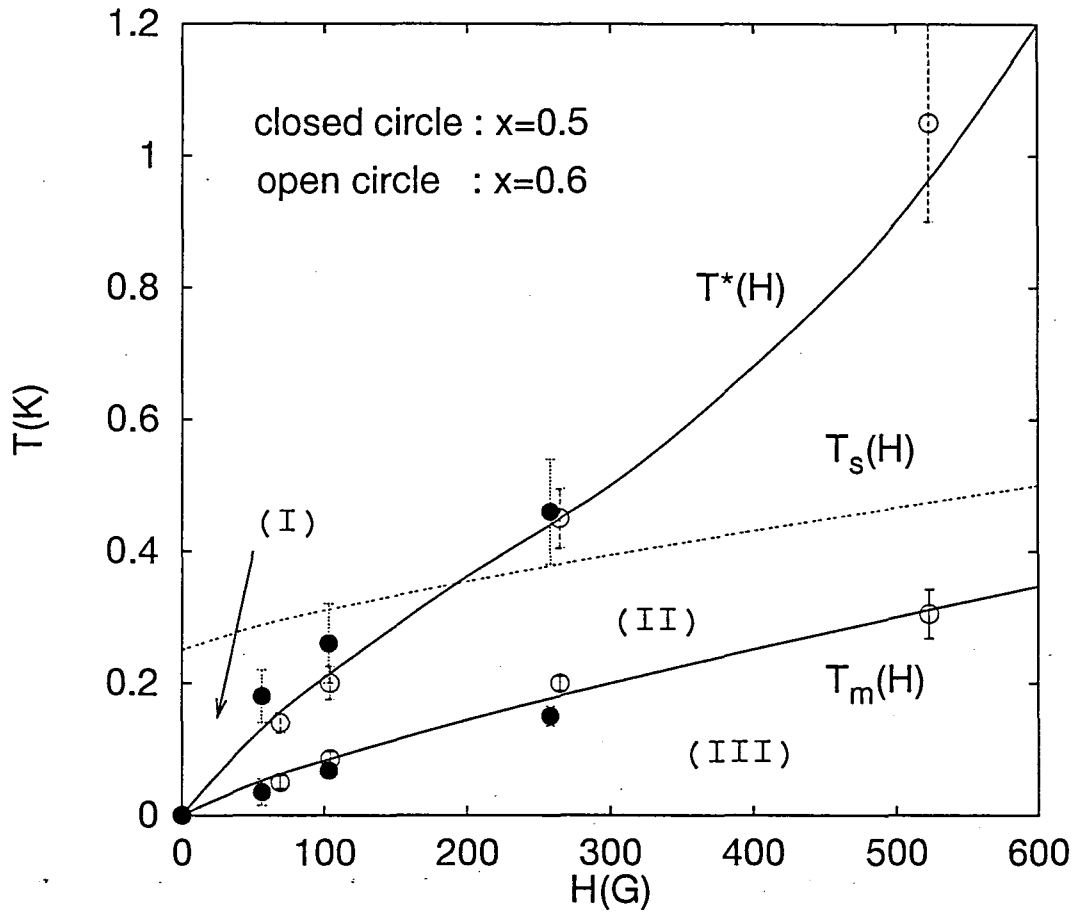

Figure 3.53: The phase diagram for $x = 0.5$ and 0.6 in HT-plain is shown. The solid and the dotted lines are guides to eyes.

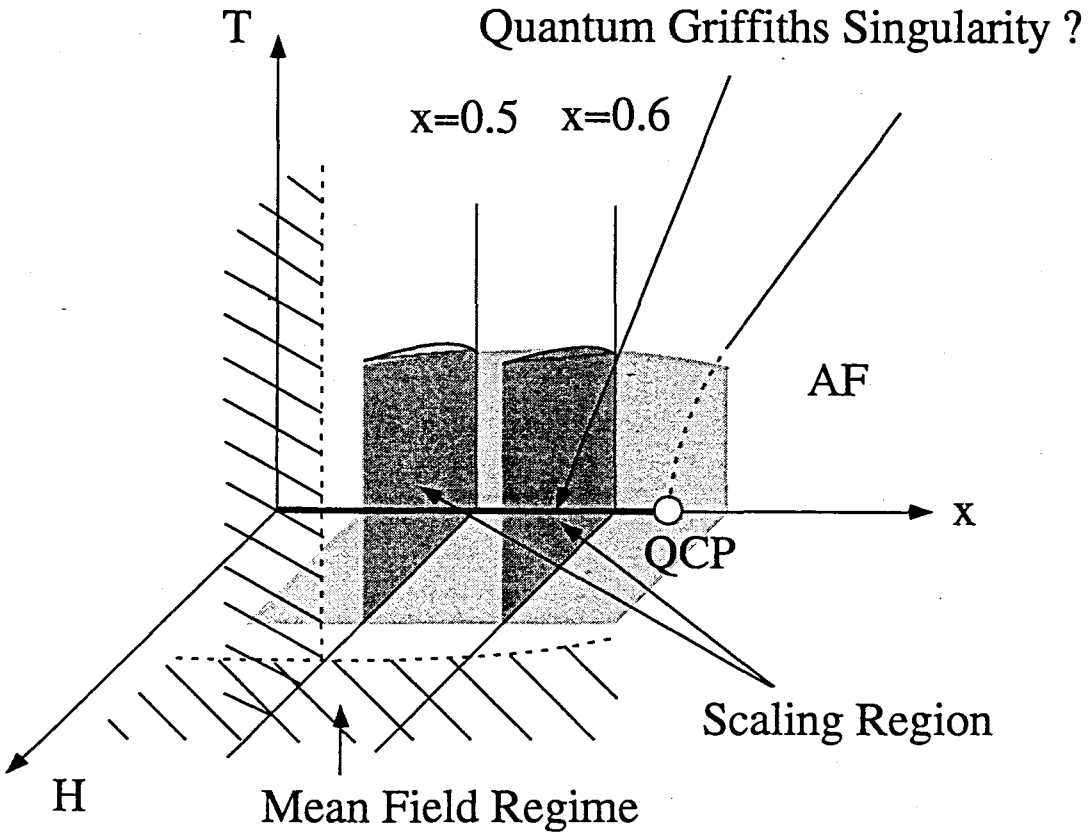

Figure 3.54: Schematic phase diagram of $Ce(Ru_{1-x}Rh_x)_2Si_2$ system near QCP

and the asymptotion to the MF behavior as increasing a field. The asymptotion to the MF can be understood as following. The divergence of the susceptibility is caused by the fluctuating large cluster, which can be suppressed by a very small magnetic field. Indeed, while the Zeeman energy of a cluster of size N grows as $\sqrt{N}$, its tunneling energy vanishes exponentially with N. The 'small' cluster still fluctuating in a moderate field gives close behavior to MF. Therefore we observe the crossover from 'Griffiths' like divergent behavior to the MF one.

Is the singularity at $T = 0$ and $H = 0$ near QCP in $Ce(Ru_{1-x}Rh_x)_2Si_2$ system really quantum Griffiths one? In that case the value of δ is expexted to be 1 from the theory[17], however we have obtained about $1.2 \sim 1.3$. In a recent results of the scaling analysis of the susceptibility for $UCu_{5-x}Pd_x$ system[67, 68], which is also 'disordered' system, δ they have obtained were also about 1.3. From these results we cannot assert that the successful scaling is the properties of a disordered system close to the QCP. Although a full understanding of this experimental fact is still lacking, we believe that the completion of the the theory of quantum Griffiths phase under a magnetic field will explain it.

I show the schematic phase diagram of $Ce(Ru_{1-x}Rh_x)_2Si_2$ near the QCP in Fig. 3.54. The QCP should be between $x = 0.6$ and 0.7. There is MF quatum critical regime comparatively far awy from the QCP, which is represented by the shaded portion in the figure. As approacing to zero temperature and zero field, the system enter to 'disorder' regime. It is represented by gray portion, where a sigularity originated from the QCP is hidden by a much stronger singularity, quantum Griffiths singularity. In the MF regime the physical quantities are scaled by the distance from the QCP $\Delta(T, H, x)$, in the 'disorder' regime

they are done by the distance from the quantum Griffiths 'line'. Thus some questions on this phase diagram, namely,

1. Is 'disorder' regime found in a weak disordered system?

2. Which singularity, originated from quantum Griffiths and QCP, is stronger just on the QCP? In the first place, does a QCP exist in such a strong disordered system as $Ce(Ru_{1-x}Rh_x)_2Si_2$?

3. Is there such a 'disorder' regime near a different type of QCP, for example ferromagnetic case?

In order to answer the first question, I show the AC-susceptibility results of $CeCu_{5.9}Au_{0.1}$ in Fig. 3.55. As I disccused in Sec. 3.3.2, $CeCu_{5.9}Au_{0.1}$ is much weaker disordered system than $Ce(Ru_{1-x}Rh_x)_2Si_2$, and shows very similar behaviors to that of $Ce(Ru_{1-x}Rh_x)_2Si_2$ at high temperature, $C(T)/T \sim -\log T$, $\chi_0(T) \sim 1 - T^{1/2}$, $\chi_2(T) \sim -T^{-1.5}$. Quite different behavior from that of $Ce(Ru_{1-x}Rh_x)_2Si_2$ is found in the figure. $CeCu_{5.9}Au_{0.1}$ shows a non-divergent behavior even in a low temperature region as at high temperature (See Fig. 3.56). And the field dependence of $\chi(T,H)$ is much smaller than that of $Ce(Ru_{1-x}Rh_x)_2Si_2$. It is consistent with the results at 1 kG reported by H. v. Löhneysen. These results can be understood by an antiferromagnetic quantum critical description well. Therefore we can conclude that there is no or very narrow 'disorder' regime beside the QCP in a weak disordered system, which is quite natural.

The second is very interesting questions, but it is open at present. The second connect to two other questions furthermore: (i) Does a finite temperature (classical) phase transition disappear as disorder is to be enhanced? (ii) Does a sharp phase transition exist in a disordered system when shifting from classical to quantum regime. The determination of the evident phase transition line between $x = 0.6$ and 0.7 in $Ce(Ru_{1-x}Rh_x)_2Si_2$ is required. It is future work. The third question is also very interesting. Following the "Harris criterrion"[69], in the case of $d\nu - 2 \leq 2$ the critical behavior of disordered system differs from that of its uniform system in the classical case. In the quantum case, this criterion may be modified to $(d+z)\nu - 2 \leq 2$. Recently R. Narayanan *et al.* have predicted that disorder modifies the critical behavior at antiferromagnetic QCP and does not affect that in the ferromagnetic case on the contrary in an itinerant electron system [70]. Although the situation is unclear in the case of the Kondo lattice system, it is worthy to compare the ferromagetic system with our $Ce(Ru_{1-x}Rh_x)_2Si_2$ in experimental.

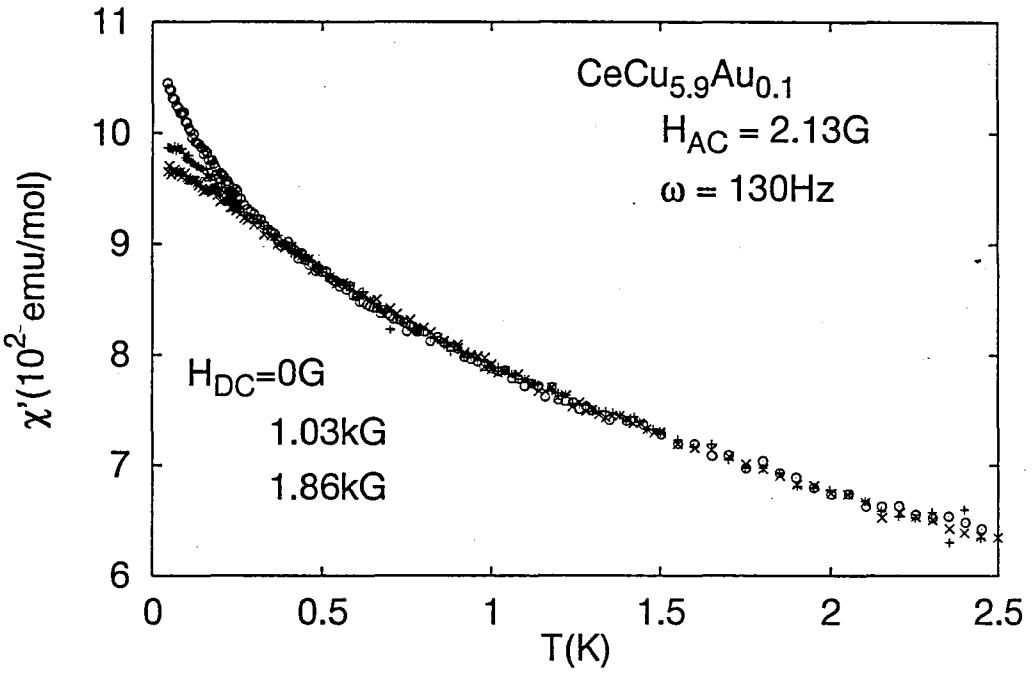

Figure 3.55: The AC-susceptibility results of $CeCu_{5.9}Au_{0.1}$ in a magentic field are shown.

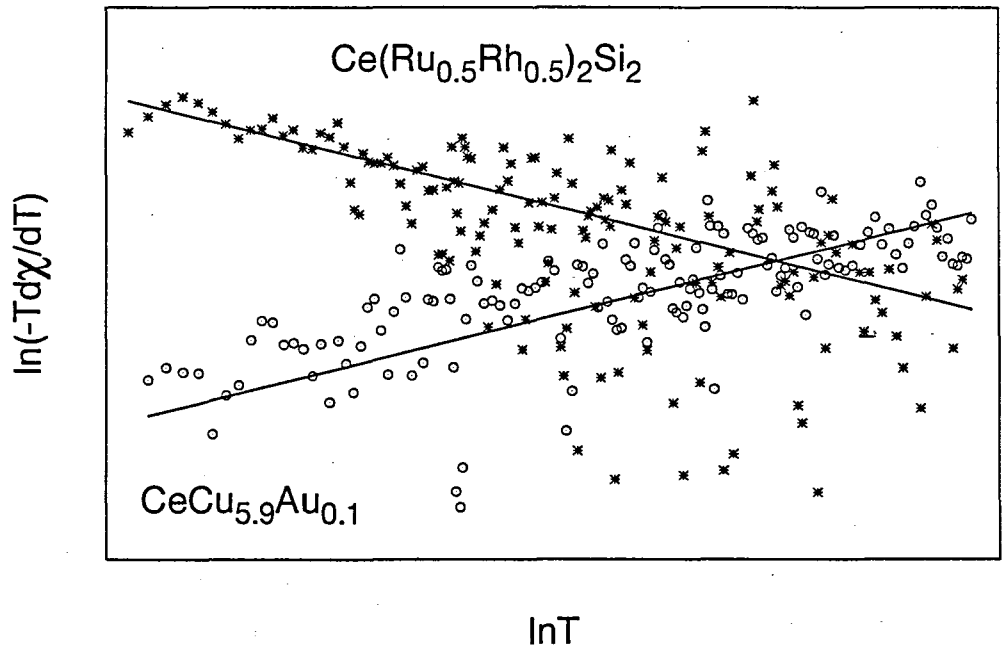

Figure 3.56: $\log(Td\chi/dT)$ vs $\log T$ plots of $CeCu_{5.9}Au_{0.1}$ and $Ce(Ru_{1-x}Rh_x)_2Si_2$ 0.50.5 at $H = 0$ are shown. The explanation of this plot is described in Sec. 3.3.2. This figure presents that $\chi_0(T)$ of $CeCu_{5.9}Au_{0.1}$ is non-divergent in contrast with that of $Ce(Ru_{0.5}Rh_{0.5})_2Si_2$.

Chapter 4

Conclusion

1. We have studied the NFL behavior in $Ce(Ru_{1-x}Rh_x)_2Si_2$ system by means of the specific heat, the susceptibility and the resistivity measurements. We found the followings as experimental results.

   (a) Near the QCP of the SDW phase on the Rh-poor side, that is at $x = 0.03$, the NFL behavior was not observed either in the specific heat, the susceptibility or the resistivity. T_{coh}, the crossover temperature below which the FL state is formed, seems to connect smoothly from the nonmagnetic side to the magnetic SDW side.

   (b) In a wide region of the intermediate Rh-concentration the NFL behavior ($C/T \sim -\log T$, $\chi \sim 1 - T^a$, $\rho \sim T^n$) was observed. The deviation from the FL is enhanced as approaching to the QCP of the antiferromagnetic ordered phase in the high Rh-concentration region. This is not the case when approaching to the QCP of the SDW phase on the Rh-rich side.

2. We tried to apply the SCR theory for the low temperature properties in the low Rh-concentration region. The parameters obtained from the macroscopic quantities, C and χ_0, and the microscopic or the dynamical quantities, χ_Q, Γ_Q and $1/T_1$, shows good agreements with each other. At least in the concentration region farther from $x = 0.03$ with respect to the QCP, the SCR theory can explain the low temperature properties in the system very well except the x-dependence of T_{coh}. Further experiment at closer concentrations to the QCP is needed in order to clarify how the QPT occurs between the nonmagnetic FL state and the SDW state.

3. We have studied the effect of a magnetic field on the NFL behavior in the intermediate Rh-concentration region. Two mechanisms for the NFL behavior coexist in this region; one is due to the quantum critical fluctuation originating in the QCP of the antiferromagnetic phase in the high Rh-concentration region and so is other to the Kondo disorder. In the high field region, the mean-field quantum critical description can be applicable. At zero field the quantum Griffiths description, which is the result of the interplay between the quantum critical fluctuation and the disorder, explains the experimental results appropriately. By a small magnetic field of 1 kG the Griffiths singularity can be hidden because of its small characteristic energy. In the low field region we found the new scaling region where the susceptibility can be scaled by H/T^δ as,

$$\chi(T, H) = T^{-\gamma} f(H/T^\delta)$$

In a much weaker disordered system, $CeCu_{5.9}Au_{0.1}$, such a scaling region was not observed. It is the feature of a disordered system near a QCP.

Bibliography

[1] K. Andres *et al.* , Phys. Rev. **B 35** (1975) 1779

[2] K. Kadowaki *et al.* , Solid State Commun. **58** (1986) 507

[3] J. Kondo, Prog. Theor. Phys. **32** (1964) 37

[4] Y. Onuki *et al.* , J. Magn. Magn. Mater. **63-64** (1987) 281

[5] A. Krimmel *et al.* , Z. Phys. **B 86** (1992) 161

[6] R. A. Steeman *et al.* , Solid State Commun. **66** (1988) 103

[7] C. Broholm *et al.* , Phys. Rev. Lett. **58** (1987) 1467

[8] G. Aeppli *et al.* , J. Magn. Magn. Mater. **76-77** (1988) 385

[9] H. v. Löhneysen, J. Phys. Condens. Matter **8** (1996) 9689

[10] C. L. Seaman *et al.* , Phys. Rev. Lett. **67** (2882) 1991

[11] A. J. Millis, Phys. Rev. **B 48** (1993) 7183

[12] M. A. Continentino, Z. Phys. **B 101** (1996) 197

[13] T. Moriya *et al.* , J. Phys. Soc. Jpn. **64** (1995) 960

[14] S. Sachdev, Phil. Trans. R. Soc. Lond. **A 356** (1998) 173

[15] E. Miranda *et al.* , J. Phys. Condens. Matter **8** (1996) 9871

[16] O. O. Bernal *et al.* , Phys. Rev. Lett. **75** (1995) 2023

[17] A. H. Castro-Neto *et al.* , Phys. Rev. Lett. **81** (1998) 3531

[18] F. M. Grosche *et al.* , Physica **B 237-238** (1997) 197

[19] F. Steglich *et al.* , J. Phys. Condens. Matter **8** (1996) 9909; Y. Aoki *et al.* , J. Phys. Soc. Jpn. **66** (1997) 2993

[20] P. Hean *et al.* , J. Low Temp. Phys. **67** (1987) 391

[21] R. A. Fisher *et al.* , J. Low Temp. Phys. **84** (1991) 49

[22] M. J. Besnus *et al.* , Solid State Commun. **55** (1985) 779

[23] S. Kambe *et al.* , J. Phys. Soc. Jpn. **65** (1996) 3294

[24] K. D. Schotte *et al.* , Phys. Lett. **55A** (1975) 38

[25] F. Lapierre *et al.* , J. Magn. Magn. Mater. **108** (1992) 167

[26] L. P. Regnault *et al.* , Phys. Rev. **B 38** (1988) 4481

[27] M. Sato *et al.* , J. Phys. Chem. Solid **60** (1999) 1203

[28] S. Quezel *et al.* , J. Magn. Magn. Mater. **76-77** (1988) 260

[29] M. Sato, Doctor thesis, Osaka University (1999)

[30] H. Aoki *et al.* , Phys. Rev. Lett. **71** (1993) 2110

[31] K. Matsuhira *et al.* , J. Phys. Soc. Jpn. **68** (1999) 3402

[32] H. Sato *et al.* , Phys. Rev. **B 57** (1998) 5891

[33] S. Kawarazaki *et al.* , Physica **B 206-207** (1995) 298

[34] C. Sekine *et al.* , J. Phys. Soc. Jpn. **61** (1992) 4536

[35] R. Calemczuk *et al.* , J. Magn. Magn. Mater. **90-91** (1990) 477

[36] S. Kawarazaki *et al.* , J. Phys. Soc. Jpn. **66** (1997) 2473

[37] Y. Miyako *et al.* , J. Phys. Soc. Jpn. **65** (1996) Suppl. B 12

[38] S. Murayama *et al.* , Phys. Rev. **B 56** (1997) 11092

[39] T. Taniguchi *et al.* , Physica **B 206-207** (1997) 123

[40] B. H. Grier *et al.* , Phys. Rev. **B 29** (1984) 2664

[41] S. Kawarazaki *et al.* , to be published in Phys. Rev. **B**

[42] Y. Yamamoto *et al.* , Doctor thesis, Osaka University (1999)

[43] S. Kawarazaki private communications

[44] R. Settai *et al.* , J. Phys. Soc. Jpn. **66** (1997) 2260

[45] Y. Kawasaki *et al.* , Phys. Rev. **B 58** (1998) 8634

[46] A. Lacerda *et al.* , Phys. Rev. **B 40** (1989) 8759

[47] M. Hatatani *et al.* , J. Phys. Soc. Jpn. **67** (1998) 4002

[48] K. Ueda *et al.* , Physica **B 259-261** (1999) 83-84

[49] K. Wilson, Rev. Mod. Phys. **47** (1975) 773

[50] R. Chau *et al.* , J. Phys. Condens. Matter **8** (1996) 9939

[51] H. v. Löhneysen *et al.* , J. Magn. Magn. Mater. **177-181** (1998) 12

[52] F. J. Ohkawa, Phys. Rev. Lett. **64** (1990) 2300

[53] D. R. Grempel *et al.* , Phys. Rev. **B 60** (1999) 4702

[54] D. R. Grempel private communications.

[55] Q. Si *et al.* , Phys. Rev. Lett. **16** (1996) 3391

[56] M. J. Rozenberg *et al.* , Phys. Rev. Lett. **81** (1998) 2550

[57] A. Georges *et al.* , Rev. Mod. Phys. **68** (1996) 13

[58] T. Taniguchi private communications

[59] M. J. Thill *et al.* , Physica **A 214** (1995) 321

[60] R. B. Griffiths, Phys. Rev. Lett. **23** (1969) 17

[61] Ch. Binek *et al.* , Phys. Rev. **B 51** (1995) 12888

[62] M. Guo *et al.* , Phys. Rev. **B 54** (1996) 3336

[63] A. M. Tsvelik *et al.* , Phys. Rev. **B 48** (1993) 9887

[64] J. S. Kim *et al.* , Phys. Rev. **B 60** (1999) 6761

[65] S. Doniach, Physica **B 91** (1977) 321

[66] H. Rieger *et al.* , Phys. Rev. **B 54** (1996) 3328

[67] A. M. Strydom *et al.* , J. Phys. Condens. Matter **11** (1999) 9691

[68] R. Chau *et al.* , J. Phys. Condens. Matter **12** (2000) 4495

[69] A. B. Harris, J. Phys. **C 7** (1974) 1671

[70] R. Narayanan *et al.* , Phys. Rev. **B 60** (1999) 10150

Published works

1. Low-temperature specific heat of $Ce(Ru_{1-x}Rh_x)_2Si_2$ and $Ce_{1-x}La_xRu_2Si_2$;
   T. Taniguchi, Y. Tabata, H. Tanabe, Y. Miyako;
   Physica **B 230-232** (1997) 123-125

2. Non-Fermi-liquid like behavior in $Ce(Ru_{1-x}Rh_x)_2Si_2$ ($0.3 \leq x \leq 0.5$);
   T. Taniguchi, Y. Tabata, H. Tanabe, Y. Miyako;
   Journal of Magnetism and Magnetic Materials **177-181** (1998) 419-420

3. Spin flutuation and magnetic phase transition in itinerant heavy electron system $Ce(Ru_{1-x}Rh_x)_2Si_2$ ($x = 0$, 0.03 and 0.05);
   Y. Tabata, T. Taniguchi, M. Sato, S. Kawarazaki, Y. Miyako;
   Journal of the Physical Society of Japan **67** (1998) 2484-2487

4. A New scaling analysis of the susceptibility and the specific heat of the non-Fermi liquid system $Ce(Ru_{1-x}Rh_x)_2Si_2$ with $x = 0.4$ and 0.5;
   J. Souletie, Y. Tabata, T. Taniguchi, Y. Miyako;
   The European Physical Journal **B 8** (1999) 43-46

5. Spin dynamics in itinerant heavy electron system $Ce(Ru_{1-x}Rh_x)_2Si_2$ ($x = 0$ and 0.03) near the magnetic instability point;
   Y. Tabata, T. Taniguchi, M. Sato, S. Kawarazaki, Y. Miyako;
   Physica **B 259-261** (1999) 70-72

6. Scaling analysis of the susceptibility of $Ce(Ru_{1-x}Rh_x)_2Si_2$ in the Fermi and non-Fermi liquid ranges;
   J. Souletie, Y. Tabata, T. Taniguchi, Y. Miyako;
   Physica **B 259-261** (1999) 372-373

7. Non-Fermi liquid behavior in $Ce(Ru_{1-x}Rh_x)_2Si_2$ ($x = 0.4$ and 0.5);
   T. Taniguchi, Y. Tabata, Y. Miyako;
   Journal of the Physical Society of Japan **68** (1999) 2026-2032

8. Systematic study of the ground state in $Ce(Ru_{1-x}Rh_x)_2Si_2$: Fermi and non-Fermi liquid behavior;
   T. Takeuchi, Y. Yamamoto, M. Sato, Y. Tabata, T. Taniguchi, S. Kawarazaki, M. Ocio, P, Pari, J. Hammann, Y. Miyako;
   Japanese Journal of Applied Physics Series **11** (1999) 151-153

9. Field effect on the non-Fermi liquid in $Ce(Ru_{0.5}Rh_{0.5})_2Si_2$
   Physica **B 281-282** (2000) 349-350
   Y. Tabata, T. Taniguchi, Y. Yamamoto, Y. Miyako, M. Ocio, P. Pari, J. Hammann

10. Non-linear susceptibility of $Ce(Ru_{1-x}Rh_x)_2Si_2$ and $CeCu_{5.9}Au_{0.1}$
    Physica **B 281-282** (2000) 356-358 T. Taniguchi, Y. Tabata, Y. Miyako, O. Tegus, A. A. Menovsky, J. A. Mydosh

11. Canonical spin glass behavior in Ce_2AgIn_3
J. Phys. Soc. Jpn. **69** (2000) 1012
T. Nishioka, Y. Tabata, T. Taniguchi, Y. Miyako

12. Field effect on the non-Fermi liquid behavior in $Ce(Ru_{0.5}Rh_{0.5})_2Si_2$
J. Phys. Soc. Jpn. Supple A**69** (2000) 47 Y. Tabata, T. Taniguchi, Y. Miyako, D. R. Grempel, M. Ocio

13. Sacling near the "Quamtum" phase transition: An analysis of the susceptibility and of the specific heat of $Ce(Ru_{1-x}Rh_x)_2Si_2$
J. Phys. Soc. Jpn. Supple A**69** (2000) 60
J. Souletie, Y. Tabata, T. Taniguchi, Y. Miyako

14. Spin fluctuation and antiferromagnetic phase transition in heavy fermions of Kramers (Ce compound) and non-Kramers (U compound) Doublets
J. Phys. Soc. Jpn. Supple A**69** (2000) 77
Y. Miyako, Y. Yamamoto, Y. Tabata, K. Marumoto, M. Sato, T. Taniguchi, T. Takeuchi, S. Kawarazaki, H. Amitsuka, M. Ocio, P. Pari, J. Hammann

15. Non-Fermi-Liquid scaling in $Ce(Ru_{0.5}Rh_{0.5})_2Si_2$
Phys. Rev. Lett. **86** (2001) 524
Y. Tabata, D. R. Grempel, M. Ocio, T. Taniguchi, Y. Miyako

Acknowledgement

This work owes much to many collaborators. The encounter with them was stimulative and fortunate for me.

First I would like to express the deepest gratitude to Prof. Yoshihito Miyako for his valuable suggestions, enlightening discussions and continuous encouragement during my present work. I also wish to express great thanks to Prof. Shuzo Kawarazaki and Dr. Tetsuya Takeuchi for their many helpful guidances and advices. I am sincerely grateful to Dr. Toshifumi Taniguchi for his stimulating discussions and valuable suggestions. He is the best collaborator and the teacher throughout my present study. I also wish to express sincere thanks to Dr. Yoshiyuki Yamamoto and Dr. Masugu Sato for their valuable discussions and many supports on sample preparation. I would also like to thank to all members in Miyako laboratory. I had enjoyed my student life with them.

In 1998 I had studied at SPEC, CEA Saclay in France, and carried out the low temperature magnetoresistance measurements there. I would like to express sincere gratitude to Dr. Miguel Ocio, Dr. Patirick Pari, Dr. Jacques Hammann and other staffs for their cooperation and the hospitality during my stay. I had obtained many interesting results with their supports. I also wish to express great thanks to Dr. Daniel R. Grempel for his theoretical support on the quantum phase transition. I would like to thank to Prof. Jean Souletie for his variable discussions and many helps during my stay in Grenoble. My study in France was very fruitful thanks to all of them.

Finally I wish to express the greatest thanks for my family for their sincere supports.